DEVELOPMENT OF ADVANCED NANOMANUFACTURING: 3D INTEGRATION AND HIGH SPEED DIRECTED SELF-ASSEMBLY

A Dissertation

by

HUIFENG LI

Submitted to the Office of Graduate Studies of
Texas A&M University
in partial fulfillment of the requirements for the degree of

DOCTOR OF PHILOSOPHY

August 2010

Major Subject: Electrical Engineering

DEVELOPMENT OF ADVANCED NANOMANUFACTURING: 3D INTEGRATION AND HIGH SPEED DIRECTED SELF-ASSEMBLY

A Dissertation

by

HUIFENG LI

Submitted to the Office of Graduate Studies of
Texas A&M University
in partial fulfillment of the requirements for the degree of

DOCTOR OF PHILOSOPHY

Approved by:

Chair of Committee,	Xing Cheng
Committee Members,	Jun Zou
	Arum Han
	Winfried Teizer
Head of Department,	Costas N. Georghiades

August 2010

Major Subject: Electrical Engineering

ABSTRACT

Development of Advanced Nanomanufacturing: 3D Integration and High Speed Directed Self-assembly.

(August 2010)

Huifeng Li, B.Eng., Shanghai Jiaotong University, China;

M.Eng., National University of Singapore, Singapore

Chair of Advisory Committee: Dr. Xing Cheng

Development of nanoscience and nanotechnology requires rapid and robust nanomanufacturing processes to produce nanoscale materials, structures and devices. The dissertation aims to contribute to two major challenging and attractive topics in nanomanufacturing. Firstly, this research develops fabrication techniques for three dimensional (3D) structures and integrates them into functional devices and systems. Secondly, a novel process is proposed and studied for rapid and efficient manipulation of nanomaterials using a directed self-assembly process.

The study begins with the development of nanoimprint lithography for nanopatterning and fabrication of 3D multilayer polymeric structures in the micro- and nano-scale, by optimizing the layer-transfer and transfer-bonding techniques. These techniques allow the integration of microfluidic and photonic systems in a single chip for achieving ultracompact lab-on-a-chip concept. To exemplify the integration capability, a monolithic fluorescence detection system is proposed and the approaches

to design and fabricate the components, such as a tunable optical filter and optical antennas are addressed. The nanoimprint lithography can also be employed to prepare nanopatterned polymer structures as a template to guide the self-assembly process of nanomaterials, such as single-walled carbon nanotubes (SWNTs). By introducing the surface functionalization, electric field and ultrasonic agitation into the process, we develop a rapid and robust approach for effective placement and alignment of SWNTs.

These nanomanufacturing processes are successfully developed and will provide a pathway to the full realization of the lab-on-a-chip concept and significantly contribute to the applications of nanomaterials.

To My Parents, Wife and Sister

ACKNOWLEDGEMENTS

I am thankful to many people for the completion of the dissertation and the entire Ph.D. journey. I would like take this opportunity to express special thanks to my advisor, Dr. Xing Cheng, for his support, guidance and patience. The belief, encouragement and motivation from him have been exemplary. I will also express my gratefulness to my committee members, Dr. Mosong Cheng, Dr. Arum Han, Dr. Jun Zou and Dr. Winfried Teizer, for their constant support.

I had the great pleasure to work with a group of nice and helpful colleagues at Texas A&M University. Thanks to Hyunsoo Park, Dehu Cui, Taohua Li and Min Shuai for the discussion and friendship. Their willingness to contribute and the experience in the material preparation and device fabrication are invaluable for this dissertation research.

MCF staff members provided great assistance with my nanofabrication and material characterization work. Thank you, Dr. Gang Liang, Dr. Jingyi Shen and Dr. Zhen Li. I want to also acknowledge ECE departmental staff, Tammy and Linda, for their assistance during my Ph.D. study here.

Finally, I want to thank my parents, sister and wife for their unconditional support and love.

TABLE OF CONTENTS

Page

ABSTRACT….. iii

ACKNOWLEDGEMENTS vi

TABLE OF CONTENTS vii

LIST OF FIGURES iix

CHAPTER I INTRODUCTION 1

1.1 Nanotechnology and nanomanufacturing 1
1.2 Current status and trend of lithography 2
1.3 Progress in the directed self-assembly 6
1.4 Organization of the dissertation 7

CHAPTER II CURRENT DEVELOPMENT OF NIL 9

2.1 Introduction 9
2.1.1 Template 10
2.1.2 Anti-sticking coating 11
2.1.3 Resist material 13
2.1.4 Parameters during thermal imprint process 14
2.1.5 Applications 15
2.2 Current progress of NIL research at TAMU 16
2.3 Summary 22

CHAPTER III AN APPROACH TOWARDS MONOLITHIC FLUORESCENCE DETECTION IN MICROFLUIDIC DEVICES 23

3.1 Introduction 23
3.2 Design methodology and fabrication process 24
3.3 MDM structure as tunable filter for lab-on-a-chip application 26
3.3.1 Principles of the tunable optical filter 27
3.3.2 Fabrication 29

Page

3.3.3 Summary 33
3.4 Optical antenna 33
3.4.1 Simulation details 34
3.4.2 Results and discussion 35
3.4.3 Fabrication 42
3.4.4 Summary 44

CHAPTER IV MANIPULATION OF CARBON NANOTUBES 46

4.1 Introduction 46
4.2 Manipulation of carbon nanotubes by micro- and nanochannels 49
4.2.1 Overview 49
4.2.2 Experimental details 51
4.2.3 Dispersing CNTs with ancillary nanomaterials 55
4.2.4 Aligned-CNT stripes on silicon and polymer surfaces 57
4.2.5 Summary 61
4.3 Guided layer-by-layer assembly 62
4.3.1 Overview 62
4.3.2 Experimental details 63
4.3.3 Polarized Raman spectra of the SWNT stripes on the substrate 66
4.3.4 Effect of surfactant on the stability and alignment 70
4.3.5 Electrical characterization 72
4.3.6 Summary 73
4.4 High speed directed self-assembly of SWNTs 74
4.4.1 Overview 74
4.4.2 Experimental setup and process design 77
4.4.3 Preparation of SWNTs suspension 89
4.4.4 Surface functionalization 92
4.4.5 Electrophoresis enhanced self-assembly 94
4.4.6 Ultrasonic agitation 96
4.4.7 Summary 98
4.5 Future work 99
4.5.1 Morphology-property relations in aligned-CNT stripes 99
4.5.2 Multidirectional CNT alignment 102
4.5.3 Microelectronic devices based on pure semiconducting CNT stripes 104

CHAPTER V CONCLUSION 108

REFERENCES 116

VITA 123

LIST OF FIGURES

Page

Figure 1. Schematics of nanoimprint process. 10

Figure 2. Schematic of the patterning process for 3D multilayer polymer structures. 19

Figure 3. SEM micrographs of 3D multilayer PMMA structures using direct thermal bonding. (a) Two-layered 700 nm period grating; (b) Three-layered 700 nm period grating; (c) Two-layered 10 μm period grating; (d) Three-layered 10 μm period. 20

Figure 4. SEM micrographs of 3D multilayer PMMA structures using SU-8. (a) Three-layered 700 nm pitch grating bonded with 1% of SU-8; (b) Three-layered 700 nm pitch grating bonded with 6% of SU-8; (c) Three-layered 700 nm pitch grating bonded with 10% of SU-8. Progressively more bottom layer structures filling is observed from (a) to (c). 21

Figure 5. Integrated multilayer optofluidic detection system. 25

Figure 6. A schematic of the microfluidic MDM structure..... 27

Figure 7. Calculated transmission spectra of MDM structures. (a) transmission spectra for different dielectric layer thickness; (b) transmission spectra of a microfluidic MDM structure with and without water..... 28

Figure 8. Schematics of the fabrication of the microfluidic MDM structure by nanoimprint and transfer-bonding. 31

Figure 9. SEM images of the side view (left) and top view (right) of the microfludic MDM structure. 32

Figure 10. Optical microscope image for MDM structure..... 32

Figure 11. (a) A snapshot of optical field distribution in a dipole antenna; (b) A profile of the optical intensity enhancement factors across the dipole antenna. 36

Page

Figure 12. Optical intensity enhancement in the gap region as a function of incident wavelengths. (a) dipole antenna with a resonant wavelength of 2 μm; (b) dipole antenna with a resonant wavelength of 8 μm. 38

Figure 13. Optical intensity enhancement in the gap region as a function of excitation wavelengths (a) bowtie aperture antenna with a resonant wavelength of 2 μm. (b) bowtie aperture antenna with a resonant wavelength of 10 μm. 38

Figure 14. Calculated field enhancement factors as a function of gap width for a dipole antenna with a resonant wavelength of 8 μm. 40

Figure 15. Calculated field distribution in the x-y plane at three different distances from the bowtie aperture antenna plane. (a) z = 0; (b) z = 0.5 μm above the antenna plane; (c) z = 1 μm above the antenna plane. 41

Figure 16. Fabrication of optical antennas 43

Figure 17. SEM images of optical dipole and bowtie aperture antennas. 44

Figure 18. Summary of schemes and applications of microchannel-aligned CNTs .. 51

Figure 19. Schematics of (a) alignment of de-roped CNTs using microchannels and (b) stripes of aligned CNTs on a substrate. 52

Figure 20. A schematic of CNT bundle reorganization. 53

Figure 21. Schematics of precision placement of CNTs on a substrate for microelectronic device and circuit applications. (a) Pattern nanoscale SAM structures for trapping surface-functionalized CNTs on the substrate; (b) Align microchannels on top of the SAM patterns and flow CNT suspension through the channels; (c) CNTs are precisely trapped at desired locations. 54

Figure 22. (a) HR-TEM images of exfoliated SWNTs prepared by our new approach. Scale bar is 100 nm. (b) Photographs of (i) pristine SWNTs and (ii) exfoliated SWNTs dispersed in water and in (iii) acetone. Sample concentration is 1,000 ppm in all three cases and images were taken after 4 months of sedimentation. 55

Figure 23. UV-vis-NIR spectra of (a) pristine SWNTs and (b) exfoliated SWNTs in water. 57

Page

Figure 24. (a) A schematic of the two-probe measurement of the conductivity of the aligned CNT stripes; (b) Optical microscope image of a sample for two-probe conductivity measurement. The vertical lines are aligned CNT stripes. The top and bottom pads are gold electrodes. 59

Figure 25. I-V characteristic from a two-probe conductivity and current density measurement. 60

Figure 26. TEM image of the cross-section of the bundled MWNT in aligned-CNT stripes and a schematic of the bundle configuration. 60

Figure 27. ESA schematic illustration of grating-guided electrostatic self-assembly process for SWNTs alignment. (a) Polymer template patterned by nanoimprint; (b) Deposit PSS-wrapped SWNT by ESA from suspension; (c) Deposit PVA on top of PSS-wrapped SWNT by ESA; (d) Deposit the 2nd layer of PSS-wrapped SWNT; (e) Deposit the 2nd layer of PVA; (f) Remove polymer template by solvent; 65

Figure 28. An SEM micrograph of aligned-CNT stripes on a silicon substrate. 66

Figure 29. Polarized Raman spectra of SWNTs stripes prepared by grating guided ESA using polyeletrolyte as surfactants (PSS and PVA). θ denotes the angle between the polarization directions of the incident laser light and the longitudinal direction of the deposited CNT stripes. (a) Before the lift-off of polymer template; (b) After the the lift-off of polymer template. 68

Figure 30. Polarized Raman spectra of SWNTs stripes prepared by grating guided ESA using small molecules as surfactants (SDS and piperidine). θ denotes the angle between the polarization directions of the incident laser light and the longitudinal direction of the deposited CNT stripes. (a) Before the lift-off of polymer template; (b) After the lift-off of polymer template. 69

Figure 31. Surfactants used in the grating guided ESA process. 71

Figure 32. I-V characteristic from a two-probe conductivity and current density measurement on 20-ESA-bilayer aligned-CNT stripes. 73

Figure 33. The schematic of the directed self-assembly process enhanced by externally imposed electric field. 79

Page

Figure 34. Working chart for nanomanufacturing of SWNTs nanostructures. 85

Figure 35. The comparison of nanoparticle assembly process in term of the ability to achieve both high-level adsorption and high contrast pattern. 86

Figure 36. Directed self-assembly of SWNTs. (a) FDTS coated surface; (b) APTES coated surface; (c) Strong electric field on APTES coated surface with PMMA template; (d) Strong electric field with ultrasonic agitation on APTES coated surface with PMMA template; (e) Same as (d) but in Teflon-AF template; (f) SWNTs strips after removal of Teflon-AF template for case (e). In all the cases, the distance between two electrodes is 1 cm. Deposition time is 3 minutes for (a) (b) (c) (d) and 1 minute for (e) (f). Deposition voltage is 20V for (a) (b), 100 V for (c) (d) and 10 V for (e) (f). 87

Figure 37. Polarized Raman spectra of SWNTs stripes prepared by high speed directed self-assembly. θ denotes the angle between the polarization directions of the incident laser light and the longitudinal direction of the deposited CNT stripes. 88

Figure 38. I-V characteristic of aligned SWNTs stripes. 89

Figure 39. Comparison of SWNTs before and after purification. (a) SWNTs aggregation of unpurified SWNTs. (b) Directed self-assembled SWNTs using unpurified SWNTs suspension. (c) SWNTs aggregation of purified SWNTs. (d) Directed self-assembled SWNTs using purified SWNTs suspension. 92

Figure 40. Electrophoretic deposition of SWNTs with different electric voltage. (a) 5 volts (b) 100 volts. 96

Figure 41. Strong ultrasonic agitation cause the polymer pattern destructed. 98

Figure 42. A schematic of CNT electrical measurement with large and narrow electrode gaps. In large gap measurements, the inter-tube transport dominates, while the intrinsic CNT properties dominate the electrical properties of the aligned-CNT stripes in narrow gap measurements. 101

Figure 43. A schematic of aligned-CNT stripes deposited from channels with different cross-sectional dimensions. Nanochannels lead to better alignment and hence better electrical properties of the stripes. 102

Page

Figure 44. A schematic of arbitrary CNT alignment and placement by high speed directed self-assembly. Left: Polymer microstructures (individual lines of various sizes, 1D line array, 2D grid and circular array) patterned by nanoimprint or electron-beam lithography for high speed directed self-assembly of aligned-CNT stripes; Right: aligned-CNT stripes after removal of the polymer template. 103

Figure 45. Schematics of the fabrication process of field-effect transistors based on pure semiconducting aligned-CNT fibers. (a) spin-coat photoresist on a substrate; (b) photolithography to define gate electrodes and alignment marks; (c) gold evaporation and lift-off to form gate electrodes; (d) sputtering or CVD oxide layer as gate dielectric; (e) PMMA template patterning and deposition of aligned-CNT stripes using high speed self-assembly process. (f) photolithography to open window for selective removal of CNTs; (g) oxygen plasma etching to cut the aligned-CNT fibers into segments; (h) discontinuous CNT segments after removing photoresist; (i) photolithography to define source and drain electrodes; (j) palladium evaporation and lift-off to form source and drain electrodes. 105

CHAPTER I

INTRODUCTION

1.1 Nanotechnology and nanomanufacturing

Nanotechnology involves the development of materials and devices in the nanoscale, usually 100nm or smaller. It is widely considered as a scientific and technological area which has huge potential to bring benefits in wide range of applications, from traditional semiconductor to upcoming biomedicine, from novel materials to renewable energy.

Due to the extremely small physical size, nanotechnology relies on very dedicated equipment and process in the fabrication of materials and devices with fundamentally new properties. Generally, nanomanufacturing can be realized by two approaches: bottom-up and top-down approach. With the bottom-up approach, small building blocks, such as atoms, molecules and nanoparticles, are assembled in a controlled or guided way to form large structures. In a top-down approach, lithography or micro-machine is used to modify large materials into engineered structures.

Robust manufacturing processes for the nanoscale devices and structures are very important and challenging for scientists and engineers to carry out research and production in many areas, such nanoelectronics, biomedicine, energy conversion and storage and novel functional materials. The fundamental understanding of the

---

This dissertation follows the style of *Nanotechnology*.

nanomanufacturing process mechanism is critical to optimize material properties and improve device performance. The advancement in the combination of top-down and bottom-up approaches will continuously contribute to the nanoscience and nanotechnology.

1.2 Current status and trend of lithography

Lithography is the key technology in the nanomanufacturing which has huge impacts on the semiconductor manufacturing industry, as well as other industrial sectors, such as MEMS, displays and so on. While optical lithography still dominates the semiconductor manufacturing, there is growing demand for other lithography technologies which will make chips manufactured with high efficiency, low cost and smaller resolution [1].

Currently optical lithography is still the dominating technology for nanopatterning in the volume production of semiconductor devices. In the optical lithography, the resolution of optical lithography is defined by

$$R = k\lambda/NA$$

where R is the minimum feature size. It is clear that R is proportional to the optical wavelength λ, and inversely proportional to the numerical aperture NA of the projection optics. The constant k is related to the process condition which is always larger than 0.25. Tremendous efforts have been spent to improve the resolution by dealing with these factors. These efforts result in derivatives of the optical lithography including the immersion lithography, double patterning lithography and EUV lithography.

Over the years, optical wavelength used in photolithography has been reduced from several hundred nanometers to the 193 nm of ArF excimer laser wavelength. Current effort focuses on the development of optical lithography system using light in extreme-ultraviolet (EUV) range with wavelength from 11 nm to 14 nm. The challenging problems associated with EUV lithography exist in the masks preparation, defects inspection, EUV sources and resists.

Higher *NA* is expected to obtain high resolution in the optical lithography. *NA* is limited to 1.0 in the air. In immersion lithography, high refractive index liquid is introduced between the final projection lens and the wafer surface, therefore the *NA* has been improved to larger than 1.3. Continuous effort aims to search for high index liquids and resists suitable for immersion lithography with greater *NA*.

In addition to using shorter optical wavelength and greater *NA*, innovation of the photolithography process has been made *k* factor smaller, resulting in improved resolution. One of the approaches is called double patterning lithography (DPL) [2]. The DPL involves the patterning of the features from masks to the wafer twice, resulting in reduced pitch size. Depending on how and when the double patterning occurs, there are several derivative forms of DPL. For example, in the double exposure double etch process, the pattern of photomask is firstly transferred to the wafer by exposure, development and etching. After removing the first layer photoresist, a second photoresist is coated and undergoes another exposure with appropriate alignment. After the second etch, the additional features are transferred on to the wafer underneath. This allowed double feature density on the wafer. DPL

requires additional processing steps, materials and efforts for alignment, resulting in increased process cost.

In addition to the optical lithography, several other lithography technologies exist in the International Technology Roadmap for Semiconductors (ITRS) 2009 Edition, including maskless lithography and imprint lithography.

Maskless Lithography is one of the candidates for high speed and multibeam electron beam writing technology. For very long time, electron beam lithography (EBL) has been used to prepare photomask for optical lithography, due to its ability to pattern structures at 10 nm and below. The low throughput has limited EBL from volume production in the semiconductor industry. Current trend is to use multiple electron beams, say thousands of beams, writing patterns in parallel to achieve resolution better than 20 nm at a reasonable throughput such as 10 wafers per hour. The challenge with maskless multibeam EBL is that each beam require huge data rate as high as 10 Gb/s, which sets too high requirement for the data transfer and storage. The progress of the maskless lithography has encouraged people to believe its promise for mass production in electronic industry, however there is still a long way before the production tools appear.

In the last two decades, nanoimprint lithography (NIL) demonstrated as an alternative lithography technology with high throughput, sub-10 nm resolution and low cost. Nanoimprint lithography is a process where nanometer scale pattern is formed by mechanical deformation of imprint resist by using a template. In the nanoimprint lithography, the pattern of the imprint template is copied to the resist and

transferred to the substrate. Since the nanoimprint process relies on the mechanical deformation of resist for pattern generation, the complicated and expensive exposure sources, projection lens are no longer necessary, significantly reducing the system cost. The resolution is only limited by the feature size of the template. Concerns with nanoimprint lithography include the throughput, defects and alignment.

Nanoimprint lithography is of special interest by many scientist and engineers because of its unique capability in the nanoscale patterning and low cost. There are emerging nanoimprint lithography tools companies offering commercial equipments for advanced nanopatterning. Molecular Imprint, an Austin-based company is the leading company to provide dedicated UV-nanoimprint lithography with their patented step-and-flash imprint lithography (SFIL) technology. Obducat, a Swedish company and the Princeton-based Nanonex are other major commercial nanoimprint tools manufactures.

Although the nanoimprint lithography is viewed as the candidate lithography technology for semiconductor industry, the applications are much beyond the semiconductor patterning. As a matter of fact, nanoimprint lithography has found many application areas, such as patterned media for data storage industry, forming ordered structures for optoelectronics, bio-MEMS and biomedicine. Due to its low cost and easy use, the nanoimprint lithography is playing more and more roles in both research and manufacturing environment.

1.3 Progress in the directed self-assembly

Bottom-up approaches of nanomanufacturing are receiving increasing attention in the academia and industry. Different from the top-down approach, bottom-up approaches build up functional nanostructures by assembling basic building blocks, such as atoms, molecules and nanoparticles. This is often accomplished by the self-assembly process, where larger and ordered structures are produced from independent building blocks in a naturally coordinated manner.

The most attractive accomplishments in the bottom-up approach include the directed assembly of diblock copolymers [3]. The complex nanoscale patterns can be generated by the top-down template-guided self-assembly of block-copolymer thin film. These new findings are particularly attractive to the patterned media technology for data storage industry. Since it is extremely difficult to form arbitrary pattern using self-assembly of block copolymers, the future of the technology in semiconductor industry is not clear.

Another attractive research area is the directed self-assembly of nanoparticles from suspensions. The nanostructure such as colloidal metal nanocrystals and semiconductor quantum dots, nanorods, nanotubes and nanoplatelets can be synthesized with controlled size and exhibit distinct properties different from traditional bulk materials. They are potentially very useful in electronics, magnetic devices and photonics. However, these applications will heavily rely on the approaches that can position and assembly these units in a controlled and efficient process. The bottom-up approaches are frequently combined with the top-down

approaches to position the nanoparticles. The speed of the process can be very slow and the assembly quality is limited. We have limited ability to control the process behaviors. There are still a lot of challenges in these research areas. One of which is the effective approach for rapid and high quality placement and alignment of one dimensional nanopaticles, for instance single-walled carbon nanotubes (SWNTs).

1.4 Organization of the dissertation

To contribute to the development of robust nanomanufacturing technology, the thesis work aims to address the most challenging problems in the nanomanufacturing.

One of the major research topics in the thesis work is to development of the approach to fabricate three-dimensional multilayer structures in the micron- and nano-scale and integrate these structures into more functional devices and systems. The study results in the optimized nanoimprint and transfer-bonding techniques to fabricate three dimensional polymeric structures in micro- and nanoscale using both thermoplastic and cross-linked polymers. The successful development of advanced nanoimprint lithography technologies allows the integration of the microfluidic system and the photonic detection system in a single chip so that an ultra-compact and cost-effective lab-on-a-chip detection system is realizable. Design and fabrication considerations have been discussed to exemplify the use of developed nanoimprint lithography to integrate three-dimensional multilayered structures for devices and systems with more functions.

Another major contribution of the dissertation is to demonstrate for the first time the high speed and accurate placement and alignment of SWNTS on a wafer level

with controlled density. The insufficient ability to manipulate SWNTs in the nanoscale has limited their applications in the large volume manufacturing of nanoelectronic devices. A fundamental and challenging problem is the efficient placement and alignment of SWNTs on a flat substrate on the wafer level. By introducing the electric field enhanced electrostatic self-assembly, as well as combining the surface chemical modification and mechanical agitation in the solution process, we present an accelerated self-assembly process, which yields high speed and high quality nanomanufacturing of patterned and aligned SWNTs stripes. The high selectivity and robustness of the process have opened up a door to the large scale and high volume production of SWNTs based structures and materials for many applications, such as nanoelectronics and sensors.

CHAPTER II

CURRENT DEVELOPMENT OF NIL

2.1 Introduction

Nanoimprint lithography (NIL) technology as an emerging lithography technique attracted a lot of research effort since Stephen Chou published the first paper in 1995 [4]. In conventional NIL, a pattern is physically imprinted into thermal plastic polymer film by a hard mold at elevated temperature and pressure. Many modifications and improvements have been made such that nanoimprint has become widely used in many research and industrial areas.

Thermal nanoimprint and UV nanoimprint are the most popular imprint processes currently. Figure 1 illustrates the process procedures for both thermal and UV imprint. In the thermal nanoimprint, a thin polymer film is formed by spin-coating. A pre-fabricated mold is applied onto the film with heat and pressure. After cooling down, the template and the substrate are separated and the pattern is replicated on the substrate. There are varieties of materials ready for thermal nanoimprint, including functional materials, making thermal nanoimprint suitable for organic electronics and functional applications. The disadvantage of thermal nanoimprint is the long time needed for the process to raise the temperature and cool down the system, limiting the process throughput. In UV nanoimprint, UV light is utilized to solidify the replicated structure made by pressed template. The resists are low viscosity monomers and cross-linking is triggered by UV light. UV nanoimprint process usually occurs at the room temperature, significantly reducing the time required by the process.

There are lots of advantages of nanoimprint lithography. It is simple and cheap while maintaining high resolution and throughput. Nanoimprint is inherently a three dimensional patterning process. A lot of materials can be used as patterned media. It is compatible to direct patterning of functional polymers. These advantages have made nanoimprint a valuable tool for many novel applications, including nanoelectronics, nanomaterials and microfluidic applications.

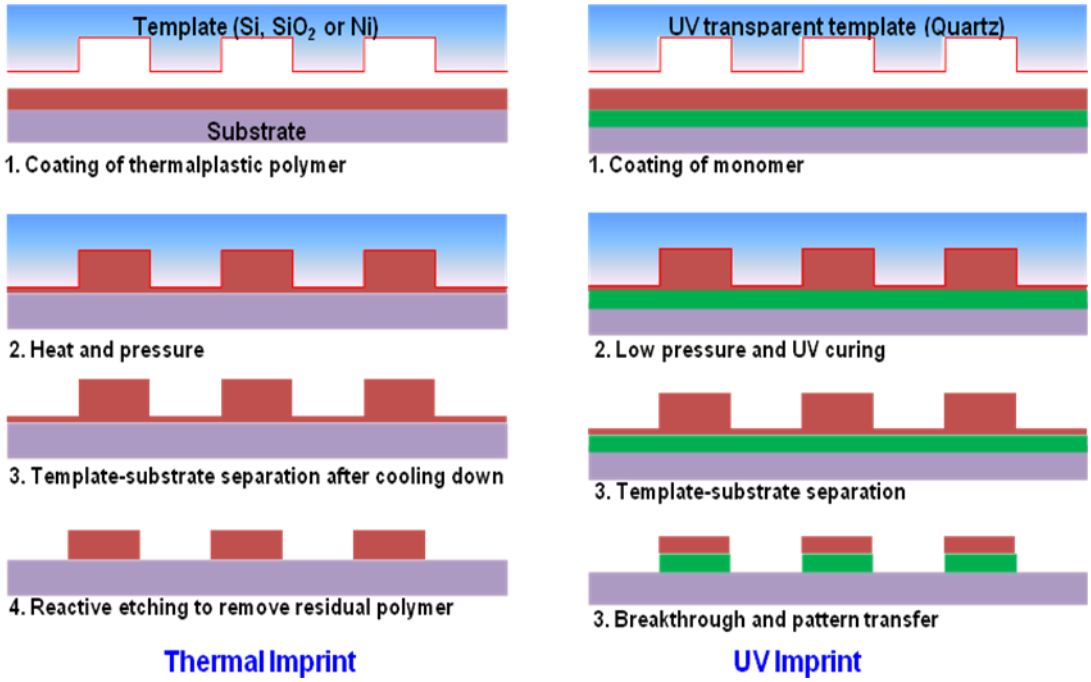

Figure 1. Schematics of nanoimprint process.

2.1.1 Template

Template preparation directly determines the feature size and quality of the nanoimprint process due to the fact of mechanical replication of the template pattern

during nanoimprint process. The nanoimprint template is usually prepared by other lithography technologies, for example EBL or FIB for high resolution template and photolithography for low resolution template. Other patterning technology such as interference lithography, AFM, X-ray lithography and directed self-assembly process can also be utilized to prepare nanoimprint template.

The application and process conditions determine what kind of material is suitable for template preparation. Thermal expansion coefficient and transparency are among the factors we need to think when choosing the material. The cheap silicon and silicon dioxide are most widely used material for thermal nanoimprint, due to its thermal expansion match with silicon substrates and its capability of being processed by a variety of dry etching process. Other materials include nickel, diamond and silicon carbide. UV transparency is a must in UV nanoimprint, where quartz is a good choice. For fast prototype where resolution and durability requirement is low, polymer on silicon can also work as templates. Example materials include SU-8, Teflon and polyimide.

2.1.2 Anti-sticking coating

One of the critical steps in the nanoimprint process is the separation of template from the patterned structure after the resist solidified. Anti-sticking treatment will ensure the fidelity of the patterned structure on the substrate by reducing the interaction forces between template and resist. This is mostly done by growing a self-assembled monolayer (SAM) on the template surface to significantly reduce the

surface energy and adhesion to resist. Table 1 listed the frequently used chemical precursors for surface SAM coating and the contact angles for various liquids [5].

An alternative approach is to add anti-sticking molecules in the imprint materials, such as Zonyl series products from DuPont. For example, Zonyl UR is an anionic phosphate fluorosurfactant which can be an effective additive to organic polymers for easy mold release for wide range of polymers. The existence of Zonyl UR also gives low liquid surface tensions for good wettability, which is good to prepare high quality thin films by spin-coating. The Zonyl additive will migrate to the surface of the polymers during the nanoimprint process and reduce the adhesion between polymer resist and template.

In a third approach, non-sticking materials are used to prepare the template. Teflon AF, such as AF-1600 and AF-2400, is a family of amorphous copolymers that retain the properties of fluorinated plastic and dissolve in some perfluorinated solvents such as FC-75. Nanoimprint template made by these materials intrinsically has low surface energy and low adhesion to resist.

Table 1. Contact angle versus surface SAM coating [5].

	FDTS	OTS	UTS	PETS	APTES	PEG 6/9	SiO_2
Water	109.6	98.2	95.0	88.0	58.0	36.0	10.0
N-Methylpyrolidone	80.5	55.0	44.6	14.7	17.8	10.0	10.0
1,2-Dichlorobenzene	80.5	42.7	30.4	9.4	13.2	5.6	10.0
Methanol	74.5	24.8	23.3	6.2	6.4	4.8	5.3
Chloroform	68.8	30.0	22.9	7.3	7.3	7.6	10.0
Toluene	62.7	10.0	10.0	10.0	10.0	10.0	10.0
Ethylacetate	58.2	31.5	10.0	10.0	10.0	10.0	10.0
n-Heptane	52.9	20.5	16.6	10.4	10.0	10.0	10.5
Isopropanol	50.5	9.5	10.0	10.0	10.0	10.0	10.0
Acetone	45.2	10.0	4.9	10.0	10.0	6.4	10.0
Fluorinert	21.6	10.0	4.4	10.0	10.0	4.4	10.0

2.1.3 Resist material

There are a variety of materials suitable for nanoimprint lithography, among which polymer is the most widely used [6]. In a traditional lithography, polymer or resist act as the pattern transfer layer in the etching process and material deposition processes. Nanoimprint allows direct patterning of functional materials by mechanical deformation of materials without hurting the polymer functionality, making it suitable for many electronic, optical and biological applications.

In the thermal nanoimprint, thermoplastic polymer such as Poly(methyl methacrylate) (PMMA) is used widely. Important factors in choosing a material for nanoimprint include the film uniformity, adhesion to the substrate, thermal stability, etching resistance and specific functionality for certain applications.

There are even more properties desired for the resist materials in the UV nanoimprint. The resists are expected to be a low-viscosity liquid at the room temperature for uniform and fast pattern filling. The material should be photosensitive and cured quickly to achieve high throughput. After curing of the material, it should adhere well with the substrate. It should be mechanically strong enough to avoid structural collapse. Etching selectivity and thermal resistance must be ensured for high fidelity patterning transfer by using reactive-ion etching process.

2.1.4 Parameters during thermal imprint process

The control of process conditions is critical to achieve high yield and high throughput nanopatterning in NIL. Imprinting temperature is the first parameter we have to consider for nanoimprint. It is mainly determined based on the thermal property of the resist material. At different temperature, the polymer exhibits different mechanical properties. At low temperature, the polymer is stiff. At sufficiently high temperature, the modulus of the elastic polymer decreases rapidly and we call this temperature as the glass transition temperature (T_g). Increasing temperature makes the polymer behavior like a viscoelastic liquid. The imprint temperature has to be higher than the glass transition temperature to achieve good patterning replication. High temperature gives a low viscosity and the polymer will flow quickly to fill the

template. Thermal expansion mismatch is another consideration during the heating process. When the template and the substrate are made of the same material, this is usually not a problem. However, low temperature is desired when different materials are used for template and substrate.

Sufficient and uniform pressure is also required for imprint process. The pressure should be large enough to ensure the polymer to fill the template. High density, large pattern or low viscosity of the polymer requires higher pressure. To ensure uniformity of the pressure, air pressure is employed to achieve conformal contact for imprint [7].

Holding time during nanoimprint also needs to be long enough to ensure full filling of polymer into the template. After nanoimprinting, the system should be cooled down to at least below the glass transition temperature before the separation of template and substrate.

2.1.5 Applications

Nanoimprint has demonstrated many useful applications in traditional electronics, as well in the data storage, bio-MEMS, optics and nanoelectronics. Through the years of research efforts by scientists and engineers, nanoimprint has found the active role for volume production of nanoscale structures for the patterned magnetic media in the data storage industry and nanoscale optical structure in the optical industry.

2.2 Current progress of NIL research at TAMU

The NIL research at TAMU is mainly conducted by Dr. Xing Cheng in the laboratory of Micro and Nano-scale Devices and Systems. The main research focuses on the fundamental issues in nanoimprint, such as surfactant coating, polymer flow and alignment during imprint progress, as well as the generic advanced lithography for three-dimensional (3D) structure fabrication and transfer bonding. Of these topics, the optimization of nanoimprint and the transfer-bonding technique for 3D polymer microstructures are extremely useful for 3D system integration.

Three-dimensional multilayer polymer microstructures may find many useful applications in electronics, photonics and bioengineering, due to their light weight, low cost, easy processing and multiple functionalities [8]. For instance, construction of multilayer microfludic channels allows the integration of more components into a lab-on-a-chip system with increased functionalities. 3D polymer structures in the micro scale may act as 3D photonics crystals. 3D polymer can also build 3D metallic structure by sacrificing itself after electroplating process [9-10].

Multilayer polymer structure in the micro- and nanoscale is built using layer-by-layer stacking techniques [11]. There is a report that polymers with progressively lower glass transition temperature are used to add new layer onto the bottom layer of the structures while preserving the bottom layer structures [12]. Apparently there are only limited number of polymers that can be used for this technique and this is not good for those applications where specific polymers are desired. In another multilayer building technique, thermoset polymer, such as UV-curable materials, are used [13-

14]. UV-cured polymer has very strong mechanical and thermal resistance, therefore adds new patterned layers on the top will not damage the existing bottom structures. The disadvantage of this technique is that the UV-cured material is extremely difficult to remove, which is not good for certain application where permanent structure is not desired. To overcome such limitation, a temperature gradient is used to directly bond multilayer structures [15]. The precise control of the temperature is very difficult and such process is not desired for good robustness.

The lack of reliable techniques to build 3D multilayer polymer structures in the micro- and nano-scale has limited its applications. We have developed an optimized nanoimprint and transfer-bonding process to build 3D polymer structures with decently high yield, with expectation of extending multilayer structure to wider range of applications.

We have adopted silicon/silicon dioxide template and PMMA with molecular weight of 15,000 (T_g=105 °C) as the material system in the development. Two templates are used in the nanoimprint process. One has a grating pattern with 700 nm period and 350nm depth, and the other has a grating pattern with 10μm period and 1 μm depth. Both of them have a 50% duty cycle and are coated with 1H,1H,2H,2H-perfluorodecyltrichlorosilane (FDTS).

As illustrated in Figure 2, cyclic combinations of nanoimprint and transfer-bonding are conducted to create the 3D multilayer structure layer by layer. In the first step, PMMA is spin-coated on a substrate followed by the standard nanoimprinting process. In the second step, PMMA is spin-coated on a substrate whose surface is

already coated with octadodecyltrichlorosilane (OTS) SAM for reduced surface energy and adhesion to the polymer. A template is patterned into the polymer and separation is accomplished by twisting the template and substrate, so that the patterned polymer structure sticks with the template. The patterned PMMA layer with the template is then transfer-bonded to the first PMMA structure in the third step. Repeating step 2 and step 3 will yield more layers added to the top for successful construction of 3D multilayered polymer structure.

The critical part of the process is the step 3, where a polymer structure is transfer-bonded to the existing bottom structure. The successful layer transfer relies on good adhesion between the structure to be transferred and the bottom structure. We accomplish this step by two different approaches. In the first approach, a temperature slightly lower than the glass transition temperature T_g is used. Base on the fact that, the polymer T_g in the surface region is usually 5−10 °C lower than that of the bulk polymer, this temperature will give enough adhesion between two polymer layers while at the same time not severely deform the existing structure, as shown in Figure 3. In the second approach, a thin adhesive layer made with SU-8 is used to ensure good bonding of the two polymer structures, as shown in Figure 4. Since the SU-8 has much lower glass transition temperature (64 ℃), bonding at a temperature a little bit above this temperature will ensure good adhesion and structure preservation.

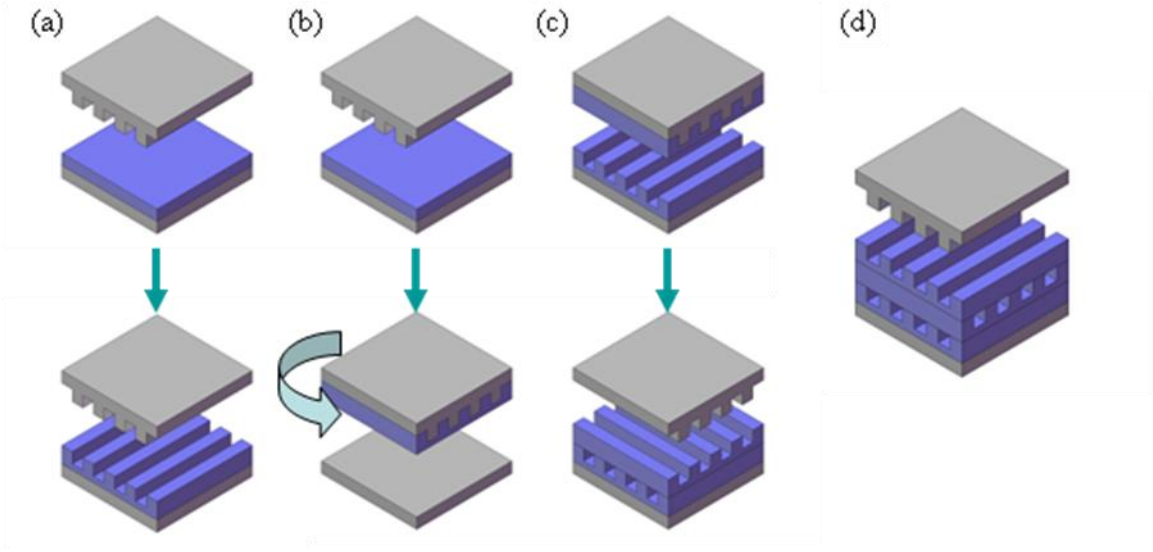

Figure 2. Schematic of the patterning process for 3D multilayer polymer structures. a) Step 1: standard nanoimprint lithography; b) Step 2: layer transfer from the OTS coated substrate to the mold using twist-demolding; c) Step 3: transfer-bonding; d) Step 4: adding more polymer layers by repeating step 2 and step 3.

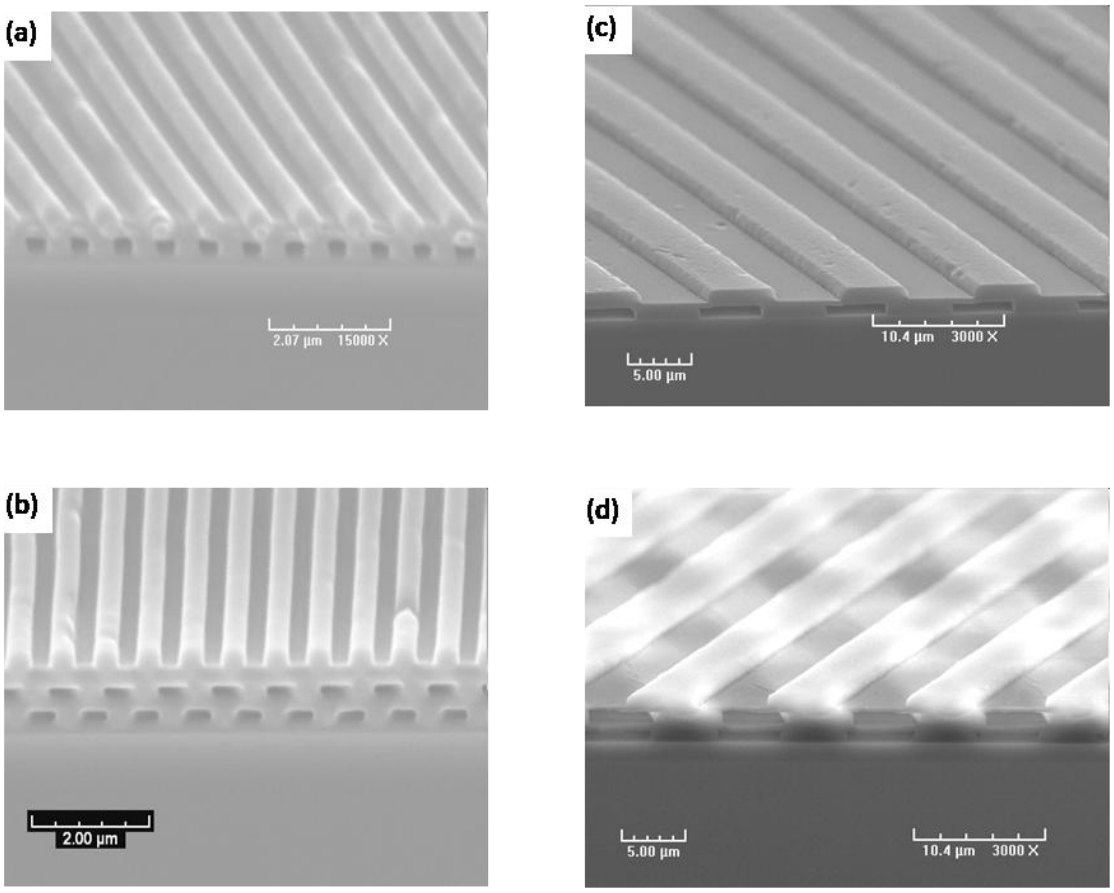

Figure 3. SEM micrographs of 3D multilayer PMMA structures using direct thermal bonding. (a) Two-layered 700 nm period grating; (b) Three-layered 700 nm period grating; (c) Two-layered 10 µm period grating; (d) Three-layered 10 µm period.

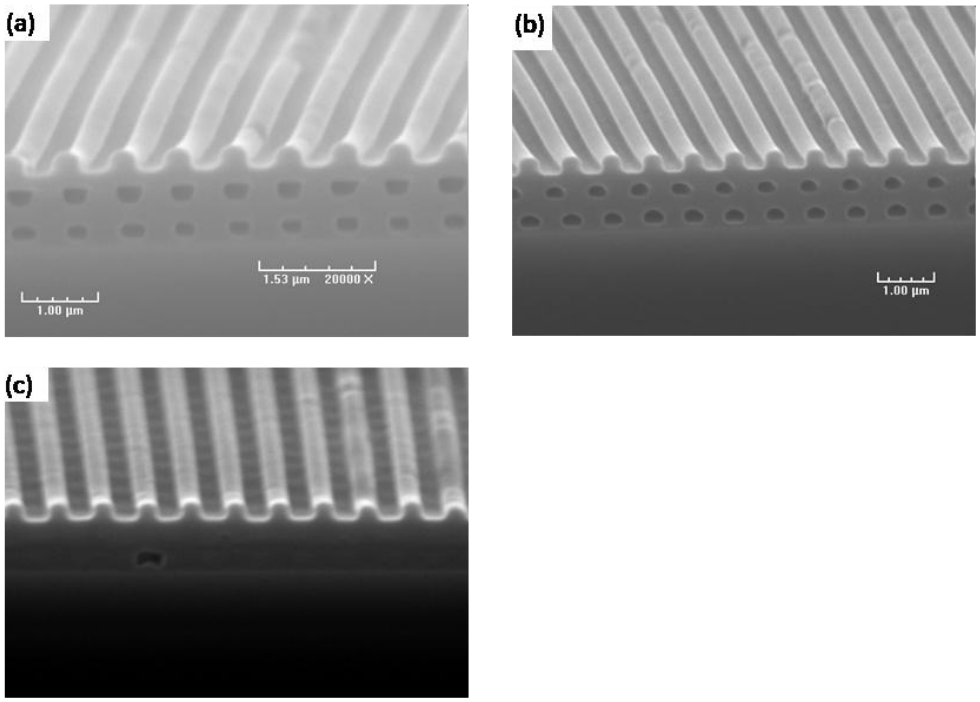

Figure 4. SEM micrographs of 3D multilayer PMMA structures using SU-8. (a) Three-layered 700 nm pitch grating bonded with 1% of SU-8; (b) Three-layered 700 nm pitch grating bonded with 6% of SU-8; (c) Three-layered 700 nm pitch grating bonded with 10% of SU-8. Progressively more bottom layer structures filling is observed from (a) to (c).

The successful development of fabrication technique for 3D multilayer polymer structure is meaningful. The direct bonding technique is suitable for all thermoplastic materials and this generic approach allows many structures stacked layer by layer with different materials and patterns used in each layer. The great flexibility in the design and fabrication opened a pathway to integrate more components into a compact monolithic system. For example, current development of

nanoimprint lithography will allow the integration of the microfluidic system and the photonic detection system in a single chip so that an ultra-compact and cost-effective lab-on-a-chip detection system is realizable.

2.3 Summary

The current state-of-the-art NIL flexibly provides nanofabrication technique with the capabilities of transfer bonding for 3D structures, patterning many different materials, and achieving ultimate resolution and low cost. All these characteristics make it a good candidate for various applications, including optics, microfluidics and electronics. NIL is particularly good for integrated structures and devices on a single chip. Combined with other techniques, such as directed self-assembly, electrophoresis and layer-by-layer assembly techniques, NIL is suitable for many nanomaterial and nanodevice applications.

Current nanoimprint technology allows us to explore many novel and practical applications. Using the optimized imprint lithography, multilayer structures can be readily constructed so that a monolithic detection system based on soft materials is not far away for practical use.

CHAPTER III

AN APPROACH TOWARDS MONOLITHIC FLUORESCENCE DETECTION IN MICROFLUIDIC DEVICES

3.1 Introduction

The ability to build 3D multilayer polymer structures in the micro- and nano-scale by using the optimized imprinting and transfer-bonding techniques is extremely useful to integrate multiple components into a single chip. We demonstrate the applicability of the developed scheme by designing and fabricating an exemplary optofluidic system, a fluorescence detection system.

Optofluidic system is a class of optical system synthesized with fluids [16]. Conventional optical systems are made with solid materials including glasses, metals and semiconductors, while sometimes fluids are desired in an optical system due to their advantages such as the ability to change the optical properties of the fluid medium within a device by simply replacing the fluid with another. In the biomedical applications, biological agents are often suspended in a liquid and fluorescence or Raman signals are desired for molecular detection and analysis. Although microfluidics can integrate multiple fluidic tasks on a chip, hybrid multi-chips and separate instruments, which are connected by optical fiber or capillary tubing, are used to accomplish the functions of the detection system. These off-chip components, such as light source sensors, lens filters and waveguides, are usually much bigger than the microfluidic devices, and thus prevent the realization of an ultra-compact lab-on-a-

chip system. For field deployment and point-of-care diagnosis, such ultra-compact and portable system with fully integrated detection system is often desired.

Fluorescence detection is an important method in bioanalysis due to its high sensitivity and selectivity. A full detection system usually consists of an excitation light source, focusing lenses, optical filters, and an optical detector. In this work, we present an approach to integrate monolithic fluorescence detection capability into an optofluidic system to fully implement the "lab-on-a-chip" concept.

3.2 Design methodology and fabrication process

The microfluidic device with monolithic fluorescence detection system is based on a vertically integrated multilayer structure as shown in Figure 5. From bottom to top, the multilayer structure has a following configuration: 1) an LED as light source; 2) a tunable optical filter; 3) a microfluidic channel for processing the fluids to be detected; 4) a tunable optical filter; and 5) a photodetector with optical antennas to improve the detection sensitivity. For broader excitation wavelengths, the light source used in this system is a top-emitting organic light emitting diodes based on semi-transparent cathode. The photodetector, which converts optical signal into electrical signal for easy and high-speed readout, is based on a photoconductor made of organic semiconductors. One or more tunable optical filters can be inserted into the multilayer structure to select excitation wavelengths for different fluorescent tags or prevent excitation light from reaching photodetector for higher sensitivity. The tunable optical filter is based on a novel microfluidic metal-dielectric-metal structure in which the transmission of the whole structure depends on the refractive index of the fluids in

the microfluidic channel. The vertical integration of light sources, tunable optical filters and photodetectors eliminates the need for optical interconnects, yielding an ultra-compact microfluidic lab-on-a-chip system with built-in fluorescence detection capability. The multilayer structure can be readily fabricated by a low-cost layer-by-layer addition technique that we discussed in the previous chapter.

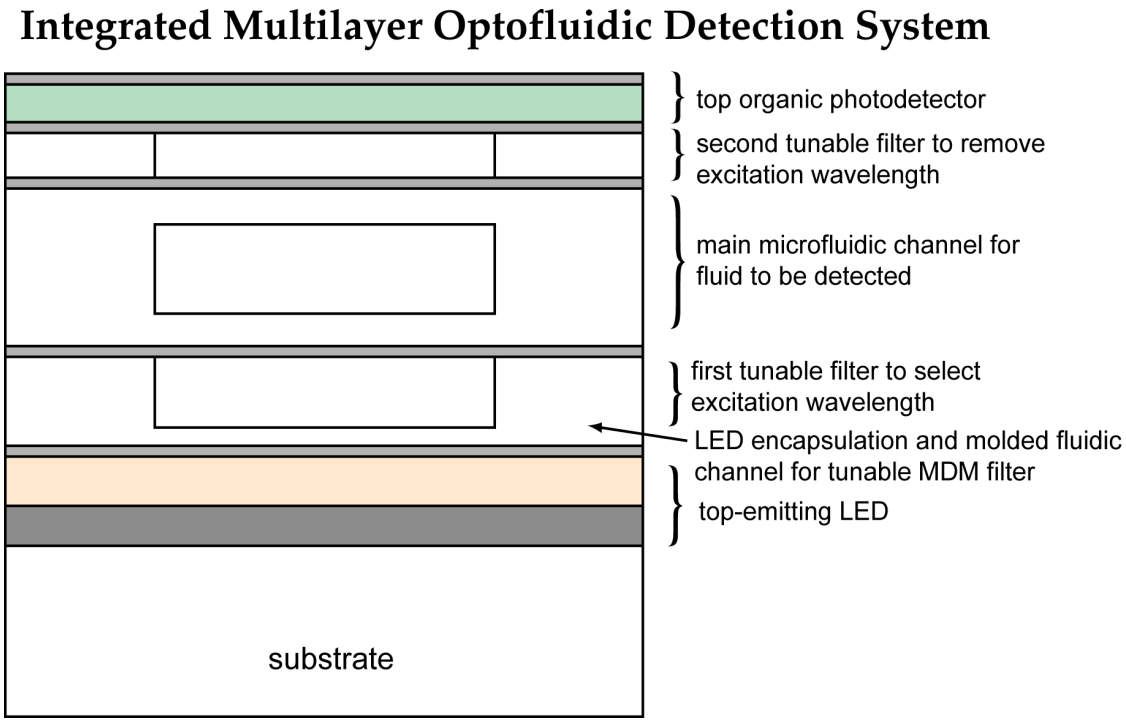

Figure 5. Integrated multilayer optofluidic detection system.

The major attractive advantages of optofluidics are the abilities of integration and reconfiguration. In the following part of this chapter, we will discuss the technical details for design and fabricating an optically tunable interference filter based on a metal-dielectric-metal (MDM) structure and fluidic reconfiguration. After that, I will

show how optical antennas can be used to improve the sensitivity of the infrared detection and integrated into an on-chip optofluidic system.

3.3 MDM structure as tunable filter for lab-on-a-chip application

Metal-dielectric-metal (MDM) structures is a Fabry-Perot resonator, which can give performance enhancement for optoelectronic devices such as light emitting diodes, photodetectors and optical filters. The microcavity theory can be used to explain the working principle of MDM structure as an optical filter. An electromagnetic stranding wave is formed at the resonance frequency, due to the reflection occurred at the dielectric/metal interface. The optical resonance inside the MDM structure also can results in an enhanced transmission by improve the coupling of the electromagnetic field on both sides of the filter [17].

Many applications, such as fluorescence detection, desire the tunability of the operating frequency for an optical filter. The thickness and the refractive index of the dielectric layer are the key parameters to determine the resonance frequency. Traditional frequency tunability can be realized by changing the dielectric layer thickness using complex micro-electro-mechanical actuators. Another approach for frequency tuning accomplished by changing the refractive index by applying an electric field to a piezoelectric polymer sandwiched between two metal layers [18]. We adopted a novel frequency tuning scheme based on changing the refractive index of the dielectric layer in an MDM structure by replacing the fluid in the channel of MDM structure. As illustrated by Figure 6, the proposed MDM structure comprises two metal films and a microfluidic channel sandwiched between them. The fluids can

be transported into and out of the middle section of the MDM structure through the fluidic channel to achieve refractive index change and resonance frequency tunability. Since refractive index of fluids can vary in a large rang, the optical filter devices can work with a wide range of resonant frequency.

3.3.1 Principles of the tunable optical filter

As shown in Figure 6, the MDM structure considered in the research consists of two metal layers, which are made of silver due to its high reflectivity and low optical absorption. Sandwiched between the metal layers is the dielectric layer, which could be organic polymers, air or liquids.

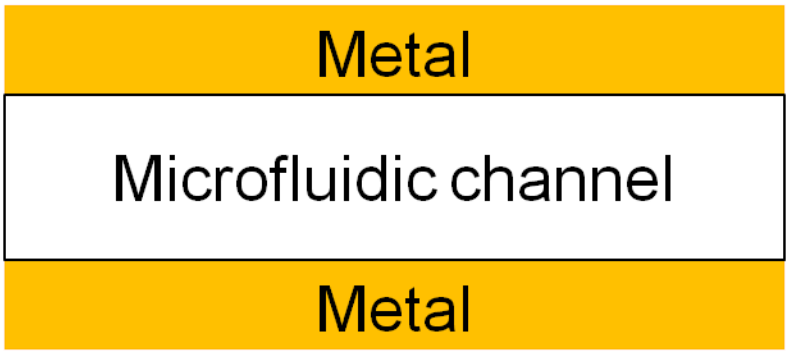

Figure 6. A schematic of the microfluidic MDM structure.

The cavity theory tell us that [19], the frequencies, at which the resonance and maximum transmission occur, are determined by,

$$\frac{1}{\lambda} = \frac{1}{2nd\cos\theta}\left(m + \frac{\varphi_a + \varphi_b}{2\pi}\right) \qquad m = 0, \pm 1, \pm 2, \ldots$$

where, λ is the optical wavelength in free space, d is the dielectric layer thickness, n is the refractive index, θ is the light incident angle, and φ_a and φ_b are the reflection phase shifts at the metal-dielectric interface.

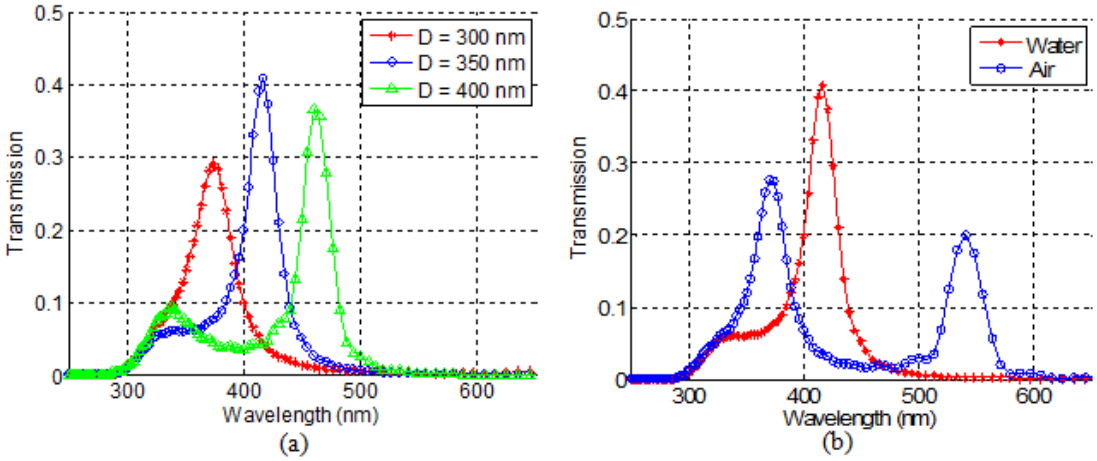

Figure 7. Calculated transmission spectra of MDM structures. (a) transmission spectra for different dielectric layer thickness; (b) transmission spectra of a microfluidic MDM structure with and without water.

Numerically, we calculated the transmission of this structure using the finite-difference-time-domain algorithm. In the simulation, semi-transparent silver layers (35 nm) are used as the top and bottom metal layers. The incident plane wave is perpendicular to the interface. Figure 7 (a) shows the optical transmission of MDM structures with the dielectric layer thickness (or the microfluidic channel height) equal to 300 nm, 350 nm, and 400 nm respectively, and the dielectric refractive index 1.33. The resonant frequencies are shifted when the dielectric layer thickness changes.

Conversely, the simulation result can be used to determine the optimal dielectric thickness (or microfluidic channel height) for a desired frequency. For example, to make an MDM structure resonate at a blue light range with a central wavelength of 460 nm, a 350 nm thick dielectric layer is desired. Under this configuration, the transmitted power can reach more than 40% of the total incident energy and the full-width-half-maximum bandwidth is about 19nm. The loss is due to the absorption of the metal layers. It should be noted that, there are resonances at multiple frequencies for a certain structure.

With nanoimprint lithography, fluidic channels can be fabricated in a polymer thin film. Since the air and the water have different refractive index, a tunable filter can be realized. Figure 7(b) illustrates that the MDM structure exhibit different resonance frequency when the microfluidic channel is filled with water or air, when the channel height is 350 nm. A resonance frequency shifts to the longer wavelength when the channels are filled with water, thus achieving tuning capability. Other liquid or liquids combination with different refractive indexes can also be transported to the microfluidic channel to achieve flexible resonant frequency tuning.

3.3.2 Fabrication

Fabrication of the MDM structure with microfluidic middle layer is a challenging task because the top metal layer cannot be deposited by simple evaporation. We adopt the transfer-bonding technique, which is discussed in the previous chapter to create the desired microfluidic MDM structure.

Experimentally, the microfluidic MDM structure is fabricated on a glass substrate using nanoimprint lithography and transfer-bonding technique, as shown in Figure 8. 5 nm thick chromium and 35 nm silver thin films are deposited onto the substrate by thermal evaporation and a thin layer of PMMA polymer is spincoated on top of the metal film. We can obtain the thickness of the PMMA layer by control the spin speed and the concentration of the PMMA solution. Microscale pattern will be created in the PMMA layer by regular nanoimprint process at 175ºC and with a pressure of 5 MPa (Figure 8(a)). On the other hand, metal layer to be transfer-bonded is prepared on a separate wafer. Self-assembled monolayer of OTS is firstly coated on the wafer to reduce the polymer-substrate adhesion. Then a thin layer of PMMA is spin-coated on the substrate followed by evaporation of 5nm nickel and 35nm silver (Figure 8(b)). Since the adhesion between the PMMA layer and the OTS surfactant coated wafer is small, the metal layer along with the thin PMMA layer is transfer-bonded onto the PMMA patterns on the first substrate by reversal nanoimprint (Figure 8(c)). The whole MDM structure is built by final removing the OTS coated wafer. The fabricated MDM structure can be characterized with transmission measurements to study the tunability of the resonant frequency, when liquids with different refractive indexes are transported into the microfluidic channel.

The microfludic MDM structure fabricated by using above approach is shown in the Figure 9, which provided the SEM images for both the side view and top view. The optical microscope image in the Figure 10 shows the tunability of the microfluidic MDM structure. The channel filled with water appears red color and channels without

water displayed as gray color. The color difference demonstrates the difference transmission peak of the fabricated structure.

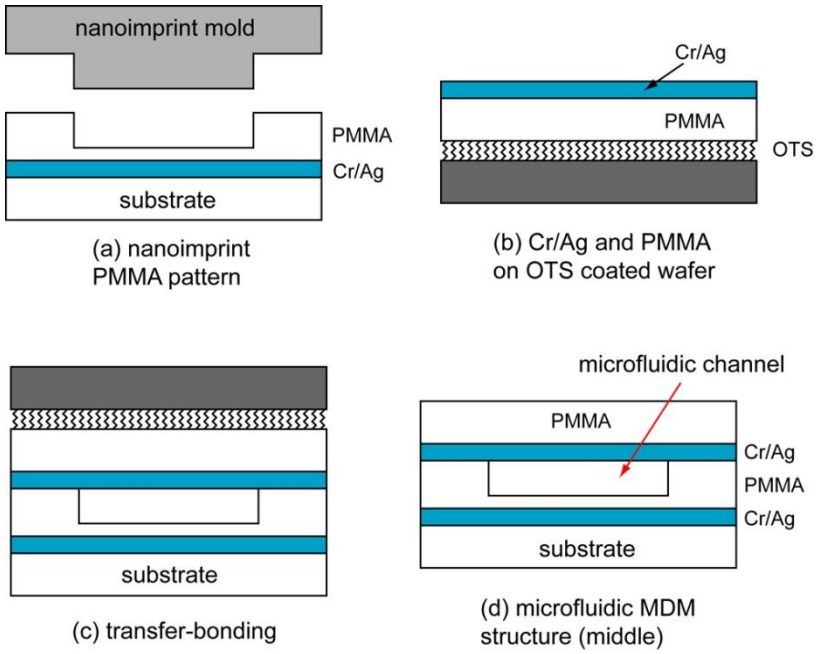

Figure 8. Schematics of the fabrication of the microfluidic MDM structure by nanoimprint and transfer-bonding.

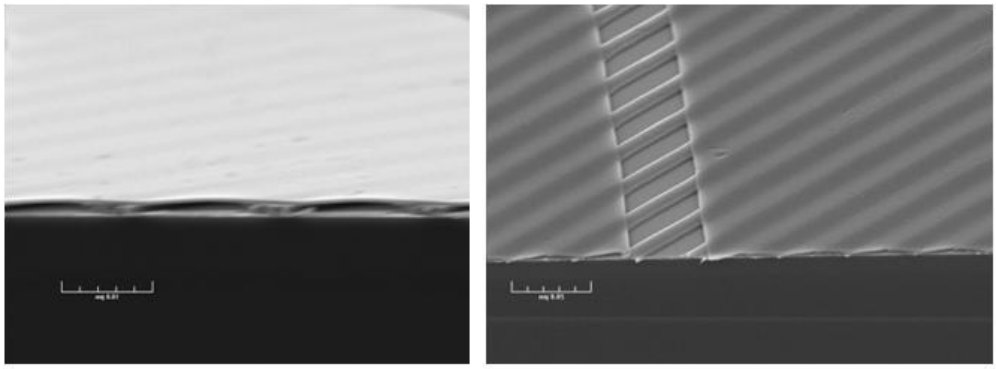

Figure 9. SEM images of the side view (left) and top view (right) of the microfludic MDM structure.

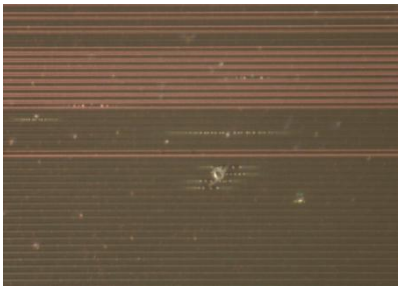

Figure 10. Optical microscope image for MDM structure

The fabrication scheme we developed allows more complex multilayer microfluidic systems to be built. For example, more components, such as layers containing organic light emitting devices and organic photoconductors can be integrated into the microfluidic system using similar fabrication techniques. By integrating the tunable optical filter to the system, flexible optical functionality can be achieved, such as the tuning of excitation wavelength to selectively excite certain biomolecules tagged with fluorescent dyes, or blocks certain wavelengths from

reaching the photodetector when detecting a specific molecule in a mixture. The successful integration of light sources, optical filters and optical detectors to a multilayer manner can yield a portable and ultra-compact lab-on-a-chip system, which is convenient for numerous point-of-care bioanalysis.

3.3.3 Summary

In summary, we designed and fabricated a novel optical filter by introducing microfluidic channels into a conventional MDM structure. Nanoimprint and transfer-bonding technique were used to address the challenging fabrication task. The frequency tunability of the optical filter is demonstrated by both numerical simulations based on a finite-difference-time-domain algorithm and experimental characterization. By using similar technique, the tunable microfluidic MDM structures can be integrated with organic light emitting devices and organic photoconductors to construct a monolithically integrated fluorescence detection system for lab-on-a-chip applications.

3.4 Optical antenna

In recent years, antennas that operate at optical frequency show huge potential in optoelectronic applications due to the strong enhancement of optical field in a confined geometry [20-22]. Optical antennas can bridge the gap between the radiated optical energy to the confined and intensity-enhanced optical energy in a local volume of a subwavelength scale. Till now, most research on optical antennas was focused on the applications in the visible light range. A disadvantage of the optical antennas

operating in visible light is their small geometries, which often require sub-50 nm lithography technique for their fabrication. One of the potential applications of the optical antennas is to enhance the sensitivity of optical detectors, particularly infrared photodetectors [23-25]. High performance semiconductor-based photodetectors such as HgCdTe photoconductors and quantum wells infrared photodetectors all require cryogenic cooling to operate [26]. Those infrared detectors are expensive and not trivial to scale down for portable infrared systems. Integrating optical antennas with infrared photodetector may present a practical approach to greatly enhance the signal-to-noise ratios of infrared detectors at room temperature and thus enable low-cost and uncooled photodetectors for infrared technology. The removal of cryogenic cooling allows compact infrared detectors to be integrated with portable systems for applications such as in-field detection of chemical and biological warfare agents.

In this work, dipole and bowtie aperture antennas that operate near mid-infrared wavelengths are explored. Theoretical simulations based on the finite-difference-time-domain (FDTD) algorithm [27] are performed to calculate the radiation enhancement factors for infrared wavelengths in designed antennas. The simulations results allow guidelines to be established for designing highly efficient optical antennas for infrared detections.

3.4.1 Simulation details

Although antenna theory in radio frequency has been well established, optical antennas have their own characteristics. The penetration of radiation into metals can no longer be neglected and the collective electron resonances (surface plasmons) must

be considered. Therefore metal has to be modeled by a more complicated theory. Rsoft FullWAVE is a commercial software based on FDTD algorithm and allows a full-wave three-dimensional modeling of complicated dispersive and nonlinear materials. In our simulation, the dielectric constants of gold at infrared wavelengths are fitted into the software from a Lorentz-Drude model [28]. The grid size used in simulation is about 1/200 λ to 1/500 λ to ensure the accuracy of the simulation results, where λ is the infrared wavelength. Perfectly matched layers are used in simulations. The incident waves are chosen to be pulsed plane waves with central frequency located at 2 μm, 8 μm and 10 μm. They consist of a Gaussian envelope function multiplied by a sinusoidal carrier.

Both dipole and bowtie aperture antennas are considered in our simulations. The infrared intensity enhancement factors at the centers of the antennas are calculated. The intensity enhancement factors are also calculated as a function of incident wavelengths to evaluate the operation bandwidth of the designed antennas. The effect of changing the gap length in dipole antenna on the intensity enhancement factor is probed. Finally, the out-of-plane distribution of infrared radiation in bowtie aperture antenna is mapped. This field distribution information will be important for multilayer integration of optical antennas with infrared photodetectors.

3.4.2 Results and discussion

A snapshot of the calculated infrared field distribution in a dipole antenna is shown in Figure 11 (a). The dipole antenna has an arm length of 2.5 μm, an arm width

of 300 nm, a gap length of 160 nm and a thickness of 50 nm. The field plot indicates strongly non-uniform field distribution across the dipole antenna. The optical field is concentrated at three locations: two ends of the antenna and the middle gap. The optical intensity distribution across the antenna length is plotted in Figure 11 (b). This log-scale plot indicates very strong intensity enhancement at the center of the gap region.

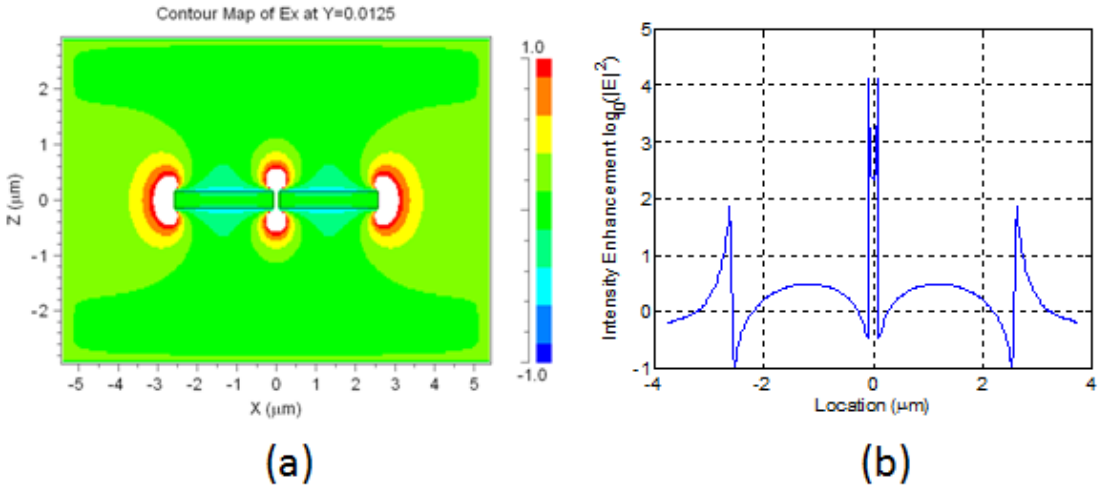

Figure 11. (a) A snapshot of optical field distribution in a dipole antenna; (b) A profile of the optical intensity enhancement factors across the dipole antenna.

For practical applications, it is often convenient to have an infrared antenna that can provide strong field enhancement over a broad range of infrared wavelengths. Figure 12 shows the intensity enhancement in the gap region of the dipole antennas as a function of incident wavelengths. In Figure 12(a), the corresponding dipole antenna has an arm length of 400 nm, an arm width of 100 nm, a gap length of 60 nm and a

thickness of 50 nm. The resonant wavelength is 2 μm and the peak intensity enhancement at this resonant wavelength is over 400 times. In Figure 12(b), the corresponding dipole antenna has an arm length of 2.5 μm, an arm width of 300 nm, a gap length of 160 nm and a thickness of 50nm. The maximum intensity enhancement is achieved at around 8 μm, the resonant wavelength, with an enhancement factor of more than 20,000. Moreover, the intensity enhancement factor is greater than 5,000 over a broad range from 7 μm to 14 μm, which indicates that the optical antenna can be used for broad-band operation. Similar results are obtained for bowtie aperture antennas as shown in Figure 13. The geometry of the bowtie aperture antenna is shown in the inset of Figure 13(a) and the thicknesses of the antennas are kept to be 100nm. For bowtie aperture antenna with a resonant wavelength of 2 μm (L1 = 500 nm, L2 = 100 nm, H = 250 nm), the intensity enhancement is up to 250 times. For the antenna with a resonant wavelength of 10 μm (L1 = 2.5 μm, L2 = 0.2 μm, H = 1.25 μm), the peak intensity enhancement factor is nearly 24,000.

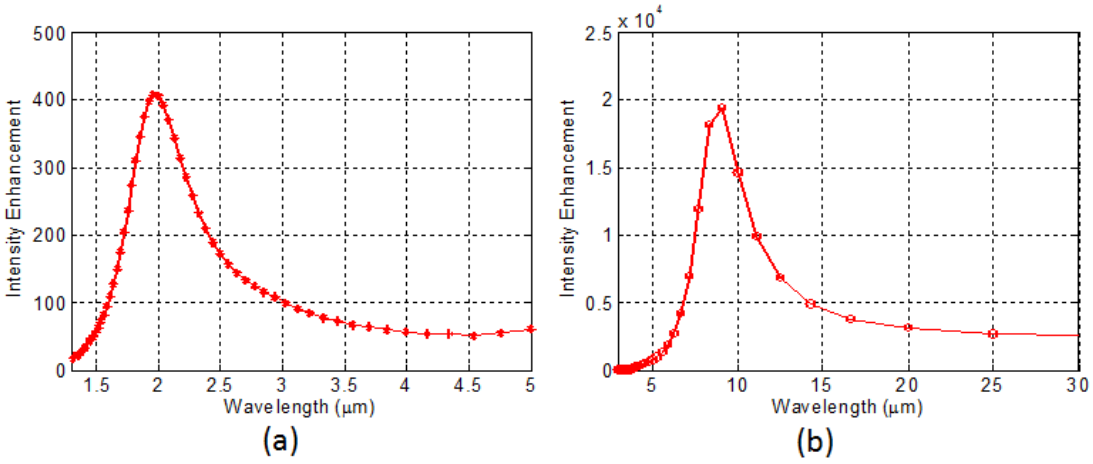

Figure 12. Optical intensity enhancement in the gap region as a function of incident wavelengths. (a) dipole antenna with a resonant wavelength of 2 μm; (b) dipole antenna with a resonant wavelength of 8 μm.

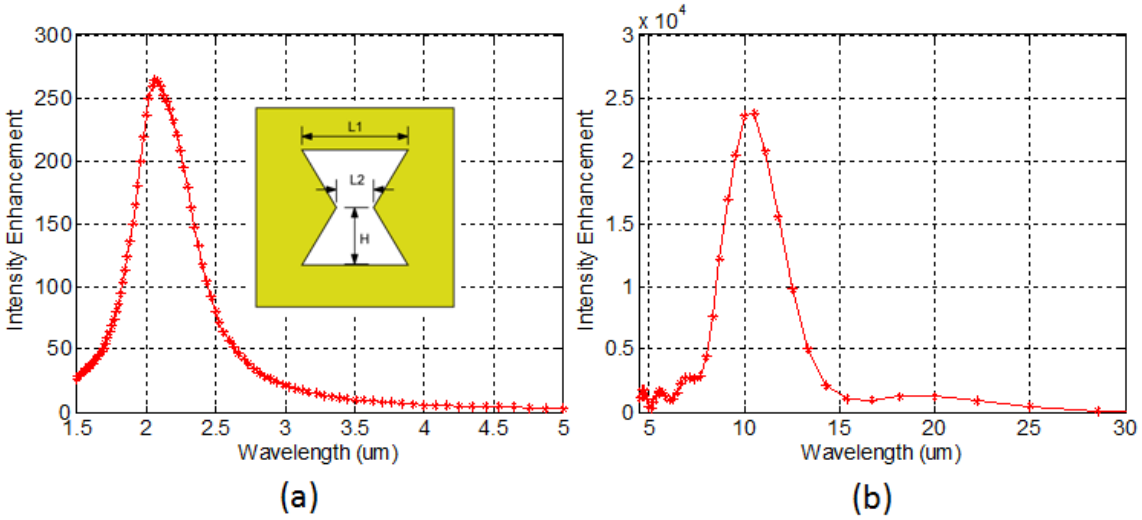

Figure 13. Optical intensity enhancement in the gap region as a function of excitation wavelengths (a) bowtie aperture antenna with a resonant wavelength of 2 μm. (b) bowtie aperture antenna with a resonant wavelength of 10 μm.

The dimensions of the optical antennas scales with the optical wavelength [29], thus optical antennas operating at infrared wavelengths are much larger than those operate at visible wavelengths. It is observed that the enhancement factors at infrared wavelength are affected by the cross-sectional capture area to the antenna gap ratio. The ability to squeeze the optical radiation impinging on a large antenna into the small gap area leads to the strong intensity enhancement at the infrared wavelength. Such strong field enhancement in the gap region suggests that the optical antennas can have the potential to greatly enhance the sensitivity of infrared detectors.

Since the optical antenna operates on the principle of focusing incident radiation into the gap area, the intensity enhancement factor of an optical antenna will depend on the width of the gap. Narrower gap means more focusing of the incident radiation and thus results in higher intensity enhancement factor. The effect of the gap length on the intensity enhancement factor for a dipole antenna with a resonance wavelength of 8 μm is shown in Figure 14. A monotonic increase in intensity enhancement factor with smaller gap size is observed. The enhancement factor increases from around 100 times at a gap length of 800 nm to around 12000 times at a gap length of 100 nm. The result indicates that the gap length, which is limited by the resolution of the fabrication techniques, can be controlled to achieve the desired enhancement factor.

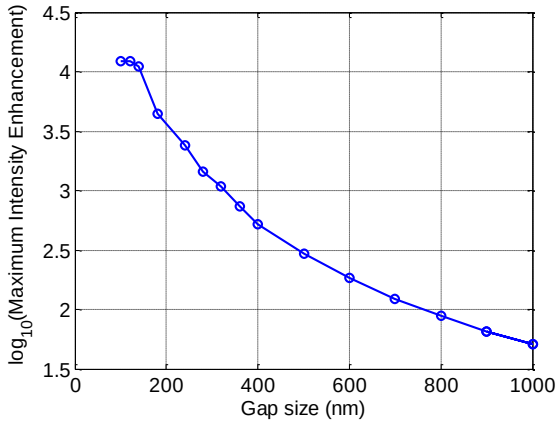

Figure 14. Calculated field enhancement factors as a function of gap width for a dipole antenna with a resonant wavelength of 8 μm.

Another attractive feature of optical antennas is their planar configuration. The planar structure allows for easy integration with infrared detectors. Since the infrared detectors will be located above or below the antenna plane, it is important to evaluate the out-of-plane optical intensity to ascertain the actual enhancement factor that can be achieved. Our simulation on a bowtie aperture antenna indicates the field enhancement is extended to a certain volume above and below the antenna plane. Figure 15 shows the simulation results for the field distribution in x-y (antenna) plane at three different distances. In the antenna plane where z equals to zero, field is strongly confined in the gap region; at 0.5 μm above the antenna plane, the field spreads out and the field amplitude reduces at the same time; at 1 μm above the antenna plane, the field spreads further. Although the intensity of the infrared radiation drops by nearly 10 times at 0.5

μm above the antenna plane, it is expected that more than 2,000 times intensity enhancement can still be achieved at a resonance wavelength of 10 μm.

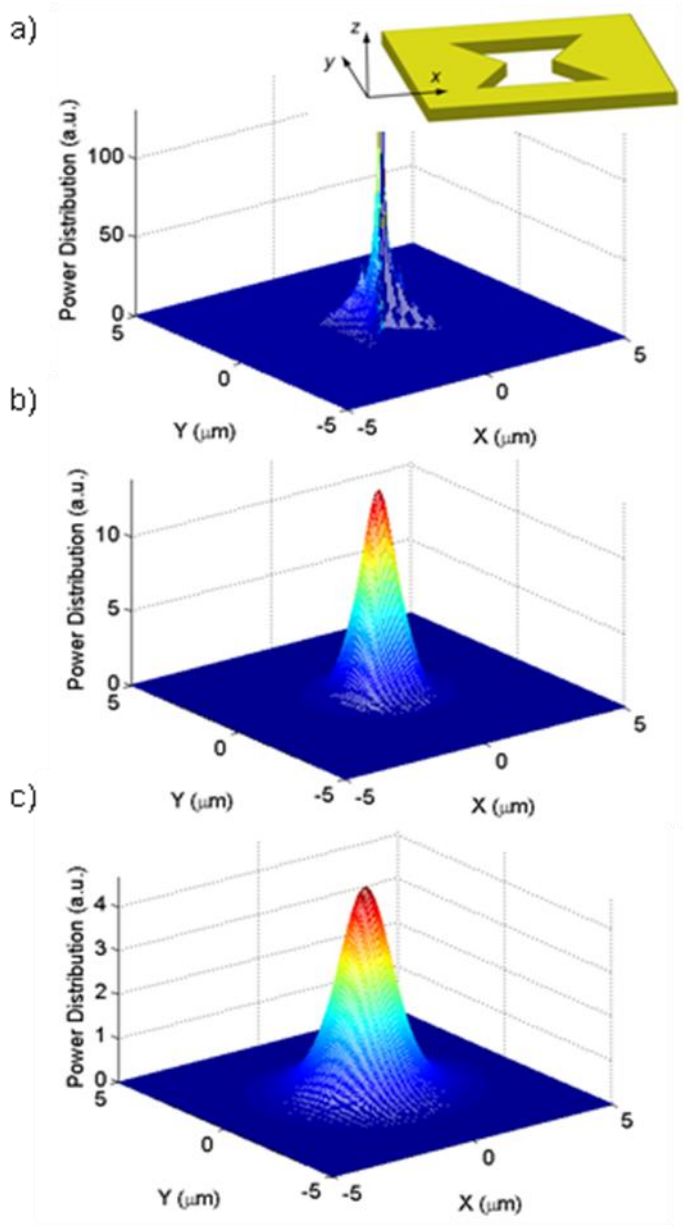

Figure 15. Calculated field distribution in the x-y plane at three different distances from the bowtie aperture antenna plane. (a) z = 0; (b) z = 0.5 μm above the antenna plane; (c) z = 1 μm above the antenna plane.

3.4.3 Fabrication

The fabrication of the optical antennas can be easily done by conventional microelectronic lithography techniques. The dimension of an optical antenna is proportional to its optical resonant wavelength. Thus an optical antenna for mid-IR wavelengths is easy to fabricate due to larger dimension. This is unlike an optical antenna for visible wavelength, which often requires sub-50 nm lithography to achieved high-enough field enhancement. For IR optical antenna, the typical size scale is between 0.1 um and several microns. This can be easily done by conventional lithography techniques such as electron-beam lithography, nanoimprint lithography and 193 nm photolithography. Here we show dipole and bowtie aperture antennas fabricated by electron-beam lithography.

First, a 950k PMMA e-beam resist is spin-coated on a substrate (Figure 16). After electron-beam exposure, the exposed PMMA is removed. A thin metal film (e.g. gold) is then evaporated onto the substrate. Lift-off in solvent will leave the optical antenna on the substrate. Figure 17 shows SEM pictures of a few IR optical antennas that we fabricated. On the top are the dipole antennas and on the bottom are the bowtie-aperture antennas.

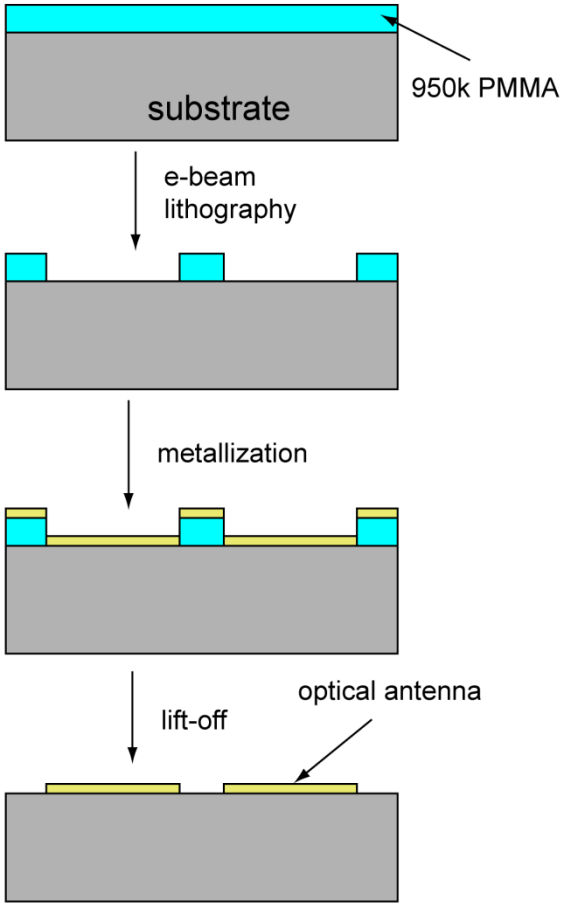

Figure 16. Fabrication of optical antennas

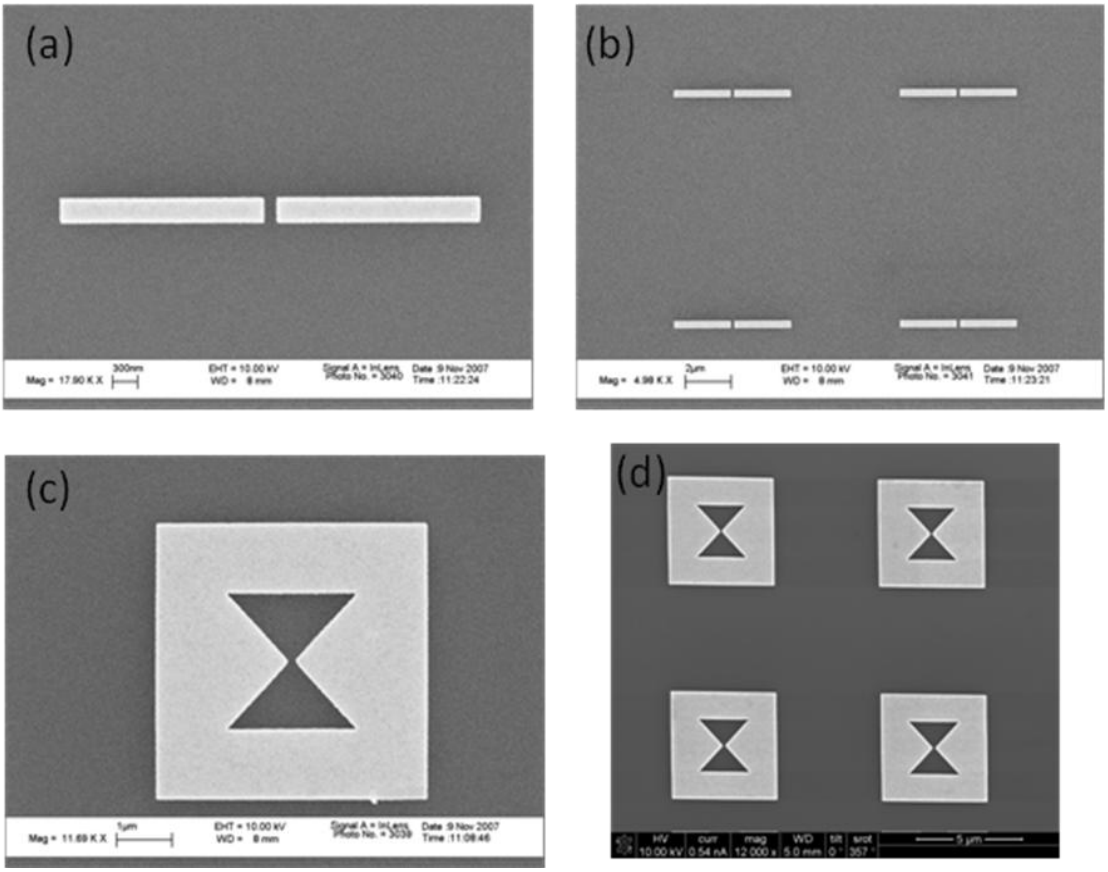

Figure 17. SEM images of optical dipole and bowtie aperture antennas.

3.4.4 Summary

In summary, we simulated and designed optical antennas that operate in mid-infrared wavelengths. Numerical simulations show that very strong field focusing and intensity enhancement can be achieved at mid-infrared wavelengths in properly designed optical antennas. The intensity enhancement factor is on the order of a thousand for a range of infrared wavelengths near resonance, which allows for broad-band operation. The intensity enhancement factor can be further increased by reducing

the gap width in the optical antenna design due to a tighter focusing of the incident radiation. There is also strong intensity enhancement at a certain distance above and below the optical antenna plane, which enables easy vertical integration of those antennas with infrared detectors.

Because infrared antenna operates at long wavelengths, their geometrical dimensions are usually in the range of 0.1 μm to several microns. Unlike optical antennas operate at visible wavelengths, which usually require stringent sub-50 nm lithography, the larger size allows infrared antennas to be easily fabricated with low cost by conventional microelectronic fabrication techniques. The advantages, such as the ease of fabrication, the planar structure for easy integration and the strong intensity enhancement will make optical antennas a viable solution for enabling uncooled and highly sensitive infrared detectors, which will have huge impact on a wide range of infrared technologies.

CHAPTER IV

MANIPULATION OF CARBON NANOTUBES

4.1 Introduction

Innovation in optical and electronic devices heavily relies on the development of engineered materials in nanoscale. To fully explore the potential application of nanomaterials for device technology, nanostructures have to be made and nanoscale building blocks should be integrated with other components of the devices and systems. Low temperature solution based process is an environmentally friendly technology, which enables us to prepare nanostructured organic and inorganic materials by assembling nanoscale building blocks with reduced energy cost. The fundamental understanding of the process mechanism is critical to optimize material properties and improve device performance. One of the most challenging works in the assembly of nanoscale building blocks is the development of a robust and controllable process to position and orient one dimensional nanoparticles, such as single-walled carbon nanotubes (SWNTs), with low cost, high accuracy and high throughput.

Carbon nanotubes (CNTs), both SWNTs and multi-wall carbon nanotubes (MWNTs), have attracted huge attention in a broad range of nanotechnology research due to their exceptional mechanical, thermal, and electrical properties, lightness and their nanoscale dimension [30-34]. For instance, metallic CNTs are capable of carrying a theoretical current of ~ 109 A/cm^2, and the thermal conductivity of CNTs is in the range of 3000 – 6600 W/m·K at room temperature [35-36]. The attractiveness of

the CNT properties have stimulated the construction of many novel devices [37-47] based on CNTs.

For most applications, the ability to control the directionality of the CNTs is often highly desired. For example, CNTs are often dispersed in polymer matrices to enhance their electric conductivity. Theoretical simulation has concluded that aligned CNT array can significantly enhance conductivity [48]. Since CNTs have high carrier mobility and extremely small physical dimension, they are also avidly pursued for building ultra-fast and ultra-dense electronic circuits for future generation of microelectronics. However, in order to achieve such goals, the first and foremost task is to acquire the ability to lay down CNTs on a substrate in a highly ordered fashion. Subsequently, complex transistor devices and circuits can be built using CNTs as an active channel material.

The ability to manipulate CNT alignment is crucial for large-scale commercial applications of CNT. Consequently, significant amount of research has been devoted in this area in the past two decades. Many novel techniques have been proposed and demonstrated with limited success. These methods include: a) gas flow control during vapor deposition [49], b) application of an in-situ electric field during vapor deposition [50], c) deposition of CNTs from a suspension with an electric field and trapping sites [51-52], d) alignment by a host material (e.g., liquid-crystal polymers) when the host material is aligned [53], e) alignment by magnetic field and magnetic particles [54-55], f) alignment by biological molecules such as peptide or nucleic acids [56], g) surface functionalization and precipitation in “V” grooved microfluidic channels [57], h)

Langmuir-Blodget self-assembly of nanowires [58], and i) flow-induced alignment in microfluidic channels [59-61].

Although significant progresses have been made, current alignment techniques are still in their early stages and need significant development in order to be practical. Many of these techniques require high temperature growth, which is not suitable for polymers, such as polymer-CNT nanocomposites. Other techniques attempt to align CNTs after purification and dispersion with various methods. However, good CNT alignment and precision placement of individual CNTs still remain elusive and process controllability is far from ideal. Easy-to-process and yet highly effective CNT alignment, separation and placement techniques are still of primary interest and paramount importance for realizing the CNTs' commercial potentials.

In this dissertation work, we systematically experiment CNT alignment and placement from a CNT suspension. The work starts with the investigation of flow induced alignment and placement by using micro- and nanochannels. The limited efficiency and lack of scalability of flow induced alignment approach motivate us further explore approaches using directed electrostatic self-assembly. By using advanced nanopatterning technology such as nanoimprint, self-assembly of SWNTs is guided to build ordered structures. The initial effort has been focused on the assembly of SWNTs by using a layer-by-layer (LbL) assembly approach. Layer-by-Layer (LbL) approach allows for the tuning of both the thickness and properties of the nanostructures and materials. However, LbL based approach still has some disadvantages such as low SWNTs loading ratio, low patterning contrast and low

manufacturing rate. Consequent research has been focused on the systematic use of chemical, physical and mechanical approaches to speed up the assembly processes and improve the assembly quality and controllability. Substrate surfaces can be functionalized to facilitate the chemical bonding in the self-assembly process. Speeding up these processes by various chemical, mechanical and physical approaches not only reduces the cost of materials preparation, but also leads to ordered structures with improved density and uniformity. A systematic understanding of these processes and an integration of these techniques will allow the construction of many useful devices for sensing, nanoelectronic and nanophotonic applications.

We use the carbon nanotubes as the material system in the research to investigate robust approach to overcome the challenge of controllable assembly of nanomaterials. The assembled CNTs stripes are characterized for their electrical properties and by Raman spectroscopy. We have developed a high-efficiency and high-throughput process to deposit and orient these CNTs on patterned solid and flexible substrates. Particularly, we have identified critical steps and factors which determine the overall process effectiveness.

4.2 Manipulation of carbon nanotubes by micro- and nanochannels

4.2.1 Overview

The main research goal of this project is to develop techniques that allow us to manipulate the morphology, alignment and placement of CNTs from suspensions and study the electrical properties of resultant CNTs materials. The basic idea is to use

micro- and nanochannels to achieve CNT alignment and precise placement on a substrate from CNT suspensions. First, the as-grown curly and entangled CNT bundles are dispersed and stabilized in aqueous or non aqueous solutions. High-resolution transmission electron microscope (HR-TEM) images show our de-roped and de-bundled CNTs are straight wires. The suspension will be forced through micro- or nanofluidic channels with a cross-sectional dimension that is much smaller than the length of the individual CNTs, and the CNTs will naturally align along the groove direction during transport due to the geometrical confinement of the channel walls. Removing the liquid component in the suspension by evaporation will deposit aligned CNTs on a substrate.

Alignment of one-dimensional (1-D) nanostructures such as nanowires by fluidic channels has been demonstrated [62]. This approach has also been applied with CNT suspensions [63, 59-60]. In this project, we employ and extend such process and its variations for several purposes: 1) reorganize CNT bundles to achieve superior properties; 2) deposit aligned-CNT stripes on a substrate for thermal, electrical and mechanical applications; and 3) place individual CNT at specific locations on a substrate for microelectronic applications. Figure 18 summarizes the general schemes for CNT alignment and placement for different target applications. We aim to systematically develop a feasible approach to achieve controlled CNT alignment and placement for numerous applications, and develop an advanced scheme for efficient and scalable CNT separation based on conductivity types.

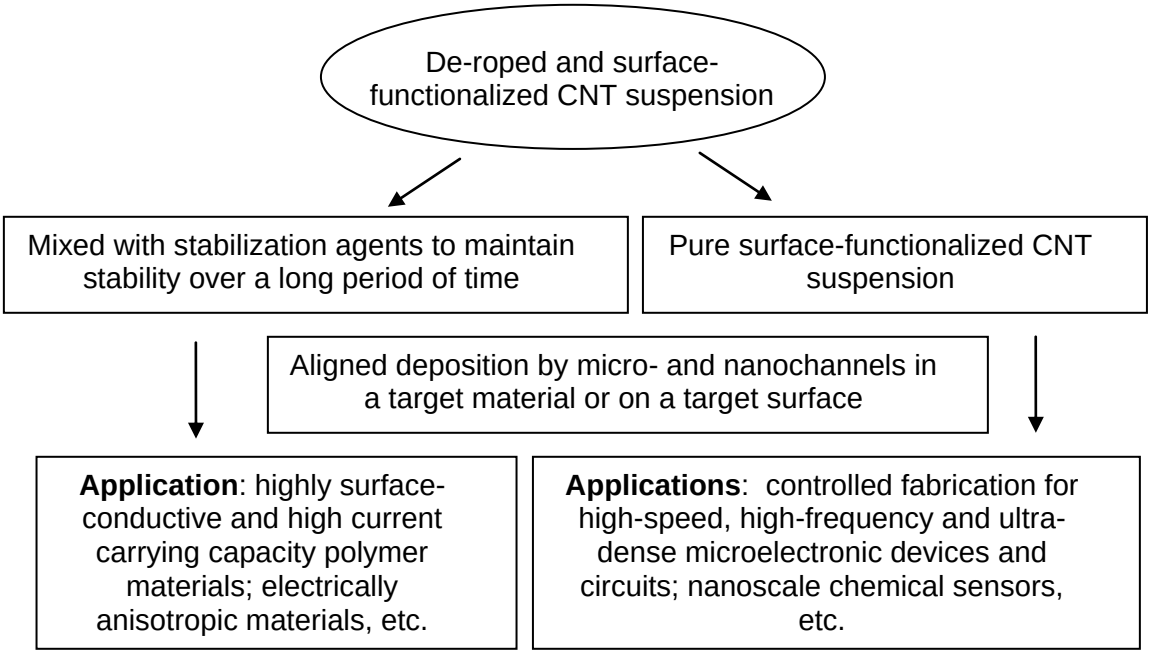

Figure 18. Summary of schemes and applications of microchannel-aligned CNTs.

4.2.2 Experimental details

The alignment of de-roped CNTs using micro- and nanochannels is depicted in Figure 19. The substrate shown in the figure can be a polymer film or sheet for creating conductive paths on polymer surfaces, or a silicon substrate for microelectronic applications. Silicon oxide or PDMS templates with micro- and nanofluidic channels are placed on top of a substrate and the CNT suspension is pushed through the channels. After drying out liquid in microchannels and removal of the channel template, stripes of aligned-CNTs will be left on the surface of the substrate (Figure 19 (b)).

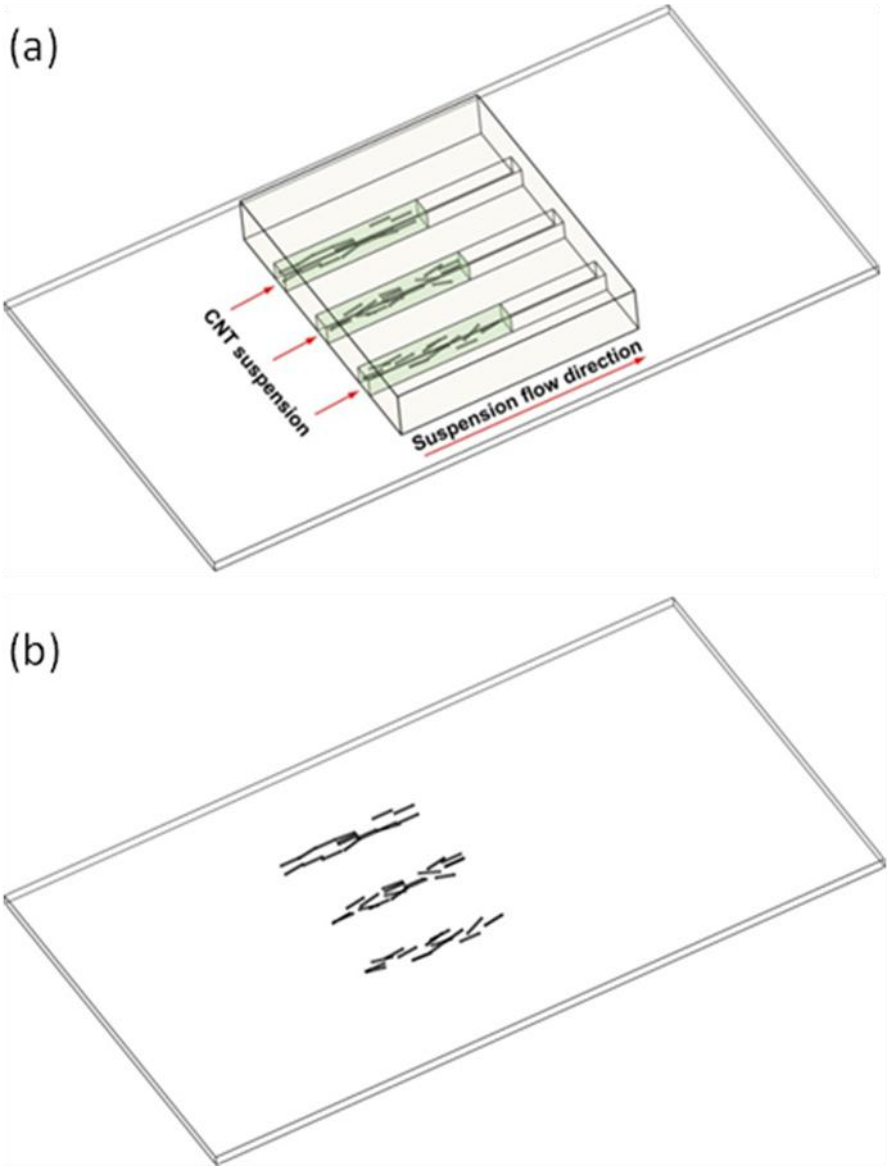

Figure 19. Schematics of (a) alignment of de-roped CNTs using microchannels and (b) stripes of aligned CNTs on a substrate.

As-grown CNT network usually have the form of long, curly and entangled ropes, in which CNTs form a partially ordered bundle. The process described here allows for the exfoliation and breakdown of the CNT ropes and reorganization of the

de-roped CNTs to form bundles with higher degree of ordering, as shown in Figure 20. In those highly ordered CNT bundles, CNTs are parallel to each other in the rope to maximize the inter-tube interaction. The enhanced inter-tube interaction can greatly enhance the electrical, thermal and mechanical properties of the CNT ropes, such as higher electric conductivity and higher tensile strength. Such CNT ropes may find important applications as a novel engineering material.

Aligned-CNT stripes or reorganized CNT bundles are novel and interesting materials whose electrical, thermal and mechanical properties can be tuned by the internal CNT morphology. Other than applications in enhancing the surface and bulk conductivity of polymer composites, aligned-CNT stripes can also be used as novel active materials for microelectronic applications such as metallic interconnects and conduction channels in solid-state devices.

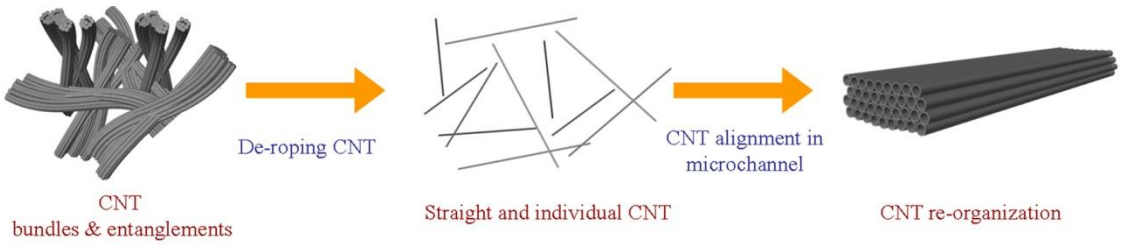

Figure 20. A schematic of CNT bundle reorganization.

For microelectronic device and circuit applications, it is imperative to place the CNTs on specific locations on a chip, which is determined by the nature of the device and the circuit to be built. The precision placement of de-roped CNTs using micro-

and nanochannels is depicted in Figure 21. The substrate shown in the figure could be a substrate of microelectronic interest, such as a silicon, GaAs or dielectric wafer.

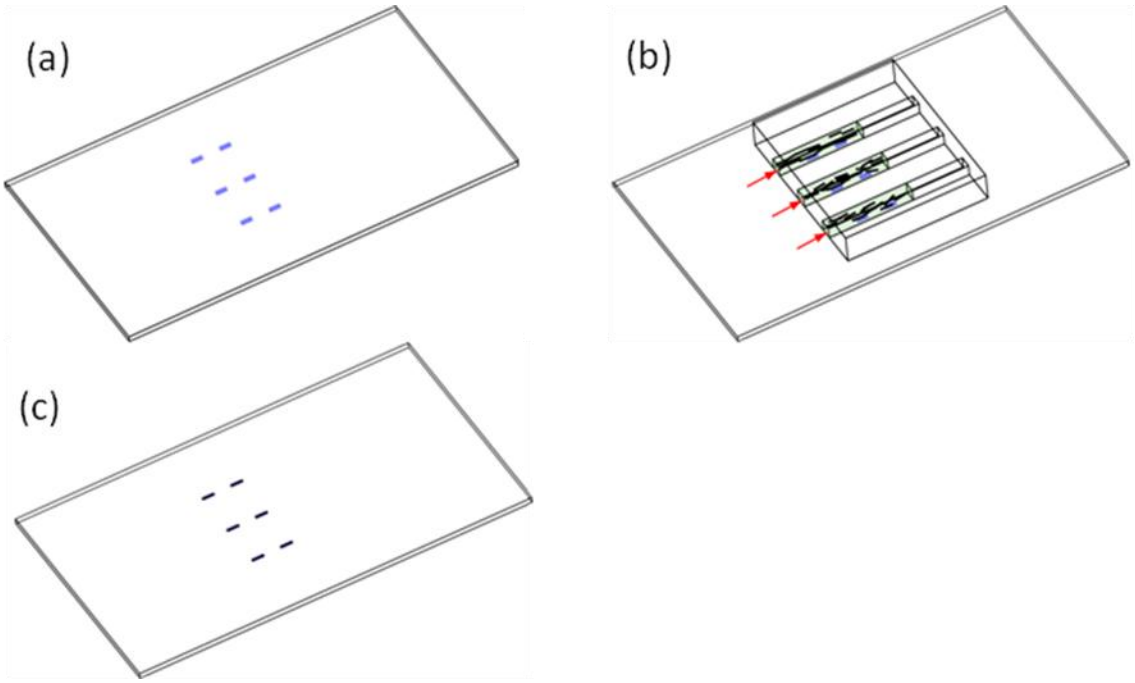

Figure 21. Schematics of precision placement of CNTs on a substrate for microelectronic device and circuit applications. (a) Pattern nanoscale SAM structures for trapping surface-functionalized CNTs on the substrate; (b) Align microchannels on top of the SAM patterns and flow CNT suspension through the channels; (c) CNTs are precisely trapped at desired locations.

A major advantage of CNT alignment using suspension is that it allows a specific type of CNTs to be pre-selected, e.g., semiconducting or metallic, prior to alignment and placement using methods such as surface modification and laser

ablation [64], dielectrophoresis [65], and sequence-dependent DNA assembly [66]. This allows for the alignment of a specific type of CNTs for different target applications. Such selectivity in CNTs types is clearly a huge advantage over vapor-based high temperature deposition techniques in which semiconducting and metallic CNTs are always coexistent and non-separable.

4.2.3 Dispersing CNTs with ancillary nanomaterials

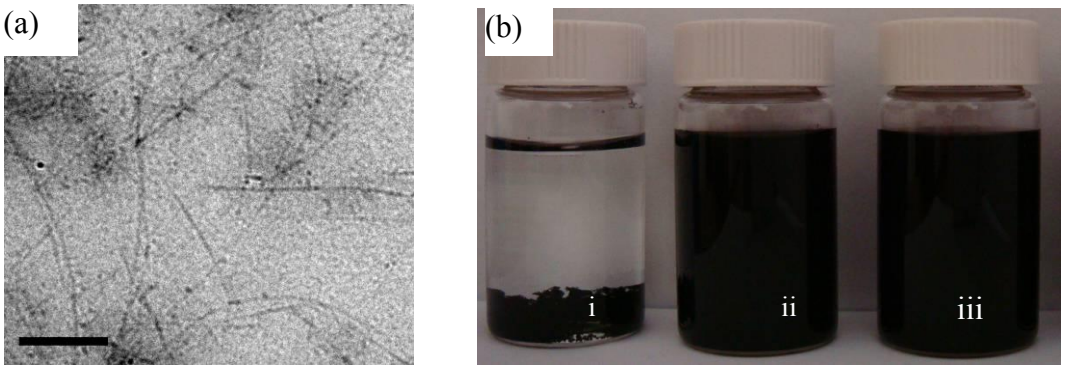

Figure 22. (a) HR-TEM images of exfoliated SWNTs prepared by our new approach. Scale bar is 100 nm. (b) Photographs of (i) pristine SWNTs and (ii) exfoliated SWNTs dispersed in water and in (iii) acetone. Sample concentration is 1,000 ppm in all three cases and images were taken after 4 months of sedimentation.

Our approach to exfoliating bundled SWNTs into individually dispersed nanotubes involves the use of secondary nanomaterials as dispersants [67]. As shown by the HR-TEM image in Figure 22(a), the SWNTs have been fully exfoliated into

individual nanotubes. Figure 22(b) shows photographs of (i) unmodified SWNTs and SWNTs exfoliated and stabilized by ancillary nanomaterials in both (ii) water and (iii) acetone. The mechanism is effective within minutes of adding the dispersant, and the subsequent dispersion is stable for at least 4 months.

It is known that SWNTs contain a variety of nanotube species of different diameters and chirality, which determine their electronic structure and, therefore, absorption spectra. The optical properties of SWNTs are strongly affected by their surrounding environment that, in a fully dispersed state, could be the liquid medium. However non-exfoliated SWNTs are nearly completely surrounded by other nanotubes contained within the aggregated bundle. Because of this, data often shows coupling and broadening of the absorption peaks. Exfoliated SWNTs at low bulk concentrations will exhibit sharp absorption peaks, as shown in Figure 23. After de-roping and dispersion through our new approach [67], the existence of more pronounced peaks strongly suggests the presence of exfoliated SWNTs. The strong absorption intensities also demonstrate that the electronic structures of the individual SWNTs after exfoliation have been mostly preserved.

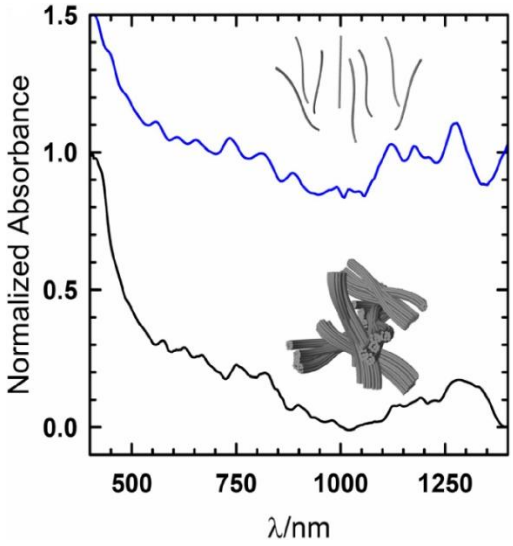

Figure 23. UV-vis-NIR spectra of (a) pristine SWNTs and (b) exfoliated SWNTs in water.

4.2.4 Aligned-CNT stripes on silicon and polymer surfaces

Traditional bulk dispersion of carbon nanotubes in a polymer matrix can only achieve a conductivity level of lower than 0.01 S/cm[68-70] due to a random orientation and distribution of CNTs in a three-dimensional space. Concentrating CNTs on the polymer surface can greatly enhance the surface conductivity due to a higher local concentration of CNTs. If the CNTs are aligned in one dimension, the conductivity can be further enhanced because the effective path for charge conduction along the aligned direction is much smaller than a random network.

Aligned-CNT stripes (XD Grade: 2/3 SWNT and 1/3 MWNT) on an insulating substrate have been achieved using the aforementioned alignment method. In our preliminary experiments, the conductivity of the aligned-CNT stripes was measured

by a two-probe technique as illustrated in Figure 24(a). After deposition of aligned-CNT stripes on a substrate, gold electrodes were evaporated using a shadow mask. Figure 24(b) shows an optical image of a sample prepared after these fabrication steps. The current between the two gold electrodes was measured as a function of applied voltages. A typical measured I-V curve is shown in Figure 25. Since in each measurement many CNTs are in parallel, the gold-CNT contact resistance is small and can be neglected. The conductivity of the aligned-CNT stripe can be estimated from the following simple equation:

$$\sigma = \frac{L}{RA} = \frac{L}{R\,N\,W\,t} \ ,$$

where L is the distance between the two electrodes, R is the measured resistance, A is the cross section area of the stripes, N is the number of CNT stripes, W is the width of each CNT stripe and t is the thickness of each stripe. For the sample corresponding to Figure 25, the values of those parameters are: L = 70 μm, R = 40,000 Ω (at 40V), N×W = 40 μm, t ≈ 0.3 μm. The calculated conductivity is 1.46 $S \cdot cm^{-1}$, and the current density at 40V is around 8300 $A \cdot cm^{-2}$. The conductivity is about two orders of magnitude higher than the highest reported conductivity of polymer-CNT composites. Those values are expected to be further improved if pure CNT suspension is used. This potentially can lead to the preparation of aligned-CNT stripes with conductivity higher than 2000 $S \cdot cm^{-1}$ [71]. A lower conductivity (0.45 $S \cdot cm^{-1}$) and current carrying capacity (2083 $A \cdot cm^{-2}$) for aligned-CNT stripes on cured-epoxy surface are recorded.

The lower values are attributed to the roughness of the epoxy surface, which often leads to CNT stripes of poorer quality.

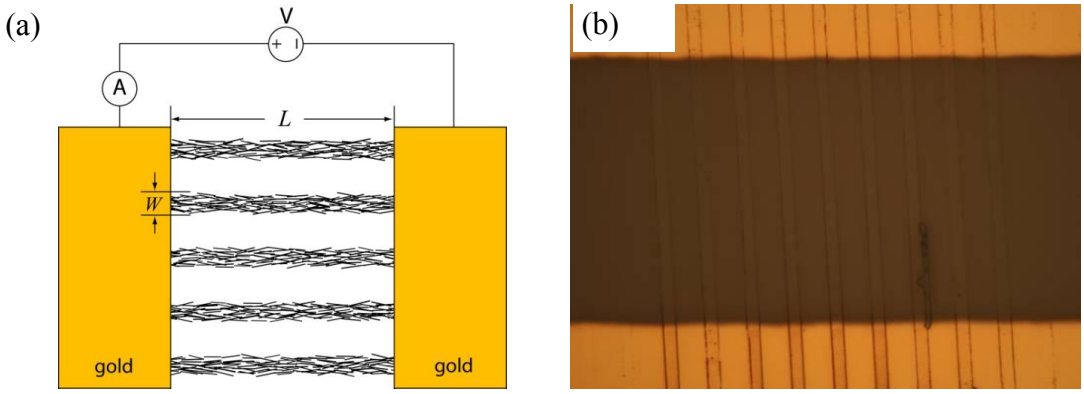

Figure 24. (a) A schematic of the two-probe measurement of the conductivity of the aligned CNT stripes; (b) Optical microscope image of a sample for two-probe conductivity measurement. The vertical lines are aligned CNT stripes. The top and bottom pads are gold electrodes.

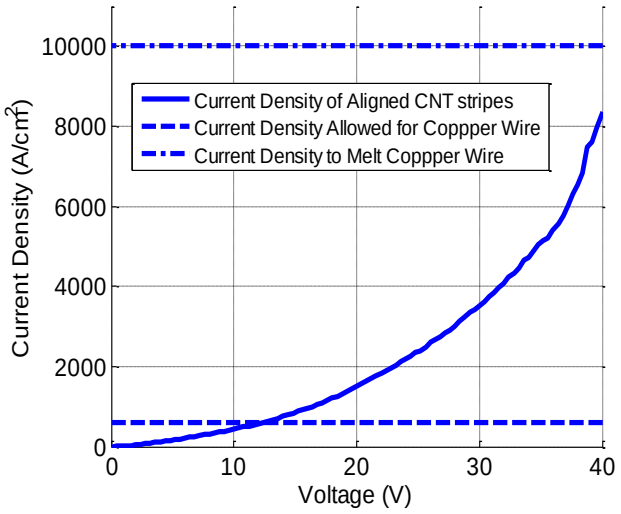

Figure 25. I-V characteristic from a two-probe conductivity and current density measurement.

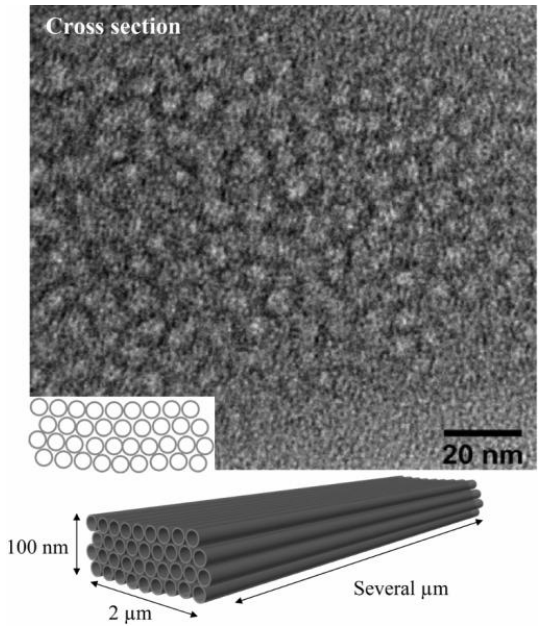

Figure 26. TEM image of the cross-section of the bundled MWNT in aligned-CNT stripes and a schematic of the bundle configuration.

Our result also indicates ordering can be achieved in aligned-MWNT stripes. MWNTs are longer in length and larger in diameter. Longer tubes result in better alignment, while larger diameter makes it much easier to observe the cross-sectional morphology of the aligned-MWNT stripes. Aligned-MWNT stripes were embedded in an epoxy resin and a thin-section of the cross-section of the aligned-MWNT stripes was cut for TEM imaging. The TEM image of the bundled MWNTs and a schematic of the buddle configuration are shown in Figure 26. The dot-like pattern indicates a reorganized MWNT bundle.

4.2.5 Summary

It is experimented that micro- and nanochannels can be used to place and align CNTs by flow-induced and geometrically confined reorganization. TEM characterization indicates the alignment of CNTs in the stripes. Electrical characterization shows higher level of conductivity and current density compared with traditional bulk dispersion of carbon nanotubes in a polymer matrix.

Although flow-induced alignment can be realized using micro- and nanochannels, it is very time-consuming to transport the CNTs dispersion into the channels and to dry out the liquid. Additionally, it is extremely difficult to scale up the process to prepare aligned CNTs on a wafer level, because of the difficulty to flow CNTs in very long and narrow channels where clogging often happens. The process discussed above can only find limited roles in the electronic and material applications.

A process with better scalability and controllability is desired to achieve the goal to effectively manipulate one-dimensional CNTs.

4.3 Guided layer-by-layer assembly

4.3.1 Overview

Many applications require SWNTs aligned and placed with good controllability to ensure the reproducibility and performance of the system. We report a simple but effective approach for SWNTs alignment and placement, which is based on grating-guided electrostatic self-assembly. Electrostatic self-assembly (ESA) is a mature layer-by-layer thin film growth technique based on electrostatic Coulomb interaction and has recently been used to prepare CNT-containing thin films with novel properties. We extended the ESA process one step further to achieve highly ordered SWNTs. The approach involves the deposition of electrostatic self-assembly layers containing CNTs in prefabricated polymer microstructures from surfactant-wrapped CNT dispersion.

The location and orientation of SWNTs can be precisely controlled by lithography technique. The residual SWNTs stripes on the substrate shows strong polarization anisotropy for polarized Raman spectroscopy, which indicates a high level alignment of the SWNTs is achieved. The choice of surfactants for the guided self-assembly process is discussed. As an easy-to-process approach, the solution processing of SWNTs alignment can be scaled up to large substrate with high

throughput. The process is compatible with semiconductor processing and flexible substrates.

4.3.2 Experimental details

HiPCO SWNTs were obtained from Carbon Nanotechnology Inc. (Houston, TX). The SWNTs were treated via sonication in 1:3 concentrated nitric-sulfuric acid for 3 hours in room temperature before dispersed into DI water assisted with surfactants. Surfactants used in the preparation of SWNTs suspensions, such as sodium dodecyl sulfate (SDS), Piperidine, polystyrene sulfanate (PSS) (1,000,000 Mw) and polyvinyl alcohol (PVA) (55,000 Mw) were purchased from Singma-Aldrich and used as received.

Nanoimprint mold with 700nm grating period and 50% duty cycle is used in the experiment to prepare polymer grating micro-structures. The grating is replicated in a thermally grown oxide layer on a silicon substrate from a commercial holographic grating (Ibsen Photonics) by nanoimprint lithography and reactive-ion etching. The mold depth is 350 nm. Poly(methyl methacrylate) (PMMA) is dissolved in toluene and spin coated onto the silicon substrate to prepared a 200nm thick thin film for nanoimprint. After thermal imprinting, the polymer grating structure was treated with brief oxygen reactive-ion etching to remove the polymer residual in the trench area. Polarized Raman microscopy was obtained by a Horiba Jobin-Yvon LabRam IR system. The SEM image was obtained by FEI Quanta 60C FE-SEM.

Figure 27 shows the schematics of the grating-guided ESA on a substrate. Submicron polymer microstructures are first created on silicon substrate by

nanoimprint lithography followed by oxygen RIE. The exposed substrtate surface at the bottom of the polymer trench is then coated with (3-aminopropyl)triethoxysilane (APTES) to improve CNT adhesion. The silicon substrate with polymer microstructure is then soaked in PSS-stablized CNT suspension to deposit a monolayer of PSS-wrapped CNTs. For SWNTs that are longer than the width of the polymer trenches, they have to align along the groove direction during deposition due to the geometrical confinement of the channel walls. After DI-water rinsing, the sample is then soaked in a positively charged polyelectrolyte solution such as PVA. A monolayer of PVA will be deposited onto the PSS-wrapped CNT surface due to electrostatic attraction. This completes a bilayer deposition and leaves the surface positively charged and the process can be repeated many times for target film thickness. The PMMA polymer template can be easily removed by solvents such as acetone to leave the aligned-CNT stripes on the substrate. After this step, stripes of aligned-SWNTs can be achieved and used for device applications.

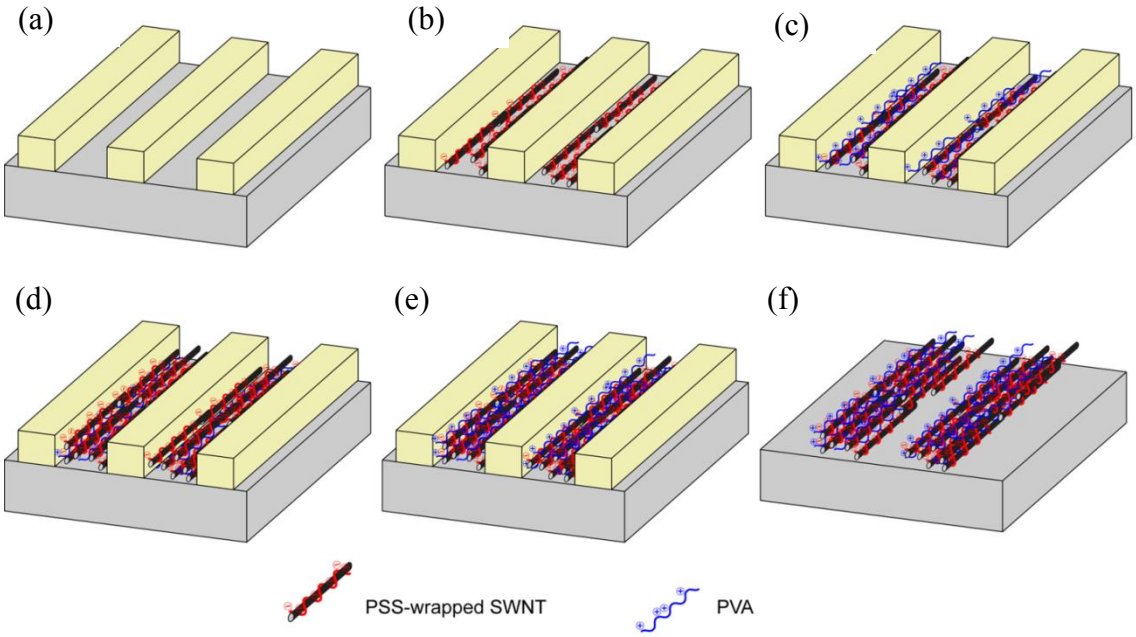

Figure 27. ESA schematic illustration of grating-guided electrostatic self-assembly process for SWNTs alignment. (a) Polymer template patterned by nanoimprint; (b) Deposit PSS-wrapped SWNT by ESA from suspension; (c) Deposit PVA on top of PSS-wrapped SWNT by ESA; (d) Deposit the 2nd layer of PSS-wrapped SWNT; (e) Deposit the 2nd layer of PVA; (f) Remove polymer template by solvent;

After grating-guided ESA and liftoff of PMMA polymer structure, we can obtain stripes with aligned SWNTs on the substrate. **Figure 28** shows the SEM image for a 5-bilayer aligned-CNT stripes after liftoff. We used analytical techniques such as Raman spectroscopy to characterize those SWNT stripes.

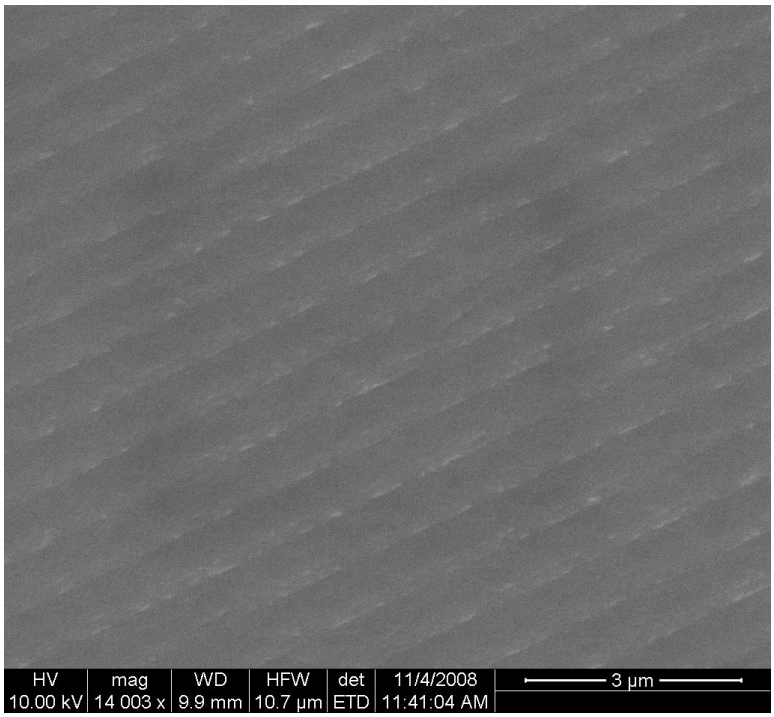

Figure 28. An SEM micrograph of aligned-CNT stripes on a silicon substrate.

4.3.3 Polarized Raman spectra of the SWNT stripes on the substrate

To probe the alignment of SWNTs after grating-guided ESA, we took polarized Raman spectra of the SWNT stripes on the substrate. In Figure 29, Raman signals of aligned-CNT stripes (prepared using polyelectrolytes PSS and PVA as surfactant) excited by probe laser with different polarization directions are plotted, where θ denotes the angle between the polarization direction of the incident laser light and the longitudinal direction of the deposited CNT stripes. The G-band (1590 cm^{-1}) Raman signatures show distinct polarization anisotropy. The signal contrast ratio at 0º and 90º is about 4.3. It was shown for isolated SWNTs that Raman scattering is

forbidden when the incident photons are polarized perpendicular to the CNT length direction. Thus, the polarization anisotropy shown in those figures indicates that the CNTs were aligned along the patterned grating direction. After polymer template liftoff, strong Raman signal is still obtained. This indicates stripes obtained from polyelectrolyte surfactants are stable, which is expected due to strong inter-chain electrostatic interaction. The signal contrast ratio at 0º and 90º is about 3.0. The level of anisotropy is only degraded very little after the lift-off process.

For grating-guided ESA of SWNTs with small molecule surfactant, signal anisotropy is also observed in polarized Raman spectroscopy, as shown in Figure 30. Similar to previous case, when the polarization direction of the probe laser is parallel (θ = 0º) to the stripes, the Raman signal of the D and G bands of SWNTs reaches a maximum, while the signal is at the minimum if the probe laser is polarized perpendicular to the longitudinal direction of the SWNT stripes (θ = 90º). In fact, the polarization contrast in Raman signal in this case is much larger than that of stripes with polyelectrolyte surfactant. This indicates small molecule surfactant can achieve better alignment results in grating-guided ESA. However, after liftoff to remove PMMA template, very weak Raman signal can be detected. This indicates most SWNT deposited during ESA is also removed by the solvent due to very weak inter-layer electrostatic force.

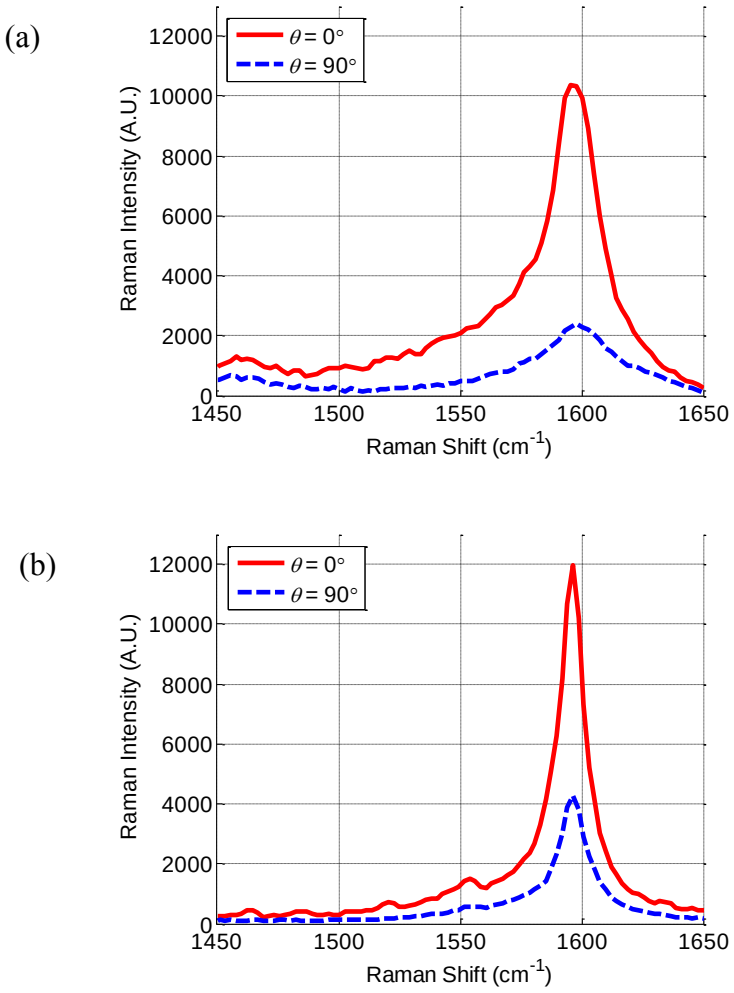

Figure 29. Polarized Raman spectra of SWNTs stripes prepared by grating guided ESA using polyeletrolyte as surfactants (PSS and PVA). θ denotes the angle between the polarization directions of the incident laser light and the longitudinal direction of the deposited CNT stripes. (a) Before the lift-off of polymer template; (b) After the the lift-off of polymer template.

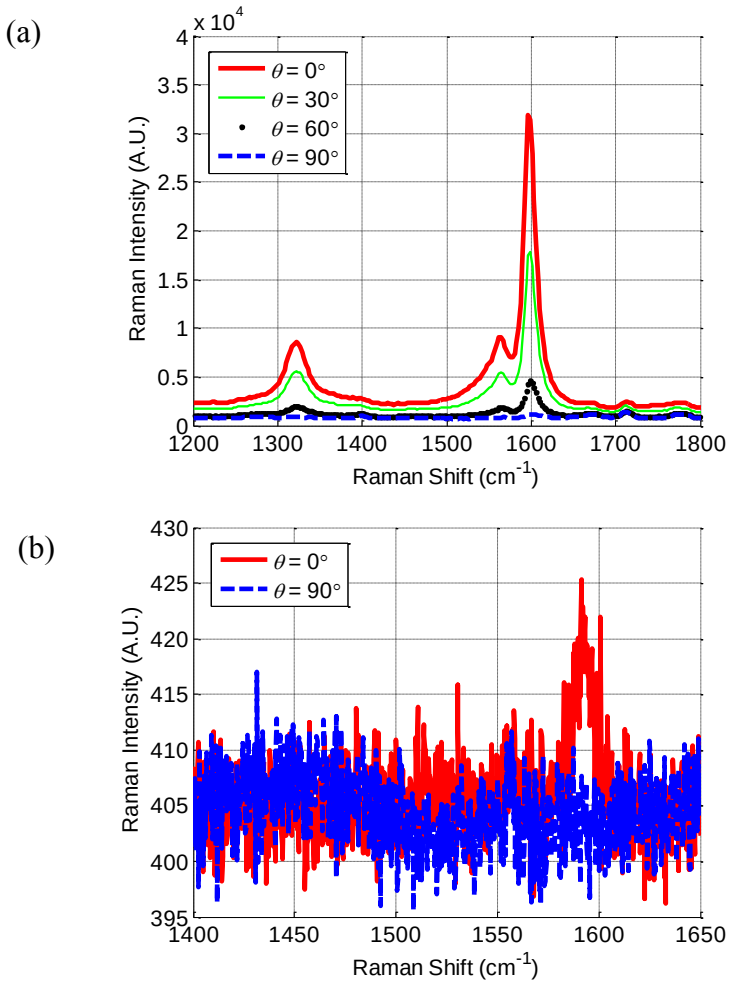

Figure 30. Polarized Raman spectra of SWNTs stripes prepared by grating guided ESA using small molecules as surfactants (SDS and piperidine). θ denotes the angle between the polarization directions of the incident laser light and the longitudinal direction of the deposited CNT stripes. (a) Before the lift-off of polymer template; (b) After the lift-off of polymer template.

4.3.4 Effect of surfactant on the stability and alignment

CNTs have poor solubility in most solvents. Recent years, lots of progress has been made to effectively disperse CNTs into solvent by surface modification with surfactants [72]. Basically, there are two methods to wrap CNTs with surfactants. One is through forming covalent bonding between surfactants and the oxidized CNT surface. The other one utilizes noncovalent functionalization of CNT with surfactants, nucleic acids, peptides, polymers and oligomers. This is usually accomplished by chain wrapping and pi-pi bonding. In this work, we choose noncovalent functionalization because it preserves the electronic properties of the nanotubes.

For electrostatic self-assembly, we need ionic surfactants that render SWNT surface charged.

Figure **31** shows the surfactants that we used in SWNTs dispersion and guided ESA. Two types of surfactants are chosen. One type is polyelectrolyte such as PSS and PVA. The advantage of polyelectrolyte surfactants are they form good wrapping on SWNT. They contain multiple charges on polymer chain, which ensures good electrostatic interaction for ESA process. The strong inter-chain interaction also leads to stable stripes that can endure polymer template removal process. However, the size and shape of SWNTs after polymer surfactant wrapping can be significantly modified, which may have negative impact on grating guided-ESA. The second type of surfactant is small molecule surfactant. SDS and piperidine are used in our experiments. In contrast to polyelectrolyte surfactant, the advantage of small molecule surfactant is that the geometry of the SWNT is not much affected by surfactant

wrapping. However, its single charge per molecule is a major disadvantage because this will lead to very weak interlayer electrostatic interaction during ESA. Also the SWNT stripes obtained after ESA is weak and can be damaged by the polymer template removal process.

Based on the results we obtained so far, we feel that ideal surfactant for grating-guided ESA should have properties in-between polyelectrolyte and small molecule. In another word, very short-chain polyelectrolyte may have both size and multi-charge advantages to yield better results.

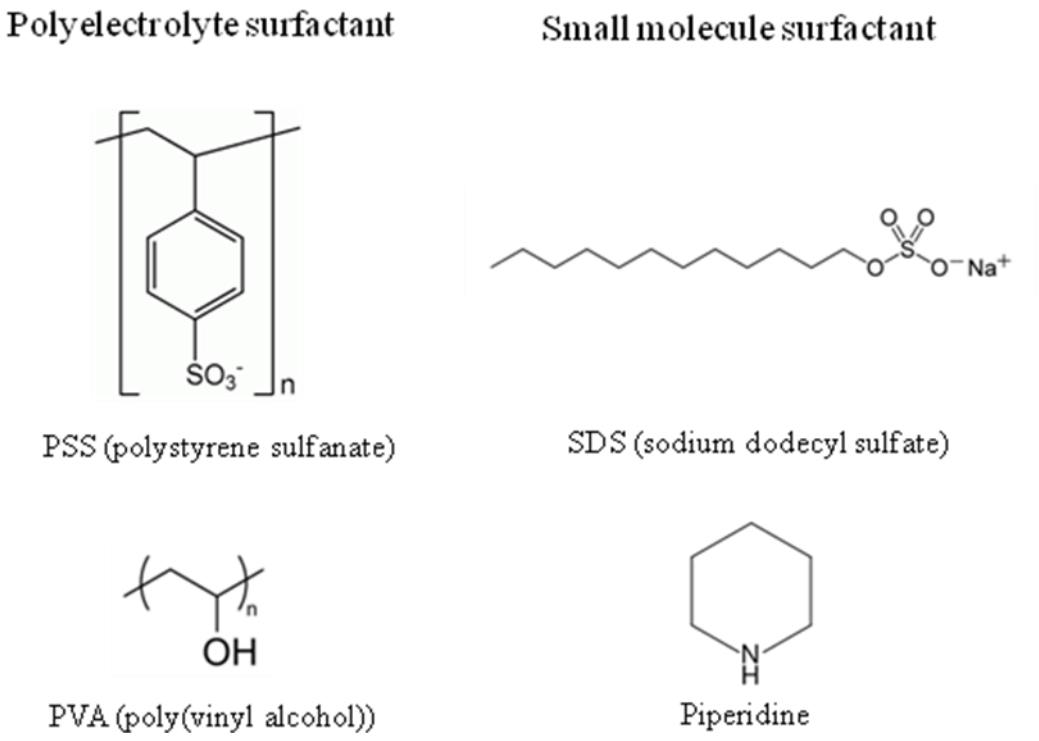

Figure 31. Surfactants used in the grating guided ESA process.

4.3.5 Electrical characterization

The electric conductivity of the aligned-CNT stripes is of interest because they can be deposited on polymer surface to render the surface conductive for many applications. In our experiments, the conductivity of the aligned-CNT stripes was measured by a two-probe technique as illustrated in Figure 24(a). After deposition of aligned-CNT stripes on a substrate, gold electrodes were evaporated using a shadow mask. Figure 32 shows measured I-V curve on 20-bilayer stripes (70 nm thick). Since in each measurement many CNTs are in parallel, the gold-CNT contact resistance is small and can be neglected. For the sample corresponding to Figure 32, the calculated conductivity is 0.04 S/cm, and the current density at 40V is around 200 A/cm^2. This conductivity is not very high due to the presence of the polyelectrolytes and the CNTs used in this preliminary are a mixture of metallic and semiconducting CNTs. Those values are expected to be greatly improved if pure metallic CNT suspension is used and the polyelectrolytes are removed from the stripes. In our research plan, we propose the research on CNT sorting based on conduction type using a multilayer fluidic device and polyelectrolyte removal by pyrolysis. The results can potentially lead to the preparation of aligned-CNT fibers with pure metallic CNTs to achieve conductivity higher than 2000 S/cm[71] for advanced applications.

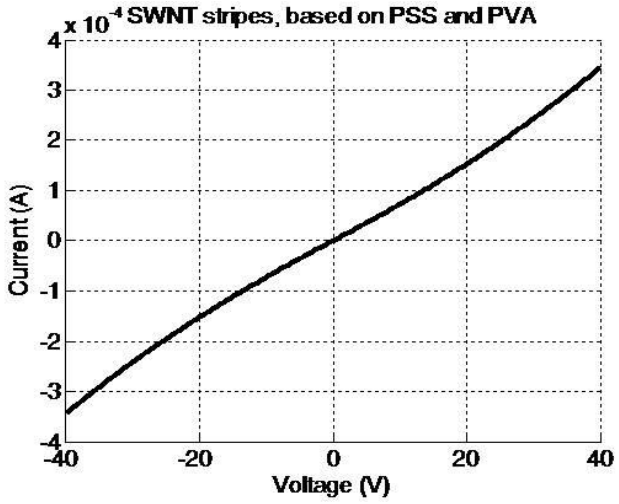

Figure 32. I-V characteristic from a two-probe conductivity and current density measurement on 20-ESA-bilayer aligned-CNT stripes.

4.3.6 Summary

In this work, we presents a simple yet effective CNT alignment technique based on the grating-guided electrostatic self-assembly. Raman spectra indicate alignment of SWNTs in grating templates is achieved. The surfactants used in SWNT dispersion and ESA played an important role to impact the SWNTs alignment. Use of polyelectrolyte surfactant results in SWNTs stripes with good stability due to strong interlayer electrostatic interaction, self-assembled SWNT stripe can survive the removal of the template. However, the level of SWNTs alignment is not as good as the results when using small molecule surfactant. Short-chain polyelectrolyte (oligomer) may yield best result in term of advantages of multicharge and short length.

With the template-guided electrostatic self-assembly, the location and the alignment direction of the SWNT are determined by the polymer template, which can be precisely controlled by lithography techniques. Solution based processing for SWNT alignment can be scaled up to large substrate with high throughput; the same approach can be applied to other nanowires and nanorods. Low temperature solution processing is compatible with semiconductor processing and flexible substrates. The approach described here may much facilitate the use of SWNTs for many advanced applications, such as electronics and sensors.

The process proposed above involves the use of polyelectrolytes to achieve the layer-by-layer assembly of CNTs. The resultant CNTs stripes also contain the surfactant materials. For many applications, the stripes containing purely CNTs are desired. The layer-by-layer assembly is also a time consuming process. The resolution of the process is also limited due to the large molecular size of the polymeric surfactants. Fast and direct deposition of pure CNTs onto the substrates with controlled placement and alignment is still desired.

4.4 High speed directed self-assembly of SWNTs

4.4.1 Overview

Carbon nanotubes (CNTs) attracted huge research effort due to its unique structure and properties. CNTs are considered as promising building blocks for wide range of material and device applications, including nanoelectronics, sensors, photovoltaics and biomedicines. One of the most fundamental and challenging

problem existing with CNTs research is the high speed, high accuracy and low cost placement and alignment of CNTs. Previous efforts to align CNTs focused on the mechanical approaches such as mechanical stretching of a nanotube composite and gas/liquid flow induced alignment. Other approaches include mechanical stretching of a nanotube composite, gas flow induced alignment during CNT growth, alignment by magnetic and electric fields, flowing CNT suspension through microfluidic channels and many others [73-76]. Current approaches have limited accuracy and scaling capability and their controllability is far from ideal. Easy to process and highly effective CNTs alignment technique is still of paramount importance to realize the potential CNTs based device applications.

Chemical functionalization of CNTs surface allows the preparation of stable CNTs suspension in organic or aqueous solvent through debundle and dispersion process. Drop or spin cast of CNTs suspension on prepatterned substrate allows the selective adsorption of CNTs on the areas which are functionalized by self-assembled monolayers (SAMs). However, both the drop and spin cast lack the ability to control the thickness, uniformity and density. It is not practical for sub-micron patterning of CNTs nanostructures using these approaches. Electrostatic self-assembly of SWNTs in the pattern guided mode is an alternative approach to place SWNTs on the substrate surface [77]. Due to the electrostatic interaction between the negatively charged CNTs and the positively charged SAMs of substrate, dispersed CNTs will be attracted to the functionalized surface and form CNTs networks. However, the applications using generic directed self-assembly are still limited by the low processing rate and low

CNTs loading ratio. Current status in the self-assembly of SWNTs is still bottleneck for the massive application of CNTs in nanoelectronics.

Electrophoretic deposition (EPD) is a simple and versatile processing technique to manufacture coatings and films from nanomaterials including carbon nanotubes. It is among the approaches which have the widest application potential for nanomaterials. With EPD processing, the charged particles, which are dispersed in solvent, are moved by the externally applied electric field and finally accumulate on the electrodes. The nanoparticles reach the electrode continuously, therefore homogeneous and dense deposit can be formed. By controlling the intensity of the electric field, the deposition time and the choice of the substrate, the thickness of the deposited film can be well controlled. In the electrophoretic deposition, the electrode is usually highly conductive material, mostly metals. Our recent research found that externally imposed electric field will significantly accelerate the assembly process on the low conductive materials such as semiconductor silicon surface and even non-conductive surface such as silicon dioxide. The electric field will mobilize the charged SWNTs in the well dispersed and debundled suspension and greatly increase the adsorption rate of SWNTs on the surface.

There are also reports that ultrasonic agitation will significantly improve the process speed and quality in the self-assembly process for microscale and nanoscale particles [78-79]. The ultrasonic agitation or vibration helps the particles to overcome the friction and stiction during the assembly process. At the same time, the diffusion process of particles on the surface is also improved due to the additional energy from

the ultrasonic agitation. This results in an acceleration of the formation of the linkage between the nanoparticles and the surface, as well as the linkage among particles. Strong enough ultrasonic agitation also removes weakly bonded particles or particle aggregations, leading to improved assembly quality. The ultrasonic agitation has been employed in our experiments and verified to be a critical factor in achieving positioning and orientating the one dimensional SWNTs.

In this part of the dissertation research, we successfully developed a scheme which combines the bottom up self-assembly process and top down lithography patterning, to effectively align and place SWNTs on flat substrates. To speed up the process and improve the assembly quality, various chemical, electrical and mechanical approaches have been used, including applying electric field, chemical functionalization and ultrasonic agitation. The experimental characteristics such as the functionalization of the substrate surface and the design of the nanotube suspension, as well as the deposition time and electric field will be discussed.

4.4.2 Experimental setup and process design

HiPCO SWNTs were obtained from Carbon Nanotechnology Inc. (Houston, TX). The SWNTs were treated via sonication in 1:3 concentrated nitric-sulfuric acid mixture for 3 hours at room temperature before dispersed into DI water with ultrasonic agitation. KOH and HCl are repeatedly used to remove the carbonaceous and metallic impurities by using a filter. The SWNTs suspension with 5 ppm concentration is prepared by 2 hour ultrasonic agitation of the purified and covalently functionalized CNTs in water. This process gives us dispersed and well debundled CNT suspension.

Nanoimprint mold with 700nm grating period and 50% duty cycle is used in the experiment to prepare polymer patterned micro-structures. The grating is replicated in a thermally grown oxide layer on a silicon substrate from a commercial holographic grating (Ibsen Photonics) by nanoimprint lithography and reactive-ion etching. The mold depth is 350 nm. PMMA and amorphous Teflon AF 1600 are dissolved into toluene and perfluoro solvent (CF-75) respectively and spin coated onto the silicon substrate to prepared a thin film resist for nanoimprint. After thermal imprinting, the polymer grating structure was treated with brief oxygen reactive-ion etching to remove the polymer residue in the trench area. Polarized Raman microscopy was obtained by a Horiba Jobin-Yvon LabRam IR system. The SEM image was obtained by JEOL FE-SEM.

APTES was purchased from Sigma-Aldrich. Silicon wafers were cleaned by piranha solution for 30 min and rinsed by DI water and dried by nitrogen flow. An amine-terminated SAM was coated by immersing the wafers in the APTES IPA solution (1%) for 20 min. After rinsing the coated wafer by IPA and annealing on 120 ˚C hotplate for 30 min, a thin layer of polymer was spin-coated on the wafer for thermal nanoimprint process.

The polymer pattern was prepared by nanoimprint lithography. NIL is a lithographic process to transfer nanoscale structures by mechanically deforming the polymer resist on the substrate at elevated temperature and pressure. It is a very rapid and low-cost process for nanopatterning. Its generic ability to process various polymer

materials gives us much flexibility in choosing the patterning materials and surface treatment.

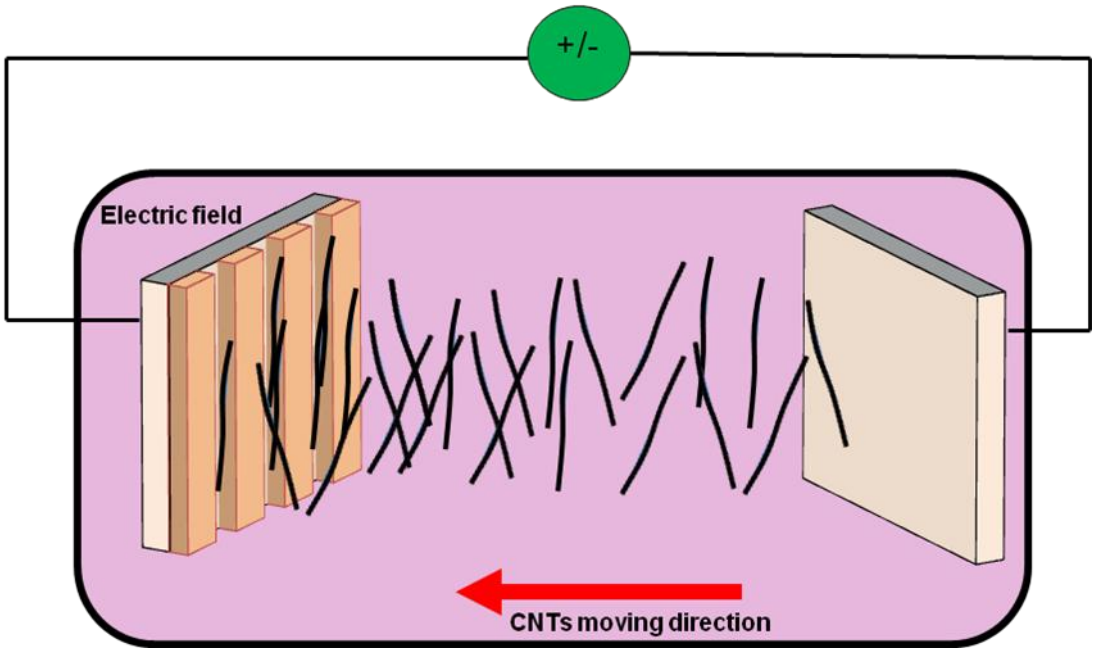

Figure 33. The schematic of the directed self-assembly process enhanced by externally imposed electric field.

As shown in Figure 33, the patterned substrate is immersed in the well dispersed SWNTs suspension and connected with power source as anode. Another metallic substrate is placed face to face, connecting with a power source as cathode. This setup will externally impose an electric field between the substrates and initialize the electrophoretic movement of the negatively charged SWNTs in the suspension. Electrostatic interaction between the functionalized SWNTs and substrate surface will immobilize the SWNTs upon they attach to the surface. Due to the geometric confinement, the SWNTs are placed and aligned along the trench area on the substrate.

The deposition container is placed inside an ultrasonic agitator and the sonication will improve the surface diffusion of the SWNTs and remove the weakly bonded SWNTs from polymer surface.

The strategy developed for this work not only combines the top-down lithographic patterning technology and bottom-up self-assembly approach, but also utilizes the externally imposed electric field and mechanical agitation to accelerate the process and improve the assembly quality.

Traditional self-assembly processes usually rely on the chemical functionalization of substrate surface and SWNTs surface. Lots of effort have been devoted to optimizing the intermolecular forces by maximizing the negative charges on the nanotube sidewalls and the positive charges of the substrate [80]. Other than the surface chemistry, we only have limited ability to control the density and the thickness of the assembled SWNTs on the substrates, such as the suspension concentration and the deposition time. The lack of the effective control of the assembly process not only makes the assembly process very slow, but also prohibits preparation of SWNT stripes with wide-range tunable properties and good robustness.

In principle, the introducing of multiple approaches would allow us to control the assembly process over wide tunable range. Figure 34 illustrates how directed self-assembly process behavior can be controlled by chemical, physical and mechanical factors, namely surface functionalization, electric field and ultrasonic agitation. We denote the curve in the figure as A-S (Adsorption vs. Sonication Strength) curve.

Ideally, for certain SWNT suspension after chemical treatment, the adsorption of the SWNTs on the dipped substrate is determined by the surface charge density and chemical group on the surfaces in a generic assembly process. Intrinsic diffusion moves the SWNTs to the functionalized substrate surface. The number of particles hitting the surface is constant with defined concentration and temperature. When external electric field is applied in the suspension and moves the negatively charged SWNTs towards the substrates, the adsorption is increased due to the concentrated SWNTs suspension immediately over the substrate surface, as well as the nanopaticles' drift due to the electric field. The interception point of the A-S curve to the y-axis with electric field enhanced assembly process is always larger than the interception point of in generic assembly process.

Applied ultrasonic agitation to the suspension will often cause desorption of weakly bonded SWNTs from the substrate surface. Ultrasonic agitation strength can be characterized using the amount of power per gallon of solution. The adsorption decreases with an increasing ultrasonic agitation strength. In an extreme case, the desorption caused by the ultrasonic agitation dominates over the adsorption caused by the electrostatic interaction, the residual SWNTs on the substrates becoming zero, where is the interception point of the curve and the x-axis. Due to the drift of SWNTs as well as the increased charge density of the substrate caused by the electric field, the adsorption for the electric field enhanced assembly would be larger than the generic self-assembly at the same chemical and mechanical condition. In our case, the electric field is configured so that the adsorption of the SWNTs onto the substrate surface is

enhanced. Larger electric field strength yields higher adsorption rate. If the electric field is reversed, the adsorption is discouraged and less SWNTs will reside on the substrate. This gives us the ability to the control the assembly rate in the nanomanufacturing process by simply controlling the electric field strength.

The surface treatment by chemical functionalization is also important to realize the nanomanufacturing of SWNTs nanostructures. It is reported that SAM patterning is used to achieve selective adsorption of SWNTs onto desired area on the substrate surface [80, 77]. In another approach, polymer pattern is fabricated by lithography process and selective adsorption is expected to occur on the exposed area without polymer coverage. In both cases, the appropriate chemical functionalization of the surface will increase the adsorption. If the surface chemistry is different, there is going to be two different A-S curves. We name this difference as the surface adsorption contrast. Surface adsorption contrast is related to the surface energy as well as the surface chemistry of the substrate. On the other hand, such surface contrast also yields different interception points with x-axis with different surface properties.

In an ideal case, the surface chemistry will lead to no adsorption of SWNTs on areas where we don't expect residual SWNTs (adsorption undesired area) and maximum adsorption on areas where we expect residual SWNTs (adsorption desired area). Practically, there is hardly realizable because there is always SWNTs residing on the adsorption undesired area, even if we did the surface treatment. This is always the case if we applied electric field during the assembly process. Nevertheless, we can

still enlarge the gap between the two A-S curves by achieving larger surface contrast between the adsorption desired area and adsorption undesired area.

During the process, if we applied weak ultrasonic agitation, the desorption caused by the agitation is not strong enough to remove the SWNTs on the adsorption undesired area. However, too strong agitation is also problematic because it may possibly reduce the adsorption in the adsorption desired area and even totally remove the SWNTs residuals in these areas. To manufacture patterned SWNTs stripes with good quality, we can only operate the system in certain ultrasonic agitation strength range, which we call working window. Practically, the working window is possibly even smaller because the polymer grating may be stripped from the substrate due to very strong agitation. A robust process needs surface chemistry to prepare the patterning with large surface contrast, so that we have wide working window to flexibly configure the manufacturing parameters.

The introducing of externally imposed electric field would elevate this problem. Figure 35 illustrates the current process ability in term of achieving the adsorption and selectivity. Dipping of substrate without any surface treatment usually only yields occasional adsorption of SWNTs on the surface. Carefully designed and uniform surface functionalization will significantly improve the adsorption and yield much denser SWNT networks. Electric-field enhanced self-assembly will dramatically improve the adsorption of SWNTs and accelerate the assembly speed. In the nanomanufacturing for nanoelectronics, clear and clean patterning of SWNTs structures are required. Nanopatterning has to be made before the deposition of

SWNTs on the surface. SAM patterning is one of the approach. The underlying idea with SAM patterning is to chemically functionalize the surface on selective areas so that the adsorption of SWNTs only occurs at the functionlized area. However, the adsorption of SWNTs on non-functionalized area is usually unavoidable. Ultrasonic agitation will improve the contrast of adsorption rate between the functionalized area and the non-functionalized area, since the mechanical agitation will remove the weakly bonded SWNTs from attaching to the adsorption undesired surface. Even with improved contrast, critical application still desire a process which yields clean and clear patterning after the SWNT deposition. Sacrificial layer of polymer may be used in the nanomanufacturing process. The lift-off of the sacrificial layer after deposition will eventually remove all the undesired nanoparticles on top of the polymer. Simultaneously utilizing the electric field, polymer patterning and the ultrasonic agitation is a viable strategy to achieve these critical requirements in the nanomanufactring. Monolayer patterning usually cannot give enough selectivity for patterned SWNT assembly. A sacrificial layer, such as polymer resist, is required to achieve high quality patterned SWNT structures.

With the anisotropic nanoparticles, such as SWNTs, when the pattern geometry becomes smaller and smaller, the nanotubes will not be easily deposited into the trench area and often sit on top of the protrusion to form a bridge across two protrusions. This may cause a big problem in the patterning of submicron SWNT structures. In our work, we adopted the highly hydrophobic material Teflon AF 1600 as the sacrificial materials. Teflon AF 1600 is an amorphous polymer which is used as

hydrophobic coating. Teflon AF is a family of amorphous copolymers that retain the properties of fluorinated plastic and dissolves in some perfluorinated solvents such as fluorinert FC-75. This makes it very suitable as the patterning resist in the directed self-assembly process.

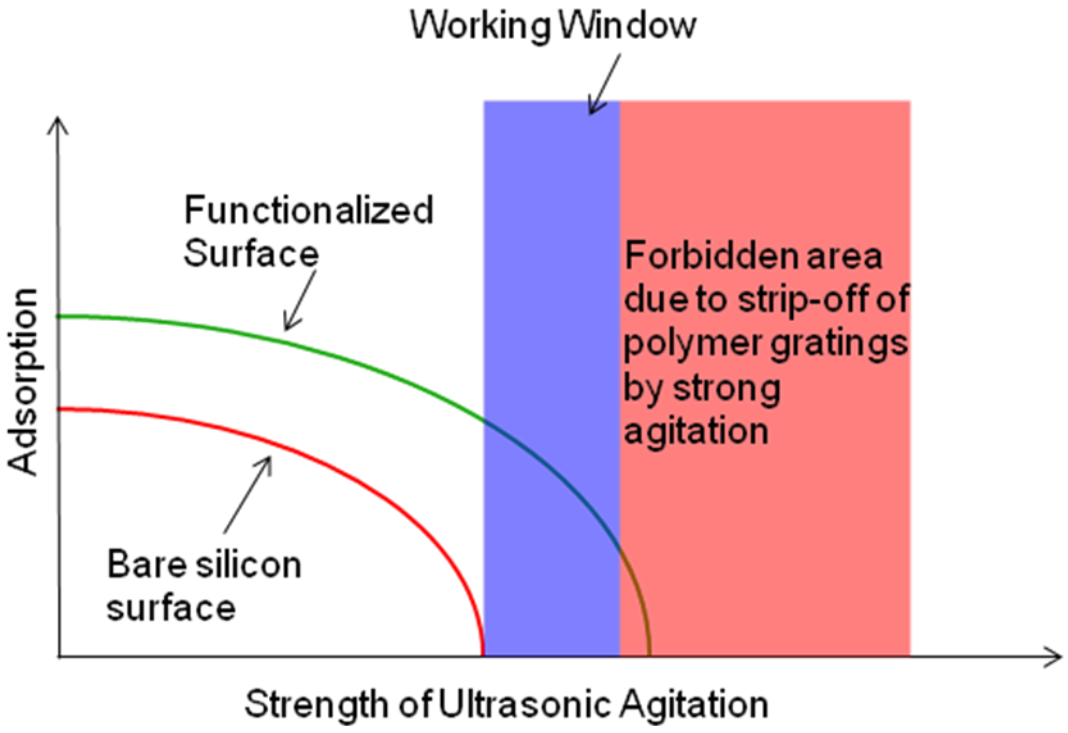

Figure 34. Working chart for nanomanufacturing of SWNTs nanostructures.

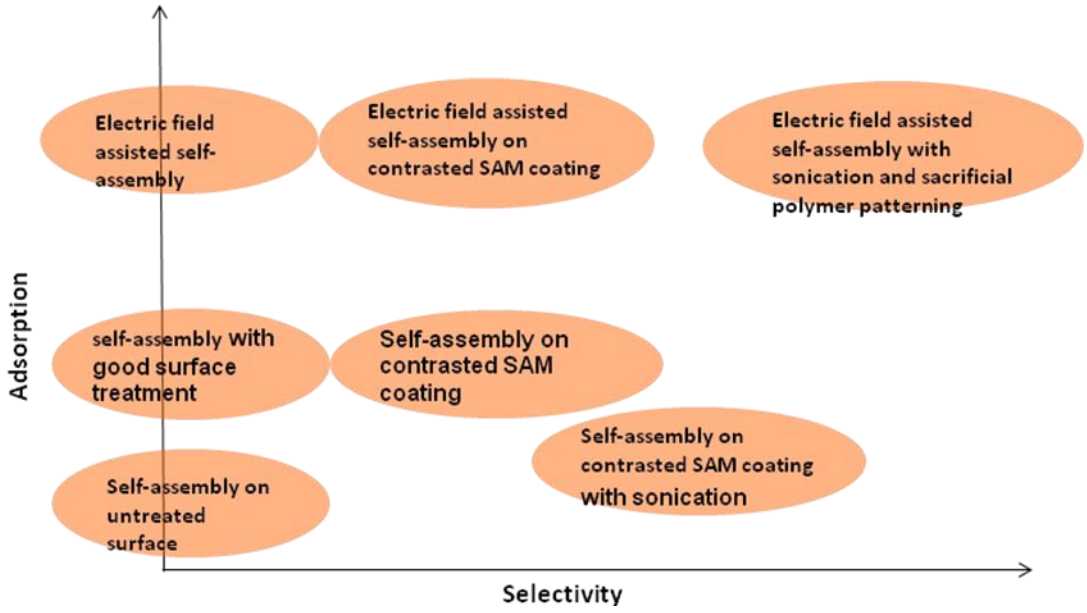

Figure 35. The comparison of nanoparticle assembly process in term of the ability to achieve both high-level adsorption and high contrast pattern.

Figure 36 shows the experimental results with different process conditions. Polarized Raman spectroscopy is used to characterize the SWNT stripes obtained from the high speed directed self-assembly. Figure 37 shows the polarized Raman spectra for a sample prepared using Teflon-AF template with 700 nm period grating (Figure 36 (e)). The process uses an electric potential of 10 V over 1 cm distance between the electrodes and a deposition time of 1 minute. The isotropic property in polarized Raman spectroscopy indicates high level of alignment of the SWNTs in the stripes obtained by the above process. According to the I-V characterization in Figure 38 for the same sample, the calculated conductivity is about 1.5 s/cm, which is much higher than the value obtained using layer-by-layer approach. This may be explained based

on the fact that the pure SWNT stripes have better inter-tube contacts compared with the tubes wrapped with polyelectrolyte.

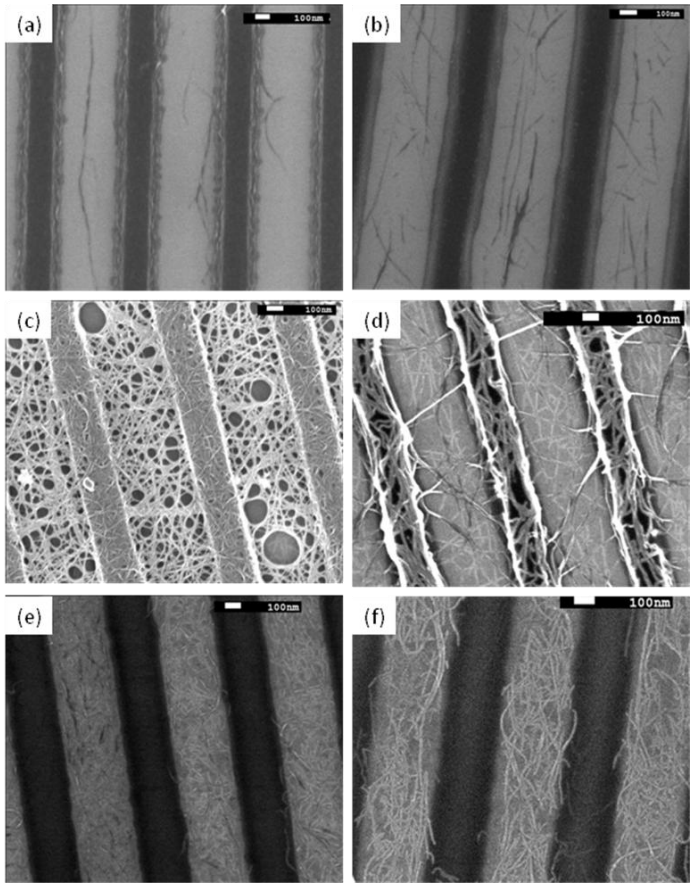

Figure 36. Directed self-assembly of SWNTs. (a) FDTS coated surface; (b) APTES coated surface; (c) Strong electric field on APTES coated surface with PMMA template; (d) Strong electric field with ultrasonic agitation on APTES coated surface with PMMA template; (e) Same as (d) but in Teflon-AF template; (f) SWNTs strips after removal of Teflon-AF template for case (e). In all the cases, the distance between two electrodes is 1 cm. Deposition time is 3 minutes for (a) (b) (c) (d) and 1 minute for (e) (f). Deposition voltage is 20V for (a) (b), 100 V for (c) (d) and 10 V for (e) (f).

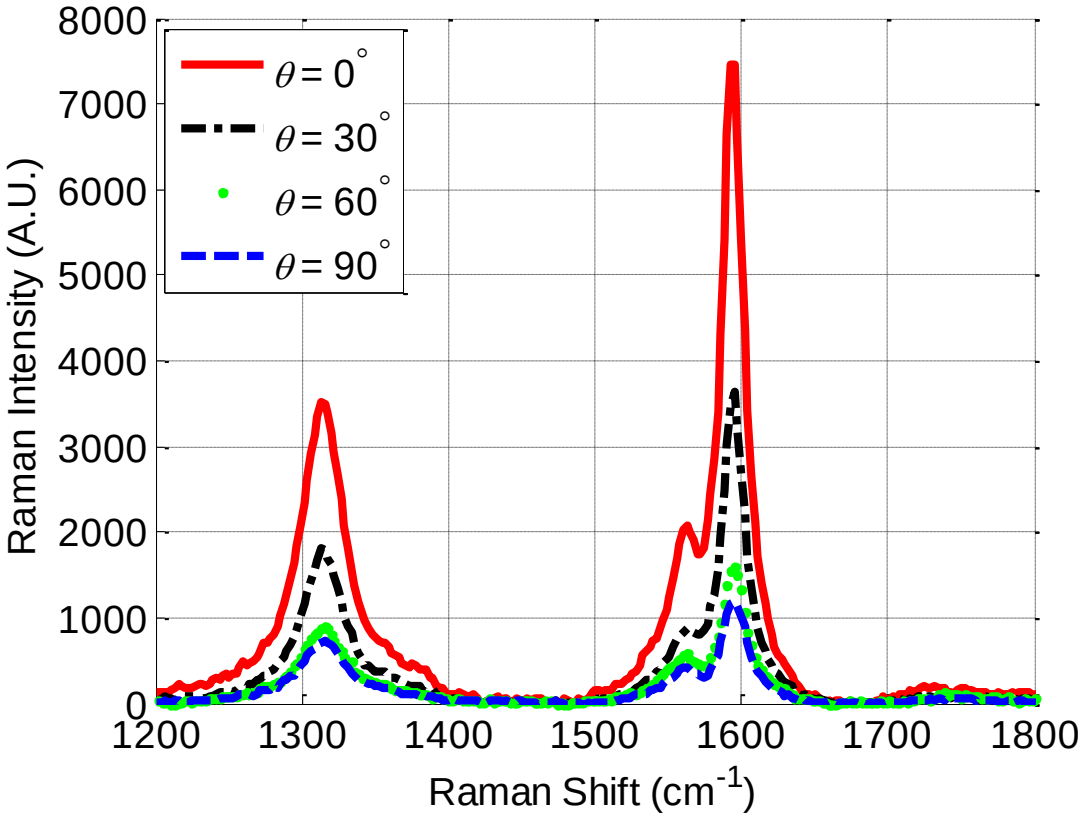

Figure 37. Polarized Raman spectra of SWNTs stripes prepared by high speed directed self-assembly. θ denotes the angle between the polarization directions of the incident laser light and the longitudinal direction of the deposited CNT stripes.

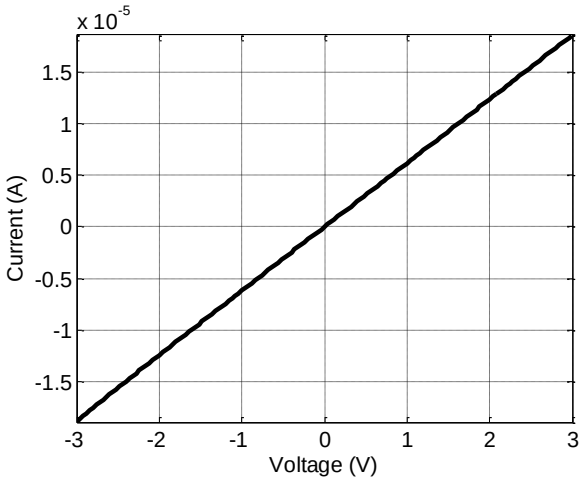

Figure 38. I-V characteristic of aligned SWNTs stripes.

4.4.3 Preparation of SWNTs suspension

To carry out nanomanufacturing of SWNTs to prepare positioned and aligned SWNT stripes on a substrate, it is important to prepare a stable dispersion of SWNTs in aqueous or organic solvent. This can be accomplished by either non-covalent functionalization of the SWNT surface or covalent funcitonlization. In our experiment, an aqueous suspension is preferred since we will use polymer gratings in the directed self-assembly process and aqueous solvent will not dissolve most of the polymers. The suspension is prepared through the treatment of the raw SWNTs with concentrated nitric and sulfuric acid together with ultrasonic agitation. The strong acidic and oxidative condition results in the introduction of carboxyl groups in the tube caps as well as defects sites on the sidewalls.

The oxidation process results in the functionalization of carbon nanotubes surface with carboxyl groups, particularly in the tips of the tubes and defects sites on

the tube surfaces. The existing of carboxyl group is critical in at least three points. Firstly, the existence of negatively charged carboxyl group on the SWNTs surface further results in the electrostatic double layer, which in turn balances the van der Waals attraction between tubes and form stable dispersion. Secondly, the charges of the carboxyl groups make it possible to use electrophoresis in the following deposition and alignment of carbon nanotubes. Thirdly, it allows further modification of carbon nanotubes because of the reaction between the acid functionalities with alcohols or amines. The reaction is the fundamental force to secure the adhesion between nanotubes and amine group terminated substrate surfaces. The further modification also enables nanotubes to find active roles in a wide range of applications such as photovoltaic and biological technologies.

The oxidation process inevitably results in partial loss of electronic structure and optical properties of the SWNTs and loss of materials as well. Some of the CNT materials also are lost during the oxidation process. New carbonaceous impurities are generated during the process. However, the oxidation process facilitates further chemical modification of the SWNTs, such as forming the amide linkage with alcohols or amines.

Carbon nanotubes are usually made from carbon monoxide or carbon sources by using arc discharge, laser ablation or catalytic gas-phase growth. The raw carbon nanotubes made from these approaches usually contain many kinds of impurities such as catalytic metallic particles and carbonaceous impurities (amorphous carbon, graphene platelets). Delicate purification processes are almost always needed prior to

further processing and device applications. A very popular purification process involves the use of strong acid and oxidative conditions together with ultrasonic agitation. Combination of concentrated nitric acid and sulfuric acid is most common this process. It is found in our research that control of the carbonaceous impurity to a low level is critical to the directed self-assembly process, because the impurities will compete with the SWNTs and form chemical bond with the chemically functionalized substrate surface, leading to less SWNTs to form the stripes. The carbonaceous impurities, such as graphene oxide platelets and amorphous carbon, are bad for the devices applications, since they are typically less conductive than SWNTs.

Hydrogen chloride and KOH are often used to effectively remove metallic impurities and carbonaceous impurities [81]. We use both the KOH and HCl in the purification process to ensure minimum loss of materials and generation of impurities. Figure 39 compares the SWNTs before and after this purification process, indicating the process can effectively remove most carbonaceous and metallic impurities. It is believed that the high purity of SWNTs is good for effective placement and orientation of SWNTs, as well as the performance of devices fabricated by these SWNTs.

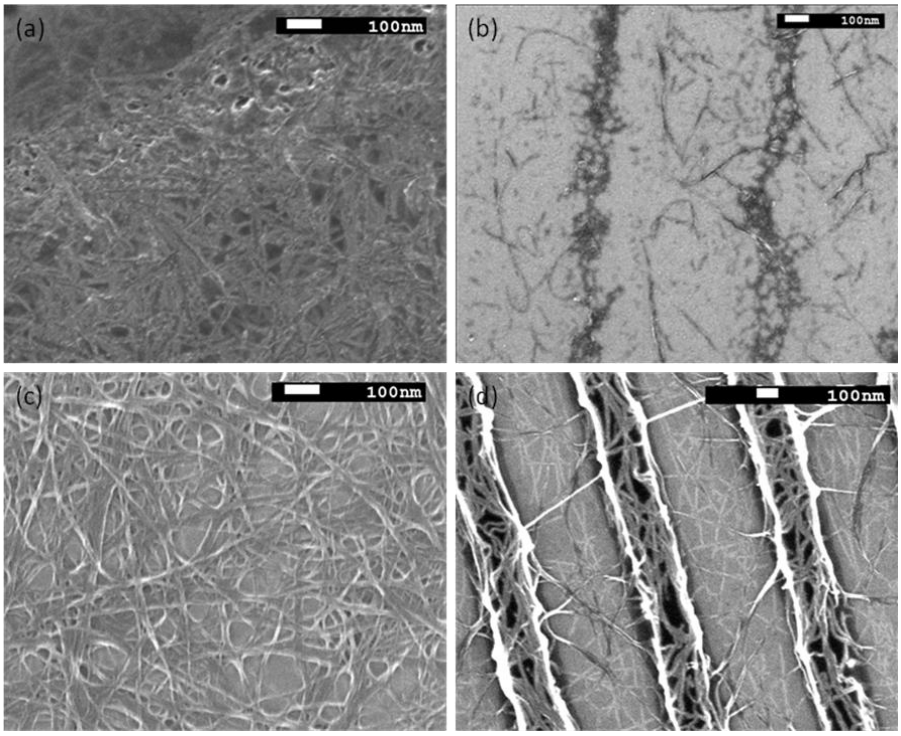

Figure 39. Comparison of SWNTs before and after purification. (a) SWNTs aggregation of unpurified SWNTs. (b) Directed self-assembled SWNTs using unpurified SWNTs suspension. (c) SWNTs aggregation of purified SWNTs. (d) Directed self-assembled SWNTs using purified SWNTs suspension.

4.4.4 Surface functionalization

Selective placement of nanoparticles can be achieved by the manipulation of surface properties, for instance surface patterning with self-assembly monolayer. This is via the successful establishment of the electrostatic or chemical bond linkage between the nanoparticles and the substrate surface and the prevention of adsorption of nanoparticle to the area, in which nanoparticles are not desired. For example, SAM pattern can be formed by growing aminosilane SAM in the area, in which adsorption

and linkage are desired, and hydrophobic FDTS SAM in the area in which adsorption is not desired. The positively charged NH_2 group at the APTES SAM would attract the negatively charged SWNTs by the carboxyl groups and form a stable electrostatic linkage. Due to the hydrophobic property and chemical inertness, SWNTs will be rarely deposited on the FDTS coated surface. Figure 36(a) and (b) demonstrated that more SWNTs will be deposited on the APTES treated surface than the FDTS treated surface. Surface treatment is critical for the process robustness, because the good surface treatment results in high adsorption contrast and wide working window, and provides much more flexibility to the directed self-assembly process for nanoparticles.

However, the traditional approach using the patterned SAM coating is not sufficient for positioning and orientating SWNTs due to two observed facts. Firstly, even with high contrast coatings, the hydrophobic coating will not eliminate the adsorption of SWNTs. SWNTs can be observed across the grating pattern with both ends of SWNTs sit on the amino group terminated surface and the middle part on the hydrophobic FDTS surface. This problem becomes worse when the applied electric field is introduced, because the electric field will force the negatively charged SWNTs to attach to the surface even the surface is hydrophobic, as shown in Figure 36(a). Secondly, the adsorption contrast by the patterned SAM surface would not give enough preference for the orientation of the SWNTs. We feel use of polymer patterning and surface functionalization is a solution to overcome the above problems. The lift-off of the polymer after SWNT deposition will ensure no SWNTs residue on the area in which adsorption is not desired. The geometrical and mechanical

confinement would give higher preference for the orientation of SWNTs. This is particularly useful for the case electric field is introduced during the directed self-assembly process.

Even with polymer patterning, there is still serious adsorption of SWNT to the sacrificial polymer, as shown in the Figure 36(c) and (d). Particular efforts have to be made to minimize this adsorption. To prevent the SWNT absorption on the polymer, we adopted the amorphous Teflon AF 1600 in the process. A thin layer of PMMA and AF 1600 are spin-coated on the APTES treated substrate. Nanoimprint process is carried out to form the polymer pattern and oxygen reactive ion etching is used to remove the residual polymer in the trench area. Finally, the sample is immersed in the APTES isopropanol solution to form a SAM layer on the trench area. This results in a sample with amino-terminated surface in the trench area for maximum adsorption of SWNTs and hydrophobic Teflon polymer surface on the protrusion area to minimize the adsorption of SWNTs. The polymer with hundred nanometer thickness will give good geometric confinement for effective SWNT alignment. Figure 36(e) shows that SWNTs can be deposited and confined into the trench area of the grating structure, while there are virtually no SWNTs adhered to the Teflon protrusion.

4.4.5 Electrophoresis enhanced self-assembly

As we discussed in the experimental design part, the generic self-assembly of nanoparticles is slow and lacks of the ability to prepared high-density and high-quality film. The introduction of electric field in the assembly process can accelerate the assembly speed as well as the assembly quality. This essentially makes the process an

EPD process. EPD is an electrochemical method very useful to prepare nanomaterials due to its simplicity and versatility. In an EPD process, electric field is applied between electrodes and the charged particles suspended in a solvent move towards the oppositely charged electrode and deposit into compact and homogeneous film. The introduction of electric field in the process gives us a lot more ability to tune the process conditions by controlling the intensity of the electric field, the deposition time and the choice of substrate.

According to the electrophoresis theory, the charged particles will be forced to move towards the electrode with an electrophoretic mobility,

$$\mu_{\epsilon} = \frac{\varepsilon_0 \varepsilon_r \zeta}{\eta}$$

where ε_0 is the permittivity of free space, ε_r is the dielectric constant of the dispersion medium, η is the dynamic viscosity of the dispersion medium and ζ is the zeta potential.

This movement results in higher concentration of SWNTs at the electrode surface and the accumulation of SWNTs will improve the opportunities to form electrostatic bonds between the functionalized electrode surface and the SWNTs. High electric field results in high assembly speed. Control of the applied electric field and deposition time will give us the ability to control the final assembly density of SWNTs, as shown in Figure 40. Our observation indicates that even the non-conductive electrode can be used for the deposition of SWNTs. We conclude that the primary

function of the electric field is to move the SWNTs towards to the electrode to accumulate.

Strong electric field will yield two facts. Firstly, the drift of the SWNTs towards the electrode is rapid. Secondly, the strong electric field yields dense SWNT films on the substrate.

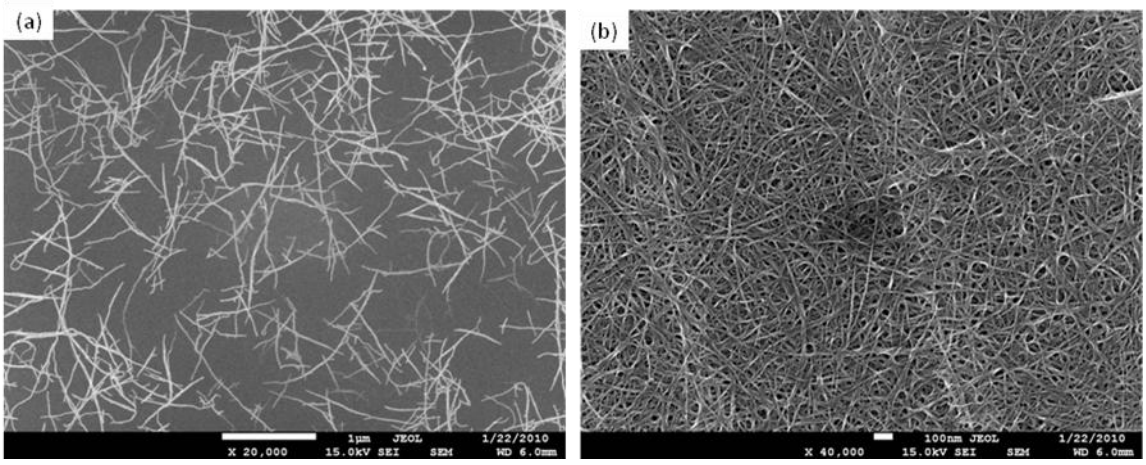

Figure 40. Electrophoretic deposition of SWNTs with different electric voltage. (a) 5 volts (b) 100 volts.

4.4.6 Ultrasonic agitation

It is found that ultrasonic agitation is a critical factor in the orientation of SWNTs in our process. The mechanical agitation will help the SWNTs to overcome the stiction and friction and thus the SWNTs have higher opportunity to drop into the grating trench and form electrostatic bond with the functionalized surface. The ultrasonic agitation will also accelerate surface diffusion of SWNTs and remove weakly bonded SWNTs. This will results in less SWNTs attached to the surface in

which the adsorption of SWNTs is not desired. These explanations are verified by the experiments. As shown in the Figure 36(c) shows a process without agitation and with strong applied electric field. The strong electric field virtually deposits SWNTs onto any substrate surface, forming a mesh to cover the patterned structure. The ultrasonic agitation does a critical role to help the SWNTs to fall into the grating trench. As shown in Figure 36, many SWNTs are found in the trench apparently.

As we discussed in the experimental design part, too strong ultrasonic agitation is also undesired, due to its destruction to the polymer pattern on the surface. Figure 41 shows the destructed polymer grating structures in the experiments. Ultrasonic agitation strength and time should be monitored in the process to ensure high yield and fidelity of the directed self-assembly process. To make a robust directed self-assembly process, it requires additional adhesion promoting process during the preparation of polymer pattern. APTES SAM coating is beneficial to improve the adhesion between the PMMA polymer and silicon surface. Thermal annealing also helps the polymer structure to more resist to the mechanical agitation.

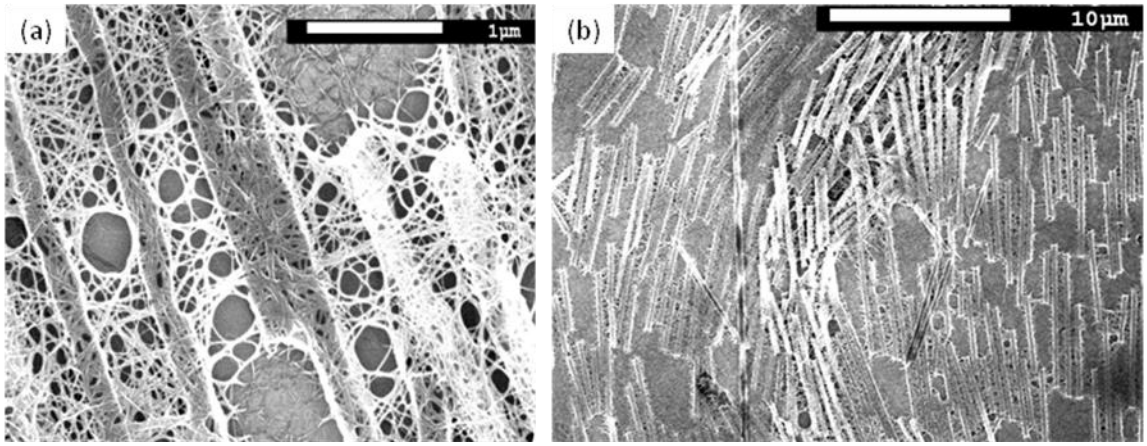

Figure 41. Strong ultrasonic agitation cause the polymer pattern destructed.

4.4.7 Summary

The insufficient ability to manipulate SWNTs in the nanoscale has limited their applications in the large volume manufacturing of nanoelectronic devices. A fundamental and challenging problem is the efficient placement and alignment of SWNTs on a flat substrate on the wafer level. By introducing the electric field enhanced electrostatic self-assembly, as well as combining the surface chemical modification and mechanical agitation in the solution process, we present an accelerated self-assembly process, which yields high-speed and high-quality nanomanufacturing of patterned and aligned SWNT stripes. The high selectivity and robustness of the process have opened up a door to the large-scale and high-volume production of SWNT-based structures and materials for many applications, such as nanoelectronics and sensors.

4.5 Future work

4.5.1 Morphology-property relations in aligned-CNT stripes

The electrical properties of the aligned-CNT stripes are highly dependent on the stripe configuration, mainly the direction and connectivity of individual CNTs inside the stripe. The electrical conductivity can be measured from a simple two-probe or four-probe measurement, and the apparent carrier mobility of the stripes can be derived from the electrical characteristics of the field-effect transistors in which those stripes act as active conduction channels. The hypothesis on electrical conductivity and apparent carrier mobility of the CNT stripes is that these parameters are highly dependent on the electrode gap size or the transistor channel width (Figure 42), as well as the alignment level of individual CNTs in the stripes (Figure 43). Most SWNTs and MWNTs in our suspension have a length from several hundred nanometers to several microns. If the gap size or channel width is around 50 nm, which is much shorter than the length of an individual CNT, the measured data will be mostly related to intrinsic carrier transport through the length of the CNTs. For gap size or channel width that is much wider (10 μm) than the individual CNT lengths, the measured data will be related to carrier transport both through individual CNTs and across different tubes, which will become highly dependent on the CNT configuration inside the stripes. To test this hypothesis and obtain data for comparison with literature models [48], conductivity and carrier mobility data will be collected in a series of measurements where the electrode gap or channel width are varied from 50 nm to 10 μm on CNT stripes with various levels of alignment. Different CNT alignment levels can be easily

achieved by using trenches of different sizes (Figure 43). After depositing the aligned-CNT stripes on a silicon substrate with a thermally grown oxide layer, metal contact pads are placed on top of the stripes by electron-beam lithography for submicron dimensions or photolithography for larger dimensions, metal evaporation, and lift-off. Palladium will be used as contact metal to avoid the formation of Schottky barriers [82] because it has high work function and good wetting on CNTs [45]. The transistor action can be easily achieved using the same platform by using the back-side silicon as a gate electrode. Several gap sizes or channel widths will be chosen according to the length of SWNTs and MWNTs in the suspension. Collected data will be analyzed to understand how connectivity and alignment level affect the electrical properties of the CNT stripes and validate electrical conduction models for CNT aggregates.

To study morphology-property relationships in aligned-CNT stripes, quantitative alignment information is needed. This can be obtained by polarized Raman spectroscopy and polarized absorption spectra. By rotating the polarization direction of the light source in Raman and UV-vis-NIR spectroscopy, it is straightforward to evaluate CNT alignment level based on the change in spectra signals. With microscope integration, polarized Raman and absorption spectra can be collected on individual stripes. Optical birefringence in aligned-CNT stripes, which is a consequence of CNT alignment, is also observed in our preliminary results and it can provide supplemental data on CNT alignment. In addition to spectroscopic measurements, direct visualization of CNT alignment will be acquired by HR-TEM, high-resolution field-emission SEM and AFM. The results obtained from analytical

tools and direct visualizations will paint a clear picture on CNT morphology in deposited stripes, which will increase our knowledge on the relationships between trench width and CNT morphology (Figure 43) in deposited stripes.

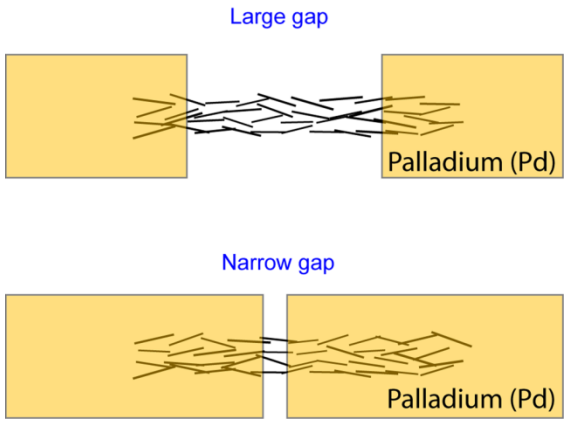

Figure 42. A schematic of CNT electrical measurement with large and narrow electrode gaps. In large gap measurements, the inter-tube transport dominates, while the intrinsic CNT properties dominate the electrical properties of the aligned-CNT stripes in narrow gap measurements.

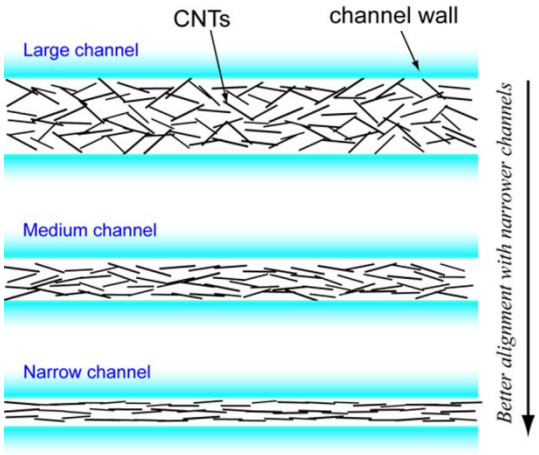

Figure 43. A schematic of aligned-CNT stripes deposited from channels with different cross-sectional dimensions. Nanochannels lead to better alignment and hence better electrical properties of the stripes.

4.5.2 Multidirectional CNT alignment

Our developed high speed directed self-assembly process has one huge advantage over other methods in that it is very simple to deposit CNT stripes with random alignment directions at specific locations. To demonstrate this, electron-beam lithography or nanoimprint lithography will be used to pattern isolated trenches of various sizes, 1D trench array, 2D trench grid and circular trench array for ESA of aligned-CNT stripes (Figure 44).

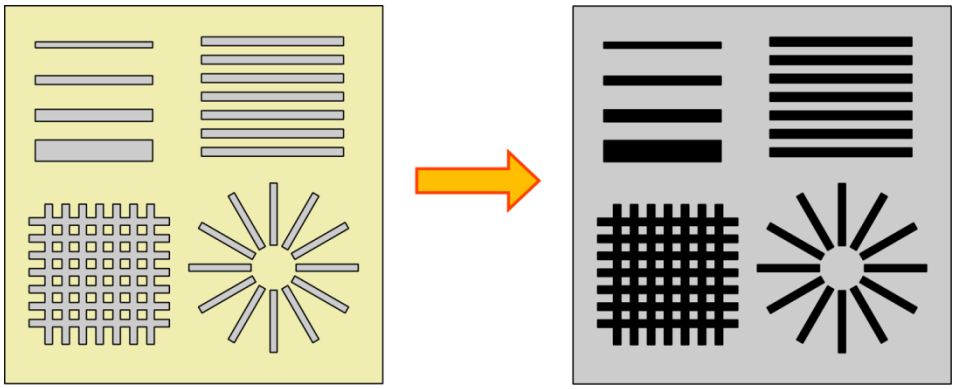

Figure 44. A schematic of arbitrary CNT alignment and placement by high speed directed self-assembly. Left: Polymer microstructures (individual lines of various sizes, 1D line array, 2D grid and circular array) patterned by nanoimprint or electron-beam lithography for high speed directed self-assembly of aligned-CNT stripes; Right: aligned-CNT stripes after removal of the polymer template.

After CNT deposition and polymer template removal, aligned-CNT stripes of various directions and placements can be achieved. This flexibility in CNT alignment and placement paves the way for building complex microelectronic circuits based on CNT stripes. If nanoimprint templates are fabricated first by electron-beam lithography and reactive-ion etching, the polymer microstructures can be replicated at low cost for mass manufacturing. It is thus envisioned that successful extension of this project will have significant impact on developing CNT-based microelectronic devices and circuits, which is the original expectation that has stimulated tremendous interests and research activities in CNTs in last two decades.

4.5.3 Microelectronic devices based on pure semiconducting CNT stripes

Pure semiconducting CNT stripes are ideal for electronic applications because of low off (leakage) current as a result of metallic CNT removal. Another distinctive advantage of using semiconducting CNT stripes as active materials in solid-state devices is that multiple CNTs are organized in parallel. The parallel configuration can greatly reduce total contact resistance and increase output current. Electronic devices based on parallel CNTs are gaining increasing attentions in recent years as a practical solution for high-frequency field-effect transistors [83-84]. Due to aforementioned advantages of our high speed self-assembly technique, multiple CNT stripes can be deposited in an array on a substrate. Using conventional microelectronic fabrication processes, the stripes can be cut into segments on which transistors can be made. Integrated circuits can then be easily constructed by wiring those transistors by metal interconnects.

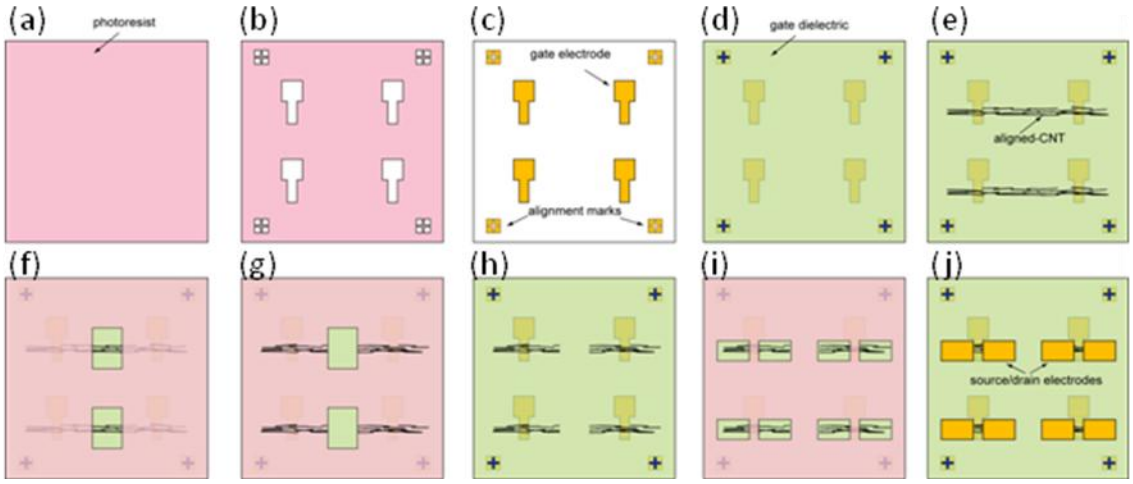

Figure 45. Schematics of the fabrication process of field-effect transistors based on pure semiconducting aligned-CNT fibers. (a) spin-coat photoresist on a substrate; (b) photolithography to define gate electrodes and alignment marks; (c) gold evaporation and lift-off to form gate electrodes; (d) sputtering or CVD oxide layer as gate dielectric; (e) PMMA template patterning and deposition of aligned-CNT stripes using high speed self-assembly process. (f) photolithography to open window for selective removal of CNTs; (g) oxygen plasma etching to cut the aligned-CNT fibers into segments; (h) discontinuous CNT segments after removing photoresist; (i) photolithography to define source and drain electrodes; (j) palladium evaporation and lift-off to form source and drain electrodes.

The fabrication of the field-effect transistors with the aligned-CNT fibers is depicted in Figure 45. Starting with a substrate, photoresist is applied on the substrate by spin-coating (Figure 45(a)). The bottom gate electrode and alignment mark patterns are patterned by photolithography (Figure 45 (b)). Gold thin film is evaporated on the

photoresist and lift-off in acetone will yield gold electrodes on the substrate (Figure 45 (c)). An oxide layer is then deposited to serve as gate dielectric by sputtering or chemical-vapor deposition (CVD) (Figure 45 (d)). A PMMA thin film is then spin-coated and patterned by nanoimprint or electron-beam lithography. The aligned-CNT stripes with pure semiconducting CNTs are then deposited by guided ESA, and followed by pyrolysis in vacuum (Figure 45 (e)). Alignment marks can ensure the placement of the CNT stripes with a precision of at least 1 μm. Since the CNT fibers are long, they must be cut into segments to provide good isolation between devices. To achieve this, photolithography will be used to open windows where sections of CNT fibers need to be removed (Figure 45 (f)). The exposed portion of the CNT fibers will be removed by oxygen plasma etching (Figure 45 (g)). After photoresist removal, short segments of aligned-CNT fibers are left on the substrate (Figure 45 (h)). The source/drain electrodes can then be defined by photolithography as shown in Figure 45 (i). Finally evaporation of palladium and lift-off in acetone complete the fabrication process. The top source/drain electrode and the choice of high-workfunction palladium with good wetting on CNTs [45] will ensure low contact resistance for better device performance.

In the future work, we propose the fabrication of an array (100×100) of field-effect transistors based on pure semiconducting CNT fibers. Devices with channel widths of 10 μm, 0.5 μm and 50 nm will be made. The field-effect transistors will be characterized with semiconductor analyzer to obtain its electrical performance. Due to 1D alignment of CNTs inside the fibers, it is expected that the fibers have anisotropic

carrier transport. For future circuit applications, this anisotropy can be circumvented by always placing source and drain electrodes along the CNT alignment direction. This can be easily achieved because high speed self-assembly allows aligned-CNT fibers to be deposited along predetermined directions. Even though carrier transport anisotropy can be addressed, statistical variation in material property among CNT fibers deposited from the same batch may still be present. The uniformity of device characteristics is important for circuit applications and will be evaluated by comparing device performances at different locations of the substrate. Deep sub-micron devices are expected to have much better performance and better uniformity because main carrier transport mechanism is through the length of the CNTs instead of cross-tube transport. High-performance circuits can be easily fabricated using this transistor arrays in future endeavor.

CHAPTER V

CONCLUSION

Robust manufacturing processes for nanoscale devices and structures are very important and challenging both for research and industrial production in many areas, such nanoelectronics, biomedicine, energy conversion and storage, and novel functional materials. Two challenging topics existing with the nanomanufacturing are three dimensional integration and rapid and controllable assembly of nanoparticles. Conventional top-down nanoimprint lithography is further developed by optimizing the process and introducing a generic transfer-bonding for fabrication of 3D polymer structures in the micro- and nanoscale. The new development allows the integration of more components into multilayer structure on a single chip to fully achieve the concept of "lab-on-a-chip". By combining the top-down lithography and bottom-up self-assembly techniques, a rapid and controllable process has been developed to position and align one-dimensional nanoparticles, for example, SWNTs.

Nanoimprint lithography is a simple and versatile process to build patterns in soft materials. It is simple and cheap while maintaining high resolution and throughput. Nanoimprint is inherently a three-dimensional patterning process. A lot of materials can be used as patterned media. It is compatible to direct patterning of functional polymers. These advantages have made nanoimprint a valuable tool for many novel applications, including nanoelectronics, nanomaterials and microfluidic applications. Many modification and improvement have been made such that nanoimprint has become widely used in many research and industrial areas.

Three-dimensional multilayer polymer microstructures are of particular interest to us because their light weight, low cost, easy processing and multiple functionalities is beneficial to many useful applications in electronics, photonics and bioengineering. We successfully developed a process to fabricate three dimensional multilayer microstructures in thermoplastic polymers using optimized layer-transfer and transfer-bonding techniques. Controlling the surface properties by growing self-assembled monolayer of surfactant coating and the twist-demolding ensures the layer to be able to be transferred to the existing bottom polymer structures. The control of the processing temperature will allow good transfer-bonding while maintaining the fidelity of the bottom structures. This generic approach to fabricate 3D polymer structures allows the integration of the microfluidic system and the photonic detection system in a single chip so that an ultra-compact and cost-effective lab-on-a-chip detection system is realizable.

The applicability of the developed approach is demonstrated by designing and fabricating an exemplary optofluidic system, a fluorescence detection system. In the proposal, the microfluidic and fluorescence detection system are integrated onto a single chip using a vertical multilayer configuration. The system possibly includes 1) an LED as light source; 2) a tunable optical filter; 3) a microfluidic channel for processing the fluids to be detected; 4) a tunable optical filter; and 5) a photodetector with optical antennas to improve the detection sensitivity. To demonstrate the major attractive advantages of the optofluidic system, we discussed the two major

components, the tunable optical filter and the optical antenna, which are essential for the realization of the integration and reconfiguration for the system.

A novel optical filter is designed and fabricated by introducing microfluidic channels into a conventional MDM structure. The frequency tunability of the optical filter is demonstrated by both numerical simulations based on a finite-difference-time-domain algorithm and experimental characterization. The layer-transfer and transfer-bonding technique are used to fabricate such structure. By using similar technique, the tunable microfluidic MDM structures can be integrated with other components, such as, organic light emitting devices and organic photoconductors to construct a monolithically integrated fluorescence detection system for lab-on-a-chip applications.

The ability of optical antennas in improving the sensitivity of detection system is demonstrated by numerical simulation for antennas that operate in mid-infrared wavelengths. Very strong field focusing and intensity enhancement can be achieved at mid-infrared wavelengths in properly designed optical antennas. The intensity enhancement factor is on the order of a thousand for a range of infrared wavelengths near resonance, which allows for broad-band operation. The intensity enhancement factor can be further increased by reducing the gap width in the optical antenna design due to a tighter focusing of the incident radiation. There is also strong intensity enhancement at a certain distance above and below the optical antenna plane, which enables easy vertical integration of those antennas with infrared detectors. Compared with optical antennas operate at visible wavelengths, optical antennas for infrared wavelength are large in size and easy to fabricate. The advantages, such as the ease of

fabrication, the planar structure for easy integration and the strong intensity enhancement make optical antennas a viable solution for enabling uncooled and highly sensitive infrared detectors, which will have huge impact on a wide range of infrared technologies.

The second challenging problem addressed in this research is the efficient approach to assemble nanoparticles. Innovation in optical and electronic devices heavily relies on the development of engineered materials at the nanoscale. Nanostructures have to be made and nanoscale building blocks should be integrated with other components of the devices and systems. Low temperature solution based process is an environmentally friendly technology, which enables us to prepare nanostructured organic and inorganic materials by assembling nanoscale building blocks with reduced energy cost. The fundamental understanding of the nanofabrication process mechanism is critical to optimize material properties and improve device performance. Particularly we aim to develop approaches to efficiently place and align SWNTs on flat substrates.

The insufficient ability to manipulate SWNTs at the nanoscale has limited their applications in the large volume manufacturing of nanoelectronic devices. A fundamental and challenging problem is the efficient placement and alignment of SWNTs on a flat substrate on the wafer level. We investigated three different approaches for this challenge.

Firstly, the flow induced alignment using micro- and nanochannel is investigated. It is experimented that micro- and nanochannel can be used to place and

align CNTs by flow-induced and geometrically confined reorganization. TEM characterization indicates the alignment of the CNTs in the stripes. Although flow-induced alignment can be realized using micro- and nanochannels, it is very time-consuming to transport the CNT dispersion into the channels and to dry out the liquid. Additionally, it is extremely difficult to scale up the process to prepare aligned CNTs residue on a wafer level, because of the difficulty in flowing CNTs in very long and narrow channels where clogging often happens. A process with better scalability and controllability is desired to achieve the goal to effectively manipulate one-dimensional nanoparticles, such as CNTs.

Secondly, we presented a simple yet effective CNT alignment technique based on the grating-guided electrostatic self-assembly. Raman spectra indicate alignment of SWNTs in grating templates is achieved. The surfactants used in SWNT dispersion and ESA played an important role to impact the SWNTs alignment. Use of polyelectrolyte surfactant results in SWNTs stripes with good stability due to strong interlayer electrostatic interaction, and the self-assembled SWNT stripe can survive the removal of the template. However, the level of SWNT alignment is not as good as the results obtained when using small molecule surfactant. Short-chain polyelectrolyte (oligomer) may yield best result in term of advantages of multicharge and short length. The process proposed involves the use of polyelectrolytes to achieve the layer-by-layer assembly of CNTs. The resultant CNTs stripes also contain the surfactant materials. For many applications, the stripes containing purely CNTs are desired. The layer-by-layer assembly is also a time consuming process. The resolution of the

process is also limited due to the large molecular chain. Fast and direct deposition of pure CNTs onto the substrates with placement and alignment is of interest.

Thirdly, by introducing the electric field enhanced electrostatic self-assembly, as well as combining the surface chemical modification and mechanical agitation in the solution process, we developed an accelerated self-assembly process, which yield high-speed and high-quality nanomanufacturing of patterned and aligned SWNTs stripes.

Chemical functionalization of CNTs surface allows the preparation of stable CNTs suspension in organic or aqueous solvent through debundle and dispersion process. This is through the oxidation process by concentrated acid, resulting in the functionalization of carbon nanotubes' surface with carboxyl groups, particularly at the tips of the tubes and defects sites on the tube surfaces. The purification of the SWNTs is critical for the directed self-assembly process, because the carbonaceous and metallic impurity would both be destructive to the assembly process and the device performance based on the SWNTs. KOH and HCl are used to fully remove impurities.

The surface treatment by chemical functionalization is also important to realize the nanomanufacturing of SWNT nanostructures. Amino-silane SAM is grown on the surface on which the adsorption of SWNTs is desired because the positive charge of the monolayer will attract the negatively charged SWNTs. While for the area in which adsorption is not desired, hydrophobic surface is prepared. In our process, the amorphous Teflon is used to form the polymer grating structure, so that minimum

adsorption of SWNTs occurs on the polymer protrusion. The existing polymer protrusion also provides the geometrical confinement for effective alignment of SWNTs.

The applications using generic directed self-assembly are limited by the low processing rate and low CNT loading ratio. Externally applied electric field is used to overcome these limitations. The charged SWNTs, which are dispersed in solvent, are moved by the externally applied electric field and accumulate on the surface of the electrode to form homogeneous and dense thin film. Due to the drift of charged SWNTs in the electric field, the concentration of SWNTs near the substrate surface is high, significantly increasing the opportunity to form bonds between the SWNTs and the surface. By controlling the intensity of electric field, the deposition time and the choice of substrate, the thickness of the deposited film can be well controlled. Our recent research found that externally imposed electric field will significantly accelerate the assembly process on materials such as semiconductor silicon surface and even non-conductive silicon dioxide.

There are also reports that ultrasonic agitation will significantly improve the process speed and quality in the self-assembly process for microscale and nanoscale particles. The ultrasonic agitation or vibration helps the particles to overcome the friction and stiction during the assembly process. At the same time, the diffusion of the particles on the surface is also improved due to the additional energy from the ultrasonic agitation. This accelerates the formation of the linkage between the nanoparticles and the surface, as well as the linkage of inter-particles. Strong enough

ultrasonic agitation also removed weakly bonded particles or particle aggregations, leading to improved assembly quality. However, too strong ultrasonic agitation strength is not desired because it will mechanically destroy the polymer patterning and result in lower deposition density.

We successfully developed a scheme which systematically utilizes these physical, chemical and mechanical approaches to achieve highly efficient process to place and align SWNTs. The high selectivity and robustness of the process have opened up a door to the large-scale and high volume production of SWNT-based structures and materials for many applications, such as nanoelectronics and sensors.

REFERENCES

[1] Willson C G and Roman B J 2008. The future of lithography: Sematech litho forum 2008. *ACS Nano* **2** 1323-8

[2] Drapeau M, Wiaux V, Hendrickx E, Verhaegen S and Machida T 2007. Double patterning design split implementation and validation for the 32nm node. In *Proceedings of the SPIE* **6521** 652109-15

[3] Poelma J E and Hawker C J 2010. Block copolymers: With a little help from above. *Nat Nano* **5** 243-4

[4] Chou S Y, Krauss P R and Renstrom P J 1996. Imprint lithography with 25-nanometer resolution. *Science* **272** 85-7

[5] Janssen D, De Palma R, Verlaak S, Heremans P and Dehaen W 2006. Static solvent contact angle measurements, surface free energy and wettability determination of various self-assembled monolayers on silicon dioxide. *Thin Solid Films* **515** 1433-8

[6] Costner E A, Lin M W, Jen W-L and Willson C G 2009. Nanoimprint lithography materials development for semiconductor device fabrication. *Annual Review of Materials Research* **39** 155-80

[7] Tan H, Kong L, Li M, Steere C and Koecher L 2004. Current status of nanonex nanoimprint solutions. In *Proceedings of the SPIE* **5374** 213-21

[8] Divliansky I, Mayer T S, Holliday K S and Crespi V H 2003. Fabrication of three-dimensional polymer photonic crystal structures using single diffraction element interference lithography. *Applied Physics Letters* **82** 1667-9

[9] Yan Q, Zhao X S, Teng J H and Chua S J 2006. Colloidal woodpile structure: Three-dimensional photonic crystal with a dual periodicity. *Langmuir* **22** 7001-6

[10] Holland B T, Blanford C F and Stein A 1998. Synthesis of macroporous minerals with highly ordered three-dimensional arrays of spheroidal voids. *Science* **281** 538-40

[11] Zhao X-M, Xia Y and Whitesides G M 1996. Fabrication of three-dimensional micro-structures: Microtransfer molding. *Advanced Materials* **8** 837-40

[12] Bao L R, Cheng X, Huang X D, Guo L J, Pang S W and Yee A F 2002. Nanoimprinting over topography and multilayer three-dimensional printing. *J. Vac. Sci. Technol. B* **20** 2881-6

[13] Hu W, Yang B, Peng C and Pang S W 2006. Three-dimensional su-8 structures by reversal UV imprint. *Journal of Vacuum Science & Technology B: Microelectronics and Nanometer Structures* **24** 2225-9

[14] Abgrall P, Lattes C, Conedera V, Dollat X, Colin S and Gue A M 2006. A novel fabrication method of flexible and monolithic 3D microfluidic structures using lamination of su-8 films. *Journal of Micromechanics and Microengineering* **16** 113-21

[15] Ooe H, Morimatsu M, Yoshikawa T, Kawata H and Hirai Y 2005. Three-dimensional multilayered microstructure fabricated by imprint lithography. *J. Vac. Sci. Technol. B* **23** 375-9

[16] Psaltis D, Quake S R and Yang C 2006. Developing optofluidic technology through the fusion of microfluidics and optics. *Nature* **442** 381-6

[17] Shin H, Yanik M F, Fan S, Zia R and Brongersma M L 2004. Omnidirectional resonance in a metal--dielectric--metal geometry. *Applied Physics Letters* **84** 4421-3

[18] Gonçalves L M, Minas G, Pinheiro C, Lanceros-Méndez S and Rocha J G 2006. A tunable fabry-perot optical filter for application in biochemical analysis of human's fluids. In *Proceedings of IEEE International Symposium on Industrial Electronics* **4** 2778-83

[19] Macleod H A 2001. *Thin-film optical filters* (Bristol: Institute of Physics Publishing)

[20] Muhlschlegel P, Eisler H-J, Martin O J F, Hecht B and Pohl D W 2005. Resonant optical antennas. *Science* **308** 1607-9

[21] Alda J, Rico-García J M, López-Alonso J M and Boreman G 2005. Optical antennas for nano-photonic applications. *Nanotechnology* **16** 230-4

[22] Sundaramurthy A, Schuck P J, Conley N R, Fromm D P, Kino G S and Moerner W E 2006. Toward nanometer-scale optical photolithography: Utilizing the near-field of bowtie optical nanoantennas. *Nano Letters* **6** 355-60

[23] Chong N and Ahmed H 1997. Antenna-coupled polycrystalline silicon air-bridge thermal detector for mid-infrared radiation. *Applied Physics Letters* **71** 1607-9

[24] Jurbergs D C, Zhao J and McDevitt J T 1996. Antenna-coupled high-Tc bolometers for visible and near-infrared detection using organic dyes as light-harvesting layers. *Applied Physics Letters* **69** 688-90

[25] Eden D D 2000. *Uncooled infrared detector.* United States Patent 6114696

[26] Rogalski A 2003. Quantum well photoconductors in infrared detector technology. *Journal of Applied Physics* **93** 4355-91

[27] Taflove A and Hagness S C 2005. *Computational electrodynamics: The finite-difference time-domain method* (Boston: Artech House)

[28] Rakic A D, Djurisic A B, Elazar J M and Majewski M L 1998. Optical properties of metallic films for vertical-cavity optoelectronic devices. *Appl. Opt.* **37** 5271-83

[29] Novotny L 2007. Effective wavelength scaling for optical antennas. *Physical Review Letters* **98** 266802

[30] Durkop T, Getty S A, Cobas E and Fuhrer M S 2004. Extraordinary mobility in semiconducting carbon nanotubes. *Nano Lett.* **4** 35-9

[31] Qian D, Wagner G J, Liu W K, Yu M F and Ruoff R S 2002. Mechanics of carbon nanotubes. *Applied Mechanics Reviews* **55** 495-532

[32] Treacy M M J, Ebbesen T W and Gibson J M 1996. Exceptionally high Young's modulus observed for individual carbon nanotubes. *Nature* **381** 678-80

[33] Wilder J W G, Venema L C, Rinzler A G, Smalley R E and Dekker C 1998. Electronic structure of atomically resolved carbon nanotubes. *Nature* **391** 59-62

[34] Zettl A 2000. Extreme oxygen sensitivity of electronic properties of carbon nanotubes. *Science* **287** 1801-4

[35] Kim P, Shi L, Majumdar A and McEuen P L 2001. Thermal transport measurements of individual multiwalled nanotubes. *Phys. Rev. Lett.* **87** 215502

[36] Berber S, Kwon Y-K and Tománek D 2000. Unusually high thermal conductivity of carbon nanotubes. *Phys. Rev. Lett.* **84** 4613

[37] Avouris P 2002. Molecular electronics with carbon nanotubes. *Accounts of Chemical Research* **35** 1026-34

[38] Bachtold A, Hadley P, Nakanishi T and Dekker C 2001. Logic circuits with carbon nanotube transistors. *Science* **294** 1317-20

[39] Baughman R H, Cui C, Zakhidov A A, Iqbal Z, Barisci J N, Spinks G M, Wallace G G, Mazzoldi A, De Rossi D, Rinzler A G, Jaschinski O, Roth S and Kertesz M 1999. Carbon nanotube actuators. *Science* **284** 1340-4

[40] Baughman R H, Zakhidov A A and De Heer W A 2002. Carbon nanotubes - the route toward applications. *Science* **297** 787-92

[41] Dai H 2002. Carbon nanotubes: Opportunities and challenges. *Surface Science* **500** 218-41

[42] Bonard J-M, Kind H, Stockli T and Nilsson L-O 2001. Field emission from carbon nanotubes: The first five years. *Solid-State Electronics* **45** 893-914

[43] Fennimore A M, Yuzvinsky T D, Han W Q, Fuhrer M S, Cumings J and Zetti A 2003. Rotational actuators based on carbon nanotubes. *Nature* **424** 408-10

[44] Heinze S, Tersoff J, Martel R, Derycke V, Appenzeller J and Avouris P 2002. Carbon nanotubes as schottky barrier transistors. *Physical Review Letters* **89** 1068011-4

[45] Javey A, Guo J, Wang Q, Lundstrom M and Dai H 2003. Ballistic carbon nanotube field-effect transistors. *Nature* **424** 654-7

[46] Rueckes T, Kim K, Joselevich E, Tseng G Y, Cheung C L and Lieber C M 2000. Carbon nanotube-based nonvolatile random access memory for molecular computing. *Science* **289** 94-7

[47] Soh H T, Quate C F, Morpurgo A F, Marcus C M, Kong J and Hongjie D 1999. Integrated nanotube circuits: Controlled growth and ohmic contacting of single-walled carbon nanotubes. *Applied Physics Letters* **75** 627-9

[48] Du F, Fischer J E and Winey K I 2005. Effect of nanotube alignment on percolation conductivity in carbon nanotube/polymer composites. *Physical Review B - Condensed Matter and Materials Physics* **72** 1-4

[49] Dai L and Huang S 2004. *Multilayer carbon nanotube films and method of making the same*. United States Patent 6808746

[50] Zhang Y, Chang A, Cao J, Wang Q, Kim W, Li Y, Morris N, Yenilmez E, Kong J and Dai H 2001. Electric-field-directed growth of aligned single-walled carbon nanotubes. *Applied Physics Letters* **79** 3155-7

[51] Banerjee S and Herman I P 2007. *Method and system to position carbon nanotubes using ac dielectrophoresis*. International Patent Application PCT/US2006/061807

[52] Smits J M, Wincheski R A, Ingram J L, Watkins A N and Jordan J D 2004. *Controlled deposition and alignment of carbon nanotubes*. United States Patent 0228961

[53] Yaniv Z and Fink R L 2001. *Alignment of carbon nanotubes*. United States Patent 6312303

[54] Filas R W, Jin S, Kochanski G P and Zhu W 2004. *Article comprising aligned nanowires*. United States Patent 6741019

[55] Haik Y, Chatterjee J and Chen C-j 2005. *Alignment of carbon nanotubes using magnetic particles*. United States Patent 0239948

[56] Mineo Y, Yuegang Z, Xing S, Lei S, A. B A, Narayanan S and 2009. *Methods of producing carbon nanotubes using peptide or nucleic acid micropatterning*. United States Patent 0169466

[57] Clarke M S 2005. *Spatial localization of dispersed single walled carbon nanotubes into useful structures.* United States Patent 6896864

[58] Jin S, Whang D, McAlpine M C, Friedman R S, Wu Y and Lieber C M 2004. Scalable interconnection and integration of nanowire devices without registration. *Nano Lett.* **4** 915-9

[59] Li S, Liu N, Chan-Park M B, Yan Y and Zhang Q 2007. Aligned single-walled carbon nanotube patterns with nanoscale width, micron-scale length and controllable pitch. *Nanotechnology* **18** 455302

[60] Yan Y H, Li S, Chen L Q, Chan-Park M B and Zhang Q 2006. Large-scale submicron horizontally aligned single-walled carbon nanotube surface arrays on various substrates produced by a fluidic assembly method. *Nanotechnology* **17** 5696-701

[61] Park J U, Meitl M A, Hur S H, Usrey M L, Strano M S, Kenis P J A and Rogers J A 2006. In situ deposition and patterning of single-walled carbon nanotubes by laminar flow and controlled flocculation in microfluidic channels. *Angewandte Chemie - International Edition* **45** 581-5

[62] Huang Y, Duan X, Wei Q and Lieber C M 2001. Directed assembly of one-dimensional nanostructures into functional networks. *Science* **291** 630-3

[63] Tsukruk V V, Ko H and Peleshanko S 2004. Nanotube surface arrays: Weaving, bending, and assembling on patterned silicon. *Phys. Rev. Lett.* **92** 065502

[64] Chattopadhyay D, Galeska I and Papadimitrakopoulos F 2003. A route for bulk separation of semiconducting from metallic single-wall carbon nanotubes. *Journal of the American Chemical Society* **125** 3370-5

[65] Krupke R, Hennrich F, Lohneysen H v and Kappes M M 2003. Separation of metallic from semiconducting single-walled carbon nanotubes. *Science* **301** 344-7

[66] Zheng M, Jagota A, Strano M S, Santos A P, Barone P, Chou S G, Diner B A, Dresselhaus M S, McLean R S, Onoa G B, Samsonidze G G, Semke E D, Usrey M and Watts D J 2003. Structure-based carbon nanotube sorting by sequence-dependent DNA assembly. *Science* **302** 1545-8

[67] Sun D, Everett W N, Chu C-C and Sue H-J 2009. Single-walled carbon-nanotube dispersion with electrostatically tethered nanoplatelets. *Small* **5** 2692-7

[68] Ramasubramaniam R, Chen J and Liu H 2003. Homogeneous carbon nanotube/polymer composites for electrical applications. *Applied Physics Letters* **83** 2928-30

[69] Barraza H J, Pompeo F, O'Rea E A and Resasco D E 2002. Swnt-filled thermoplastic and elastomeric composites prepared by miniemulsion polymerization. *Nano Letters* **2** 797-802

[70] Bliznyuk V, Singamaneni S, Kattumenu R and Atashbar M 2006. Surface electrical conductivity in ultrathin single-wall carbon nanotube/polymer nanocomposite films. *Applied Physics Letters* **88** 164101-3

[71] Ma W, Song L, Yang R, Zhang T, Zhao Y, Sun L, Ren Y, Liu D, Liu L, Shen J, Zhang Z, Xiang Y, Zhou W and Xie S 2007. Directly synthesized strong, highly conducting, transparent single-walled carbon nanotube films. *Nano Letters* **7** 2307-11

[72] Vaisman L, Wagner H D and Marom G 2006. The role of surfactants in dispersion of carbon nanotubes. *Advances in Colloid and Interface Science* **128-130** 37-46

[73] Limin H, Cui X, Dukovic G and O'Brien S P 2004. Self-organizing high-density single-walled carbon nanotube arrays from surfactant suspensions. *Nanotechnology* **15** 1450

[74] Li S, Liu N, Chan-Park M B, Yan Y and Zhang Q 2006. Large-scale submicron horizontally aligned single-walled carbon nanotube surface arrays

on various substrates produced by a fluidic assembly method. *Nanotechnology* **17** 5696

[75] Lay M D, Novak J P and Snow E S 2004. Simple route to large-scale ordered arrays of liquid-deposited carbon nanotubes. *Nano Letters* **4** 603-6

[76] Yan Y, Chan-Park Mary B and Zhang Q 2007. Advances in carbon-nanotube assembly. *Small* **3** 24-42

[77] Valentin E, Auvray S, Goethals J, Lewenstein J, Capes L, Filoramo A, Ribayrol A, Tsui R, Bourgoin J-P and Patillon J-N 2002. High-density selective placement methods for carbon nanotubes. *Microelectronic Engineering* **61-62** 491-6

[78] Karl-Friedrich Bohringer M, Michael C, Ken G, Roger H and Al P 1997. Electrostatic self-assembly aided by ultrasonic vibration. In *AVS. 44th National Symposium*, San Jose, CA.

[79] Lee J S, Ha K, Lee Y-J and Yoon K B 2005. Ultrasound-aided remarkably fast assembly of monolayers of zeolite crystals on glass with a very high degree of lateral close packing. *Advanced Materials* **17** 837-41

[80] Cabana J, Paillet M and Martel R 2009. Directed assembly of swnts by electrostatic interactions and its application for making network transistors. *Langmuir* **26** 607-12

[81] Qi H, Qian C and Liu J 2006. Synthesis of high-purity few-walled carbon nanotubes from ethanol/methanol mixture. *Chemistry of Materials* **18** 5691-5

[82] Heinze S, Tersoff J, Martel R, Derycke V, Appenzeller J and Avouris P 2002. Carbon nanotubes as schottky barrier transistors. *Phys. Rev. Lett.* **89** 106801

[83] Burke P J 2004. Ac performance of nanoelectronics: Towards a ballistic thz nanotube transistor. *Solid-State Electronics* **48** 1981-6

[84] Yu Z and Burke P J 2005. Aligned array FETs as a route towards thz nanotube transistors. In *Proceedings of the SPIE* **5790** 246-53

VITA

Huifeng Li completed his B.Eng. in electrical engineering at Shanghai Jiaotong University, China, in 2002, He received his M.Eng. degree in electrical engineering at National University of Singapore in 2005. He entered the doctoral program in electrical engineering at Texas A&M University in August 2004 and received his Ph.D. degree in August 2010. He can be reached at the following address:

Huifeng Li

214 Zachry Engineering Center, TAMU 3128, College Station, TX 77843